67-1980

TAPPE, John, 1932-

THE CHEMISTRY, PETROLOGY, AND STRUCTURE OF THE BIG TIMBER IGNEOUS COMPLEX, CRAZY MOUNTAINS, MONTANA.

University of Cincinnati, Ph.D., 1966
Geology

University Microfilms, Inc., Ann Arbor, Michigan

THE CHEMISTRY, PETROLOGY, AND STRUCTURE OF THE BIG TIMBER IGNEOUS COMPLEX, CRAZY MOUNTAINS, MONTANA

A dissertation submitted to
The Graduate School
of
the University of Cincinnati

in partial fulfillment
of the requirements for the degree of

DOCTOR OF PHILOSOPHY
1966

by

John Tappe
A.B. University of Cincinnati, 1958

UNIVERSITY OF CINCINNATI

AUGUST 12 19 66

I hereby recommend that the thesis prepared under my supervision by JOHN TAPPE

entitled THE CHEMISTRY, PETROLOGY, AND STRUCTURE OF THE BIG TIMBER IGNEOUS COMPLEX CRAZY MOUNTAINS, MONTANA

be accepted as fulfilling this part of the requirements for the degree of DOCTOR OF PHILOSOPHY

Approved by:

Howard L. Landes

William T. Jenks

Frank L. Rowley

Form 668—Grad. Sch.—1M—7-63

PLEASE NOTE:
Figure pages are not original copy and tend to "curl". Several pages have small indistinct print. Filmed as received.

University Microfilms, Inc.

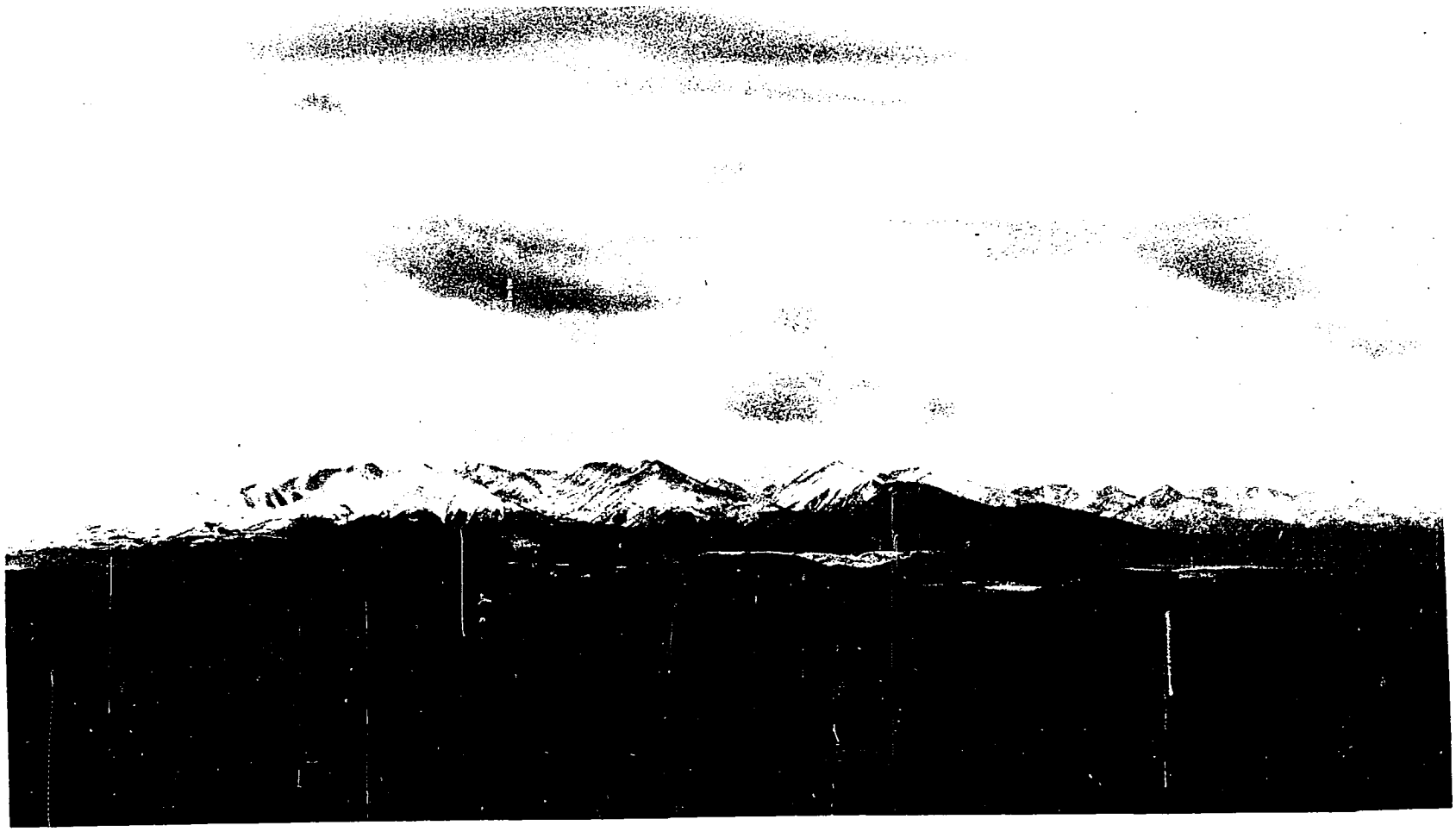

Frontispiece. View of Big Timber Igneous Complex from Big Timber, Montana. (toward northwest)

THE CHEMISTRY, PETROLOGY, AND STRUCTURE OF THE BIG TIMBER IGNEOUS COMPLEX, CRAZY MOUNTAINS, MONTANA

by

John Tappe

TABLE OF CONTENTS

LIST OF ILLUSTRATIONS

PREFACE

Although this paper does not claim to solve all the geologic problems present in the Big Timber igneous complex, it is hoped that the research it represents will serve as the basis for future investigations in this area. As is repeatedly noted throughout the text, there remain many problems which have as yet been studied only superficially or not at all. These problems are particularly apparent in the area of petrography, the complete study of which will require years of additional extensive research.

The area in which the most complete study has been made, the geochemistry section, is, oddly enough, one of the shortest sections of the paper (in text) due to the use of charts and diagrams and the peculiar nature of geochemical data which lends itself to brief and concise exposition. For reasons of time and finances the precise chemical procedures used in the chemical analyses have not been included in this dissertation. They will be published in the near future under the auspices of the University of Cincinnati Department of Geology and will serve as a guide for future students in geochemical research at the University of Cincinnati.

In spite of the four years of extensive research spent on this project, it now appears that I have managed

to scratch only the surface of this complex geologic area. As depressing and humbling as this discovery is, it does suggest innumerable possibilities for future study. As has been said, the first step in the long road to wisdom consists of realizing how much one does not know.

INTRODUCTION

General Statement

The Crazy Mountains in general and the Big Timber igneous complex in particular have frequently been referred to in geologic literature as an excellent example of a pluton from which a radial dike pattern emanates. This complex consists of multiple plutonic intrusions and several associated injections of dikes. In view of the "textbook nature" of this pluton it may seem strange that all previous work performed in the area has been of a purely reconnaissance nature and that no detailed study of the pluton has been undertaken. There are many possible reasons for this lack of attention, the most obvious being the extremely rugged terrain. Since roads leading into the area are few and poor and terminate several miles outside the area being mapped, field work must be performed by back-packing into the higher elevations and establishing a base camp. Although part of the area can be traversed by horse-back, most of it can be covered only on foot.

A second but less restricting difficulty is found in the fact that there are no large-scale topographic maps of the area. The only map which covers this area, the White Sulphur Springs sheet of the 1:250,000 series of the United States Geological Survey, is completely inadequate for

geologic mapping. Partially compensating for this lack, however, are the quite adequate aerial photographs available from both the U.S.G.S. and the Soil Conservation Service.

Despite the aforementioned difficulties the writer has undertaken and partially completed a detailed study of this pluton. Although a systematic collection of plutonic and dike rocks on a one-quarter-mile grid has been initiated, the difficult terrain and very short field season have prevented a complete collection in the area. The entire pluton has been mapped, but only about one-half the collecting has been completed to date. A thorough reconnaissance and photogeology has been performed on the remaining part of the area, and it is anticipated that with additional field work a more complete geologic picture of the area will emerge.

Location and Physiographic Setting

The area being studied is located in Southcentral Montana, approximately eighty miles north of the northern boundary of Yellowstone National Park. The Crazy Mountains are located on the Central Montana Platform (Central Montana Rockies of Eardley, 1962, p. 351) and are part of the "Transverse Igneous Belt" which cuts diagonally across the regional structural lineaments. All the igneous bodies within this transverse belt are Tertiary in age and have

been studied in broad detail by Larsen (1940). The Crazy Mountains are the southwesternmost member of this transverse belt and form an outlier to the Rock Mountain front proper which is thirty miles to the west.

Weed (1899, p. 1) described the Crazy Mountains as:

> the highest and most conspicuous mountains of the quadrangle [Little Belt Mountain Quadrangle]. Surrounded on all sides by low and open bench lands, their rugged snow-capped peaks and sharp crests are visible for many miles. The mountains form a group of connected peaks and not a range. The mountain mass is from 10 to 20 miles wide and 30 long, and lies almost wholly within the limits of the quadrangle. The highest peaks reach an elevation of over 11,000 feet, or 6000 feet above the bench lands. In both elevation and ruggedness they far surpass the other mountains of the quadrangle and indeed most mountains of the State. Yet they form an isolated mountain group that does not belong to the Rocky Mountain system, either in geographic relation and position or in geologic structure. They afford a remarkable example of a residual mountain range in flat-bedded rocks carved out simply by stream erosion.

The Crazy Mountain igneous complex is located axially to the Crazy Mountain basin which is bounded on the north by the Little Belt and Castle Mountains, on the west by the Bridger Mountains, and on the south by the Absaroka and Beartooth Mountains. Toward the east the basin is lost against the Lake Basin Fault Zone and the Pryor Arch.

The igneous rocks and the metamorphic aureole of the Big Timber complex form the highest peaks within the area (See frontispiece). Within the area studied elevations vary from 6,000 to slightly over 11,000 feet.

Pleistocene glaciation within the area has been severe. Excellent exposures have been created by deep U-shaped valleys which have cut into the complex and its metamorphic aureole. Valley train and scree material have covered much of the valley floors and lower walls, but generally exposures of the pluton, dikes, and metamorphic aureole are excellent.

Purpose of the Study

The igneous rocks within the Crazy Mountain basin have been intruded as sills, dikes, laccoliths, and stocks and vary widely in composition from the mildly alkalic rocks to the oversaturated rocks of the calc-alkaline types. This study has as its principal purpose the presentation of field and laboratory data pertaining to the chemistry, petrology, and structure of the Big Timber igneous complex and is intended to be a segment of a larger study of all the igneous rocks located within the Crazy Mountain basin.

The chemical and petrographic study of the plutonic and dike rocks has been undertaken to describe the variation and determine the type of differentiation and assimilation in the formation of the wide variety of rock types present.

Comparison has been made of the chemical analyses (Simms, 1966) of the mildly alkalic rocks of the area north and west of the writer's area to determine whether or nor there exists any chemical relationship between the two different rock suites.

Since erosion has not cut through the base of the epizone (estimated to be between four and six miles in depth (Buddington, 1959)), the study of the physico-chemical conditions under which the pluton was intruded could provide information regarding the method of emplacement of epizonal plutons.

Geologic Setting

The Big Timber igneous complex is the largest of a series of igneous intrusions into the Crazy Mountain basin. The precise relationship among the various igneous phases is a matter of serious debate due largely to the great diversity of rock types present. The Crazy Mountain igneous series (all the igneous rocks intruded into the basin) is the southwesternmost part of the Central Montana Rockies (Eardley, 1962, p. 351) which includes all the Tertiary intrusives east of the Cordillera. These intrusives, none of which has been affected by the Laramide orogeny, are part of the Montana Petrographic Province of Larsen (1940); they include the area from the Little Belt Mountains on the

west to the Porcupine Dome on the west and from the Sweetgrass Hills on the north to the Crazy Mountains on the south.

Figure 1 is a generalized geologic map of Southcentral Montana showing the Crazy Mountain basin. Shown also are the gravity data (presented by Kelley, 1966) as specifically related to the Big Timber igneous complex and the Loco Mountain stock.

The Big Timber igneous complex and the smaller Loco Mountain stock ten miles to the north have been intruded coaxially to the Crazy Mountain basin.[1] These intrusions penetrated in excess of 20,000 feet of sedimentary rocks. A stratigraphic column of the basin is shown in Figure 2.

Rocks of the Big Timber igneous complex are, for the most part, in direct contact with the sediments of the Fort Union formation. The sediments in contact with the pluton vary generally from coarse argillaceous sandstones to rather clean fine-grained siltites and were sufficiently well-indurated at the time of the intrusion of the early basic phase to withstand lateral thrusting. This thrusting is well-exposed on the north wall of Big Timber canyon above the Lazy K Bar Ranch. As yet no detailed investigation of these sediments has been made.

---

[1] The axis of the Crazy Mountain basin varies on different maps due principally to a lack of detailed geological mapping within the basin. The most recent work by McMannis (1957) shows the axis to be essentially parallel to the Bridger Range (The Rocky Mountain Front).

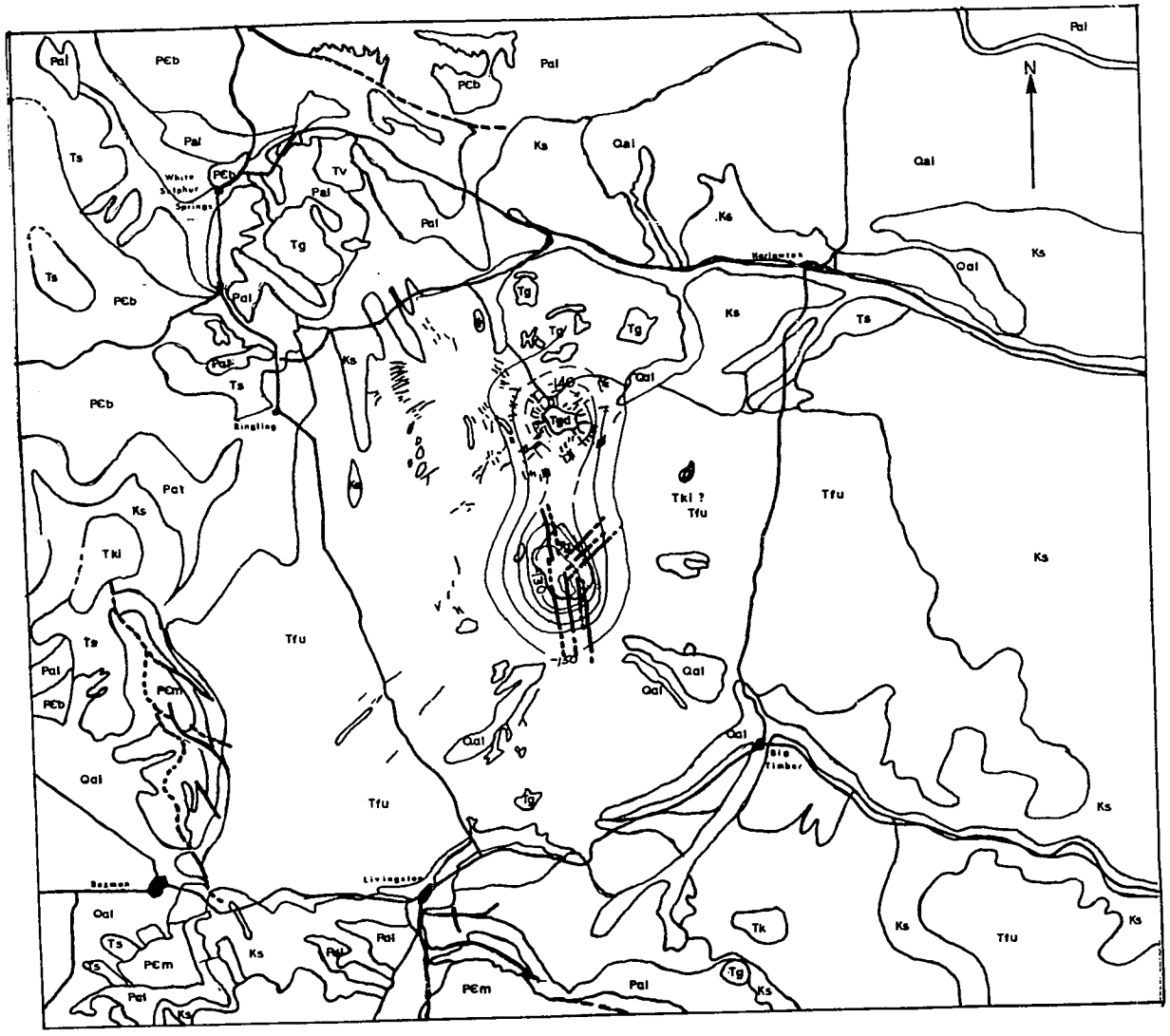

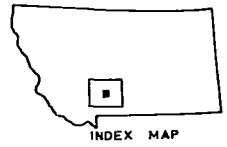

Figure 1

Simplified Geologic Map
With Gravity Data

Sedimentary Rocks		Igneous Rocks	
Quaternary Deposits	Qal	Tertiary Intrusives (Sills and Laccoliths)	Tg
Tertiary (Undif.)	Ts	Crazy Mountain Diorite	Tgd
Fort Union Fm.	Tfu	Tertiary Dikes	
Livingston Fm.	Tki	Tertiary Volcanics	Tv
Cretaceous (Undif.)	Ks	Cretaceous Volcanics	Kv
Paleozoic (Undif.)	Pal		
Pre-C Belt Series	PEb		
Pre-C Metamorphics	PEm		

Fault — — — — Contact — — — —

Bouguer Anomaly

Contour Interval: 5 milligals — -150 —

Modified from: Iddings & Weed (1894), Weed (1898), Moore (1957), U.S.G.S. Montana Geologic Map (1955), & Kelley (1966).

0 Miles 10

SCALE

Figure 2 STRATIGRAPHIC COLUMN (Roberts, 1963)

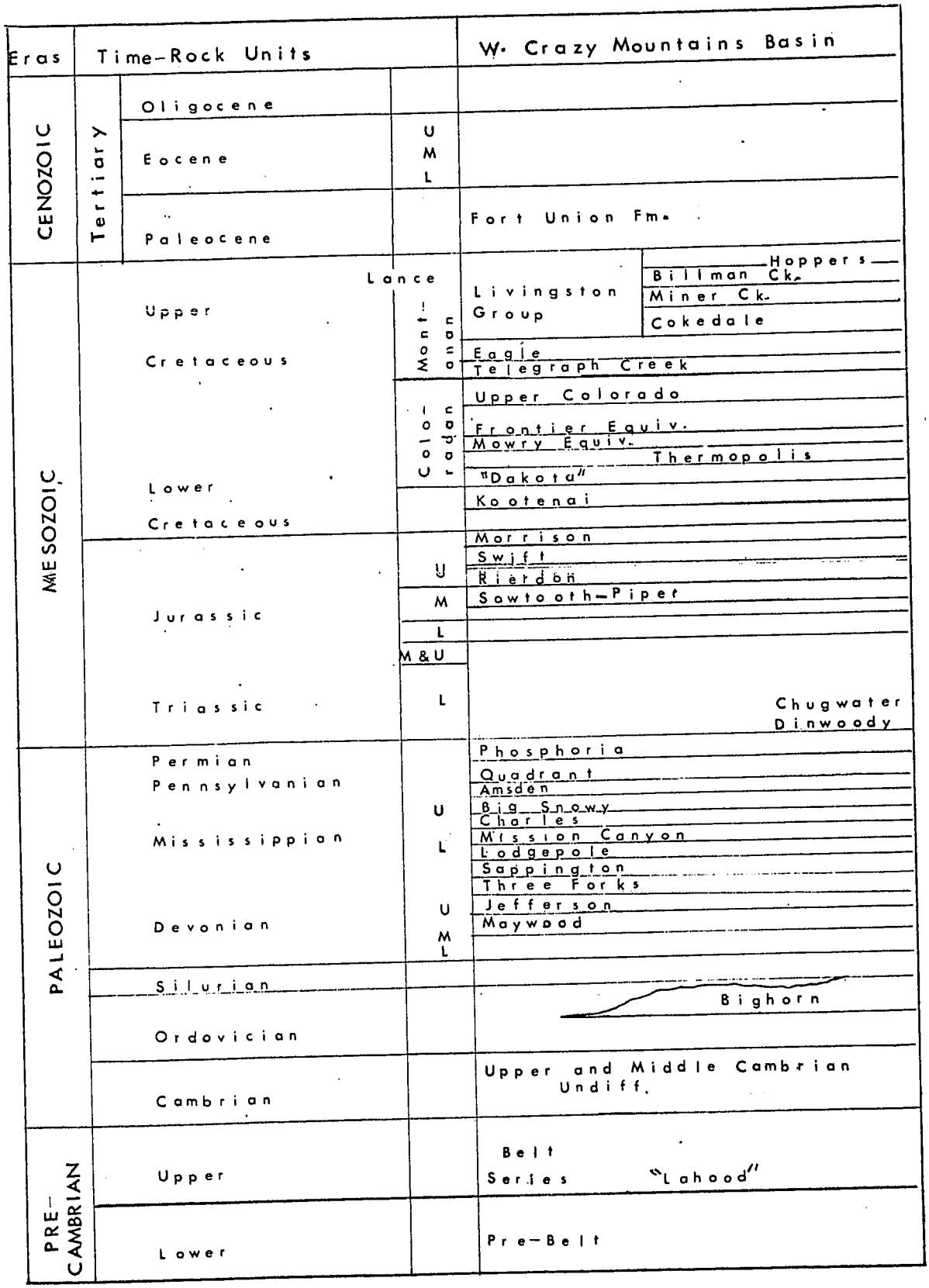

Post-Paleocene sedimentation has not been found within the area, although it has been reported in spotty instances within other parts of the basin as high level bench gravels. The dating of these deposits is questionable (Pryor, personal communication), but they have been used by several investigators (Weed, 1899 and Simms, 1966) in the dating of the igneous events within the basin.

Recent gravity work by Bonini (personal communication) and Kelley (1966) shows a very strong positive Bouguer anomaly over both the Big Timber igneous complex and the Loco Mountain stock (See Figure 1). These data strongly support the field relationships of the igneous phases as found by the writer.

Previous Work

The Crazy Mountains were first observed by Lewis and Clark in 1806 while traversing east on the Yellowstone River. Later F. V. Hayden (1872) made note of the distant mountain range as the "Crazy Woman Mountains." Later surveys also mentioned the mountains, but none made any detailed observations within the mountains proper.

The first study within the Big Timber complex was done by Iddings and Weed (1894) and later by Weed (1899); the most extensive work was performed by Wolff (1938). Both Iddings and Weed (1894) and Weed (1899) made broad

reconnaissance studies of large areas (mapped on a scale of 1:250,000). In view of the wide range of these studies, only a brief petrographic description of the igneous rocks was presented. Wolff made an extensive survey of the Crazy Mountain basin north of the writer's area but spent only a few days within the Big Timber complex. He stated on p. 1581: "The outline which follows is based on a few days of study in a region difficult of access, and much may be added by further work." Mansfield (1909) spent a few days in the area and has given a brief description of the glacial geology within the area.

None of the aforementioned writers concerned himself with the structure present in the area, and the few chemical analyses presented by Wolff are biased, since they were collected from scree slopes.

Acknowledgements

The writer would like to express his gratitude to the many individuals who have helped to accomplish this investigation of the Big Timber complex. Thanks are particularly due to Drs. Leonard H. Larsen, William F. Jenks, and Frank L. Koucky who have given of their time to the writer and have made numerous valuable suggestions during the four years spent on this project.

Particular gratitude is also extended to the members of the Van Cleve family, especially Paul "Spike" Van Cleve who supplied the writer with pack animals and mounts during the three summers spent in the area. His knowledge of the difficult terrain made the work less difficult than it would ordinarily have been. The writer was also ably assisted by two summer field assistants, Terry Rowekamp and Edward Davis.

A regular National Science Foundation fellowship during the academic year 1964-1965 and summer fellowships during the summers of 1964 and 1965 were of great assistance to the writer. Acknowledgement is also made to NSF Grant G19281 which covered computer time costs in the calculation of the normative minerals and the plotting of numerous diagrams.

METHODS

Collection

All rock samples were systematically collected. A one-quarter mile grid was superimposed on the Forest Service Planimetric 2 inch map (See Plate I, in pocket), and samples of the plutonic rocks were collected at each grid intersection. Dike rocks were similarly collected, although no grid system was completely adequate due to the pattern in which the dikes have been intruded.

Mapping

The preliminary geologic map (Plate I, in pocket) was made from Map 610-4-3, a 2 inch planimetric map of the U.S. Forest Service. Field mapping was performed using two sets of aerial photographs: (1) a Soil Conservation series of scale ca. 1:15,000 and (2) a U.S. Geological Survey series of scale ca. 1:30,000. The geological data was transferred by means of a Caesar-Saltzman projector to the 4 inch base map, enlarged from the aforementioned 2 inch map.

Analytical Procedures

From recent literature detailing experimental procedures and from results of other petrologic studies it has become increasingly evident that whole rock chemical data are vital to the understanding of the physico-chemical

processes operating during the consolidation of a rock melt. The writer undertook the chemical analysis of a suite of rocks, the collection of which has previously been described.

There are many analytical procedural schemes in both chemical and geological literature (Shapiro and Brannock, 1952 and 1956; Riley, 1958; Ahrens et al., 1963; Debras-Guedon and Voinovitch, 1963; Oki et al., 1962; and others). Since an investigation of these various procedures proved that no one scheme was adequate for the particular laboratory facilities at hand, the writer was forced to undertake a search of chemical literature and to modify existing procedural schemes.

Following is a brief description of procedures used in the estimation of the principal oxides of rocks. The analyses were carried out in four parts: (1) silica, (2) metal oxides and phosphorous pentoxide, (3) ferrous oxide, and (4) water.

Sample preparation. Approximately 200 grams of the representative sample was taken, broken into walnut-size fragments using a rock-splitter, and passed through a jaw-crusher three times. The sample was then quartered using a riffle splitter. Three-quarters of the sample has been stored in screw cap jars, and the remaining quarter was ground in a motorized mortar and pestle to pass a 100 mesh sieve. This was then thoroughly mixed and oven-dried at 110° for four hours.

Determination of silica. The dried and ground sample was decomposed by fusing with sodium hydroxide in a silver crucible in a muffle furnace at 830° C. The fusion was leached in an acid-water solution, acidified to a pH of 1.5 and diluted to volume by weight. Silica was determined spectrophotometrically in this solution by molybdenum yellow complex method developed by the writer.

Determination of metal oxides and phosphorous pentoxide. A portion of the rock sample (ca. 0.5 grams) was dissolved using either a mixture of hydrofluoric and perchloric acids in a teflon beaker with a tight-fitting lid or hydrofluoric acid alone in a teflon-lined bomb. The solution and precipitate were fumed to near dryness twice with perchloric acid to remove fluoride and silica. The residue was dissolved in hot perchloric acid and diluted with water to 500.0 ml. by weight. This solution was used in the estimation of TiO_2, total iron as Fe_2O_3, Al_2O_3, MnO, CaO, MgO, Na_2O, K_2O, and P_2O_5. The use of perchloric acid instead of sulfuric acid has been outlined by Riley (1958) and also by Langmyhr and Sveen (1965).

1.) Titanium dioxide was determined spectrophotometrically by the use of Tiron (disodium 1, 2-dihydroxybenzene-3, 5-disulfonate). The yellow color was measured at 380 mμ. This method has high sensitivity, excellent stability and is exceptionally free from interference from other elements.

2.) Total iron oxide was estimated spectrophotometrically at 510 mμ as the red complex of 1, 10 phenanthroline.

3.) Aluminum oxide was determined using an oxine-chloroform extraction. Iron was complexed as the ferrous-dipyridyl complex; the pH was adjusted with sodium acetate buffer to 4.9-5.0; and aluminum was extracted with a chloroform solution of 8-hydroxyquinoline. The density of the yellow extract was measured spectrophotometrically at 390 mμ, and a small correction was made for titanium dioxide.

4.) Manganese oxide was estimated spectrophotometrically at 575 mμ as the permanganate. Oxidation of manganese was performed using persulfate, since it gives more consistent results than does periodate when working with small amounts of manganese.

5.) Calcium plus magnesium oxide as CaO were estimated chelatometrically at pH 10.0 using calmagite as the indicator (Mallenkrodt Chemical). Iron was complexed with potassium cyanide in triethanolamine prior to titration. The solution was titrated with EDTA to the disappearance of the last trace of red.

6.) Calcium oxide was estimated by flame photometry using 20% glycerin (v/v) in the final solution as a buffer. Flame emission was measured at 422 mμ, and estimation was made us ng a standard calibration curve.

7.) Sodium and potassium oxides were estimated by flame spectrophotometry. A portion of the solution was passed through an anion exchange column (IRA-400) in the citrate form. This passage removed most divalent and trivalent ions which could cause serious flame interferences. The solution was buffered with ammonium sulfate prior to introduction into a sheathed oxygen-hydrogen flame.

8.) Phosphorous pentoxide was estimated by the molybdenum blue method as described by Riley (1958).

Determination of ferrous oxide. Ferrous oxide was estimated by a modified method of Van Loon (1965). Standard methods used in the estimation of ferrous oxide allow for subsequent oxidation of the ferrous ion; therefore, a method which prevents this oxidation has been used. Slightly higher values have been found for ferrous iron in standard rock samples (See Figure 3). Approximately 0.5 grams of dried rock powder were weighed into a teflon beaker containing a solution of potassium iodate. Hydrofluoric acid was added to the beaker, and its contents were heated until the sample was dissolved. The solution was neutralized with ammonia, and an excess of potassium iodide was added and the solution immediately titrated with sodium thiosulfate using starch as the indicator.

Estimation of water. Water was estimated on a 0.5 gram sample using the modified method of Riley (1958).

Accuracy and precision. Analytical procedures were compared to the standards, diabase W-1 and syenite S-1, and with additional analyzed samples obtained from C.O. Ingamells. The results are presented in Figure 3. In all instances accuracy and precision were well within the limits set by the U.S.G.S. (Fleischer and Stevens, 1962).

From the chemical analyses computations of the normative minerals, ionic and cationic equivalents were made using an IBM 1620 computer. All variation diagrams were plotted utilizing an on-line IBM 1627 Plotter.

Figure 3. Comparison of Values for W-1 and S-1

Analyses by the writer were performed in triplicate and run along with rocks for the Big Timber igneous complex. Precision is within the limits of acceptability as set by Stevens et al., 1960.

W-1-I - preferred values (Ingamells and Suhr, 1963
W-1-II- analysis by J. Tappe (average of 3)
S-1-I - mean values (Webber, 1965)
S-1-II- analysis by J. Tappe (average of 3)

	W-1		S-1	
	I	II	I	II
SiO_2	52.60	52.76	59.45	59.32
TiO_2	1.08	1.11	0.49	0.49
Al_2O_3	14.94	15.17	9.58	9.48
Fe_2O_3	1.38	0.77	2.27	1.08
FeO	8.71	9.34	5.44	6.51
MnO	0.17	0.18	0.40	0.42
MgO	6.52	6.50	4.07	4.04
CaO	10.92	10.95	10.32	10.74
Na_2O	2.15	2.19	3.24	3.47
K_2O	0.63	0.68	2.75	2.63
P_2O_5	0.14	0.15	0.20	0.23
H_2O	0.53	0.48	0.60	0.51
Total	99.77	100.28	98.81	98.92
Total Fe as Fe_2O_3	11.05	11.13	8.31	8.30

STRUCTURE

Since no previous detailed structural work has been attempted within the area mapped by the writer and since structural data immediately outside the map area is lacking, this section has as its purpose the presentation of evidence of tectonism within the Big Timber igneous complex. Magma tectonics have been only partially explored and cannot be evaluated until post-magmatic structures have been quantitatively investigated.

General

The Crazy Mountain basin is considered by McMannis (1955) to be of particular significance in the structural evolution of southwestern Montana. Smith (1965) has shown that there was operative within the Montana Platform a series of Tertiary igneous intrusive centers which could well be related to the Lewis and Clark megashears (See Figure 4). The two megashears of particular significance to the study of the Crazy Mountain basin are the Lake Basin lineament and the Nye-Bowler lineament.

The Lake Basin lineament was first described by R.T. Chamberlin (1919) who interpreted the series of *en échelon* faults exposed at the surface as expressions of tension resulting from movement along a buried sinistral transcurrent fault.

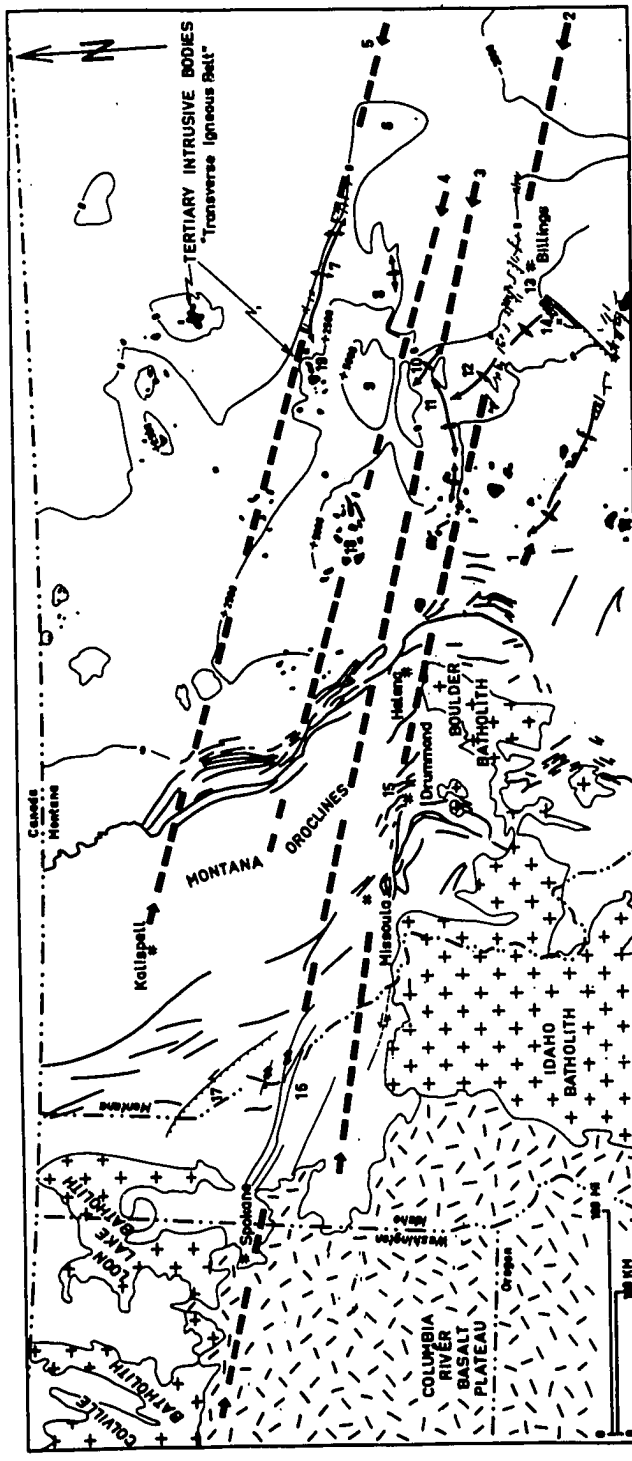

Figure 4. Lewis and Clark lineaments (megashears), surficial manifestation of deep-seated sinistral transcurrent movement (From Smith, 1965).

In 1936 Wilson reported a structural zone paralleling the northeastern margin of the Beartooth Mountains for which he proposed an origin similar to that of the Lake Basin lineament. This structural belt, the Nye-Bowler lineament, has associated with it a series of en échelon faults, folds, and volcanic centers. The lineament is about 120 miles long; the work of McMannis (1955) suggests that it may be traced even further west.

The apparent effect of movement along these lineaments and along the Osburn, Big Snowy, and Cat Creek lineaments further to the north has been to crenulate the original trend of the Cordilleran mobile belt (Smith, 1965, p. 1403). The Lake Basin and the Osburn lineaments have been traced for several hundreds of miles from the Central Montana Platform toward the west. A lack of detailed structural data has prevented the establishment of a probable similar extension of the other lineaments.

All the aforementioned lineaments have sinistral movement and are considered by Smith (1965) to be fundamental faults (master faults) and surface manifestations of deep-seated shear zones.

Faulting Within the Big Timber Complex

Faulting within the Big Timber igneous complex has been extensive, consisting principally of normal and scissors

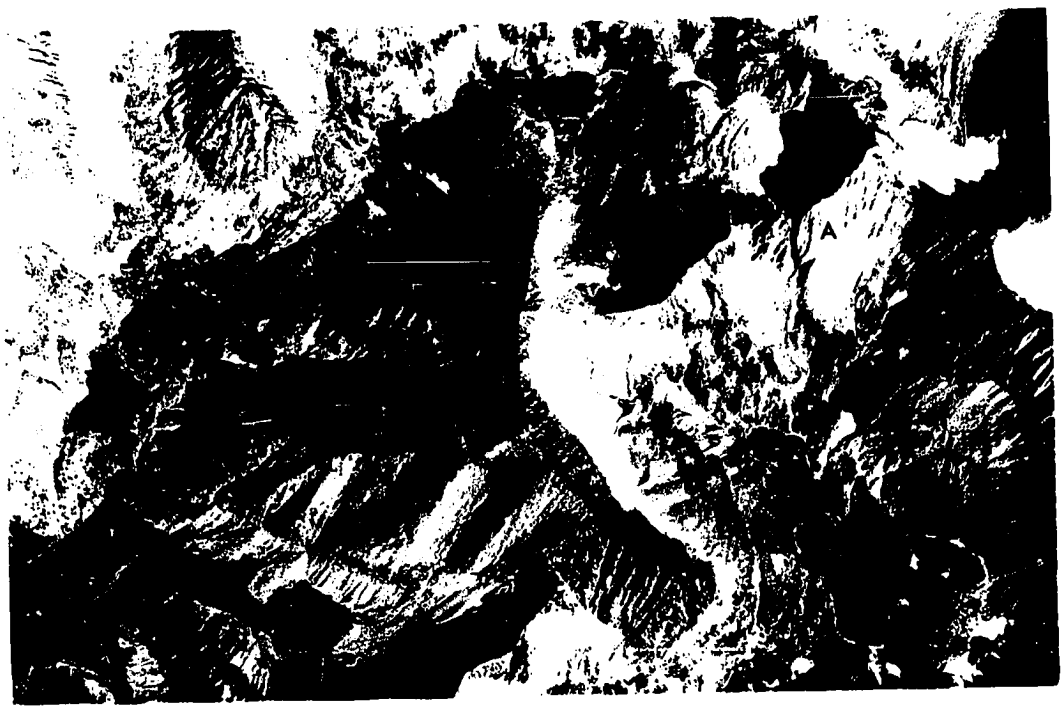

Figure 5. Aerial photograph showing vicinity of Rock Lake. Note faulting causing offset in ridge (A) north of Lake.

faults and dextral strike-slip faults. These faults can easily be recognized on aerial photographs as shown on Figures 5, 6, 7, and 8 and are also expressed topographically on the Fairview Peak quadrangle (7 1/2 minute series) of the U.S. Geological Survey. Broad fault gouge zones, steep "step" faults and deep notches in arêtes caused by faulting are easily recognized in the field and are shown in Figures 9, 10, 11, and 12.

On Plate I the principal faults can be seen as trending essentially north-south with a second series trending essentially northeast to southwest. Movement along these

Figure 6. Aerial photograph showing large fault (A) in the vicinity of Rock Lake. Note wide zone of fault gouge associated with fault.

faults has varied from essential grinding movement (no determinable direction), as can be seen in the vicinity of Swamp Lake, to very strong normal faulting along the fractures forming Crazy Lake, Smeller Lake, and Druckemiller Lake. The fault cutting Druckemiller Lake and Granite Peak is shown in Figures 9 and 14. Strike-slip movements along these fractures can be determined from the slickensided surfaces exposed near Swamp Lake and below the fault near the Mine Lakes. The amount of movement is difficult to determine, since no piercing points have been found. However, in the vicinity of Blue Lake a mineralized shear

Figure 7. Aerial photograph of area of Blue Lake, Druckemiller Lake and Twin Lakes. Note high angle fault cutting ridge of Granite Peak at A and strike-slip fault "cutting off" end of Granite Peak at B.

zone, striking ca. 300° azimuth, appears to have been offset approximately three-quarters of a mile. This fault is shown in Figure 13.

From the aerial photographs presented in Figures 5 through 8 it appears that many of the faults have undergone recent movement. This can be seen from the offset ridges between stream channels in Figures 5 and 7. Many of the fault zones show strong microbrecciation with much of the fault gouge being extremely friable. Since the area has undergone extreme Pleistocene valley glaciation and the glaciers could easily have removed this material,

Figure 8. Aerial photograph showing faulting in vicinity of Crazy Lake and Pear Lake. Figure 10 was taken at A. The twin peaks of Crazy Peak (B) have been caused by faulting.

this fault gouge must have resulted from post-Pleistocene faulting. However, since the andesitic dike phase has been intruded parallel and subparallel to this fault zone, it appears that faulting within the zone must have occurred several times since its inception.

Photogeological and reconnaissance mapping of the northern part of the pluton indicate that the degree of faulting has not been as severe here as in the southern half of the pluton (See Plate I). Faulting in the vicinity of Campfire Lake is shown in Figure 15.

Top: Figure 9. View of Granite Peak looking north from notch south of Pear Lake showing large fault. Note joints paralleling fault pattern.

Bottom: Figure 10. Wide notch in arête above Pear Lake caused by fault. Note small faults in Ridge to Iddings Peaks (Right).

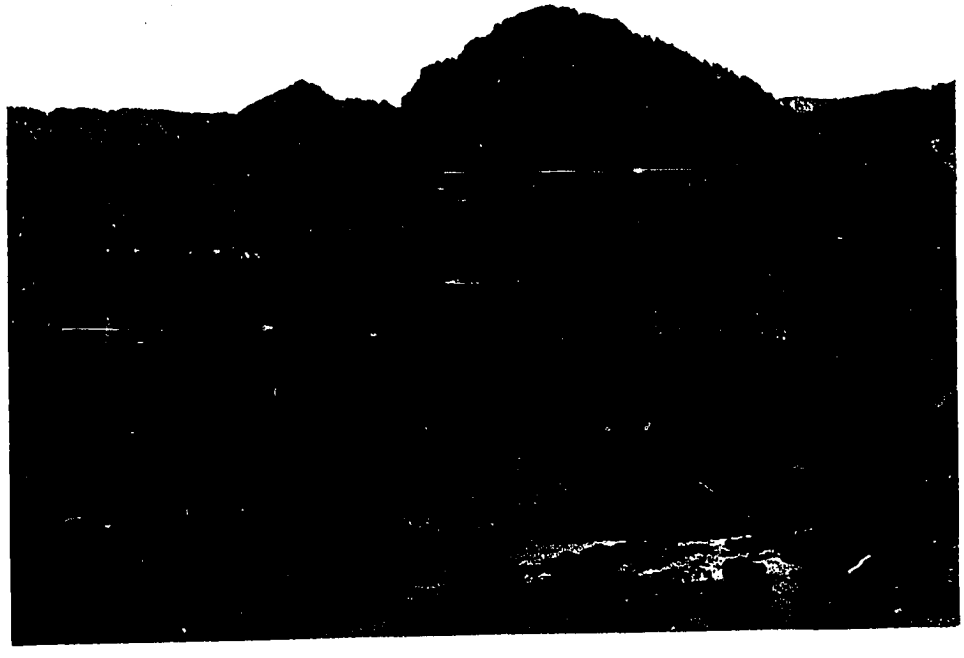

Top: Figure 11. "Step faults" at head of the North Fork, Big Timber Creek.

Bottom: Figure 12. "Step faults" at head of North Fork, Big Timber Creek. Photograph taken to the left of Figure 11.

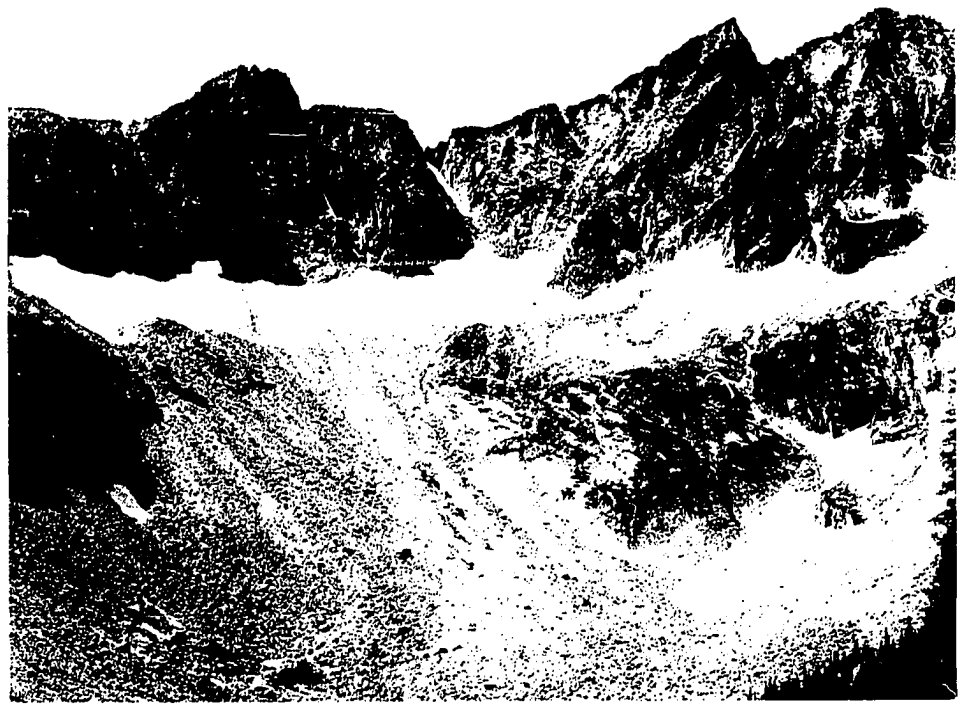

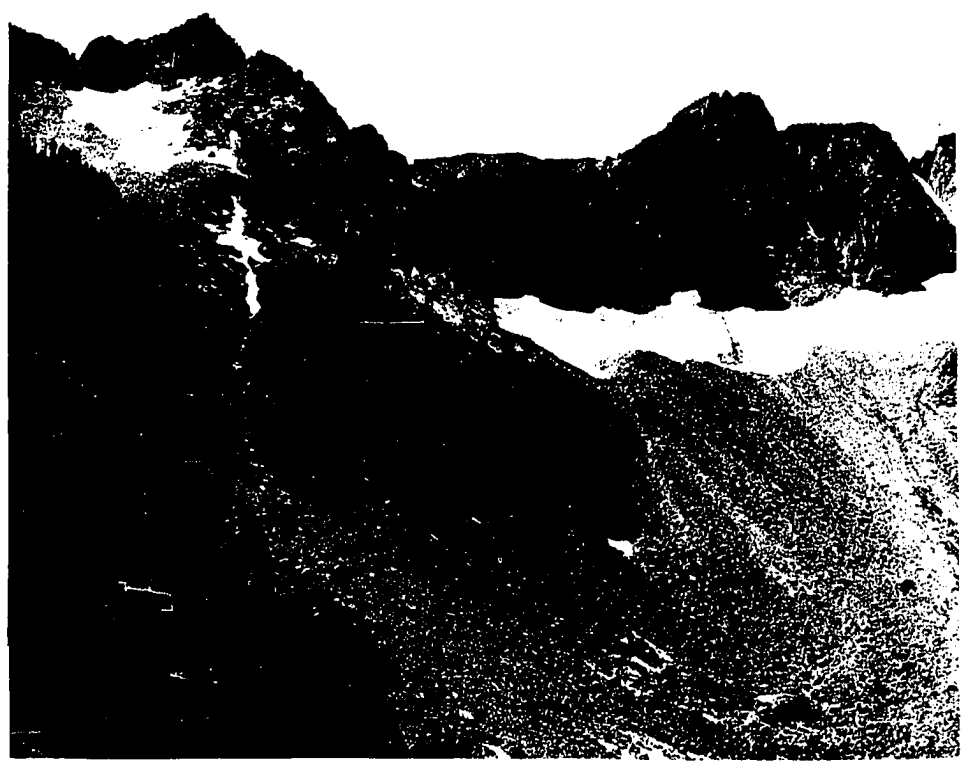

Top: Figure 13. Strike slip fault cutting through Blue Lake and "cutting off" the east end of Granite Peak.

Bottom: Figure 14. High angle fault on north face of Granite Peak. See also Figure 9.

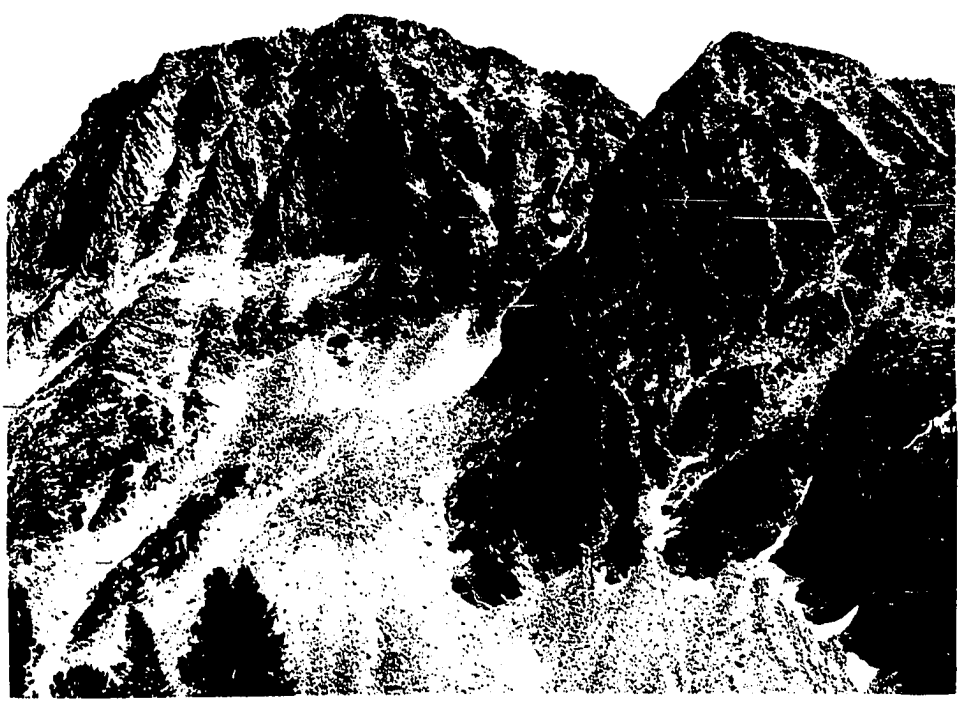

Figure 15. Faulting at head of middle fork, Sweetgrass Creek at Campfire Lake, cutting through metamorphic aureole.

Joints

Joint patterns within the pluton represent several generations. Although no quantitative evaluation of the joint data has been attempted, several directional trends present within the pluton are probably related to both the intrusion and the consolidation of the magma and to later faulting within the area. An initial set of joints, probably related to both the intrusion of the basaltic dike phase and to the final consolidation of the plutonic magma, can also generally be applied to the later intrusion of the aplitic dike phase. Whether these sets of joints are related to a cooling contraction of the magma or to a set of northeast to southwest trending faults has not been established.

Later joint sets, apparently genetically related to the strong north-south trending set of faults and andesitic dikes, are shown on Figure 6. This set of joints essentially parallels the faults and dikes, adding to the general north-south grain within the pluton.

Magma Tectonics

Due to the high degree of post-plutonic structural activity no attempt has been made by the writer to evaluate the primary structures present within the pluton. Flow-layering and banding is widespread throughout the inter-

mediate plutonic phase, and all directional measurements made on these features reveal an inward dip. However, post-plutonic faulting has been sufficiently severe to cause rotation of many primary structural elements.

Faulting associated with the forceful intrusion of the pluton has been only casually investigated. A thrust fault immediately outside the metamorphic aureole in Big Timber Canyon has a thrust plane dipping gently (5°) inward toward the pluton. Additional faulting (normal?) and fracturing has been observed in the valleys of Swamp Creek, Milly Creek, and the Middle Fork of Sweetgrass Creek, all indicating the forceful east-west nature of intrusion. The gentle dips of the metasediments and general lack of fracturing along the northern and southern limits of the pluton indicate that the stresses operative in these directions were less severe than in the east-west direction.

Analysis

Recently Chinnery (1966b) has re-evaluated the causes and results of secondary faulting associated with master faults (megashears of Smith, 1965). All previous investigations (Anderson, 1951; Moody and Hill, 1956; Lensen, 1960; and Crowell, 1962) of primary faults and associated secondary and tertiary faults have considered the stress to be a force vector (See Figure 5 of Moody and Hill, 1956,

p. 1213). By reanalyzing the stress field associated with master fault systems Chinnery (1966a) has been able to show that the stress within a system does not have vectorial properties but can be analyzed only in terms of tensors.[1]

From this analysis Chinnery (1966b) has proposed six different modes of secondary fault formation for both conditions of pure shear and conditions of uniaxial compression. These six fracture patterns are shown in Figure 16.

Using the aforementioned patterns of fracture development, Chinnery (1966b) has evaluated three areas in which strong secondary faulting is associated with a master fault (See pp. 183-189, op. cit.). Of these the Garlock fault, associated with the San Andreas fault, shows strong similarities to the Lewis and Clark megashears of the Montana Platform.

Applying the principles set forth by Chinnery (1966b) to the evaluation of the faulting associated with the Big Timber complex, a strong similarity can be drawn between Chinnery's "Type B" secondary faults, resulting from uniaxial compression, and those found within the complex. This similarity can be extended further to include

---

[1] The reader is referred to Chinnery, 1966a for a thorough mathematical treatment of the use of tensors in the interpretation of secondary faults.

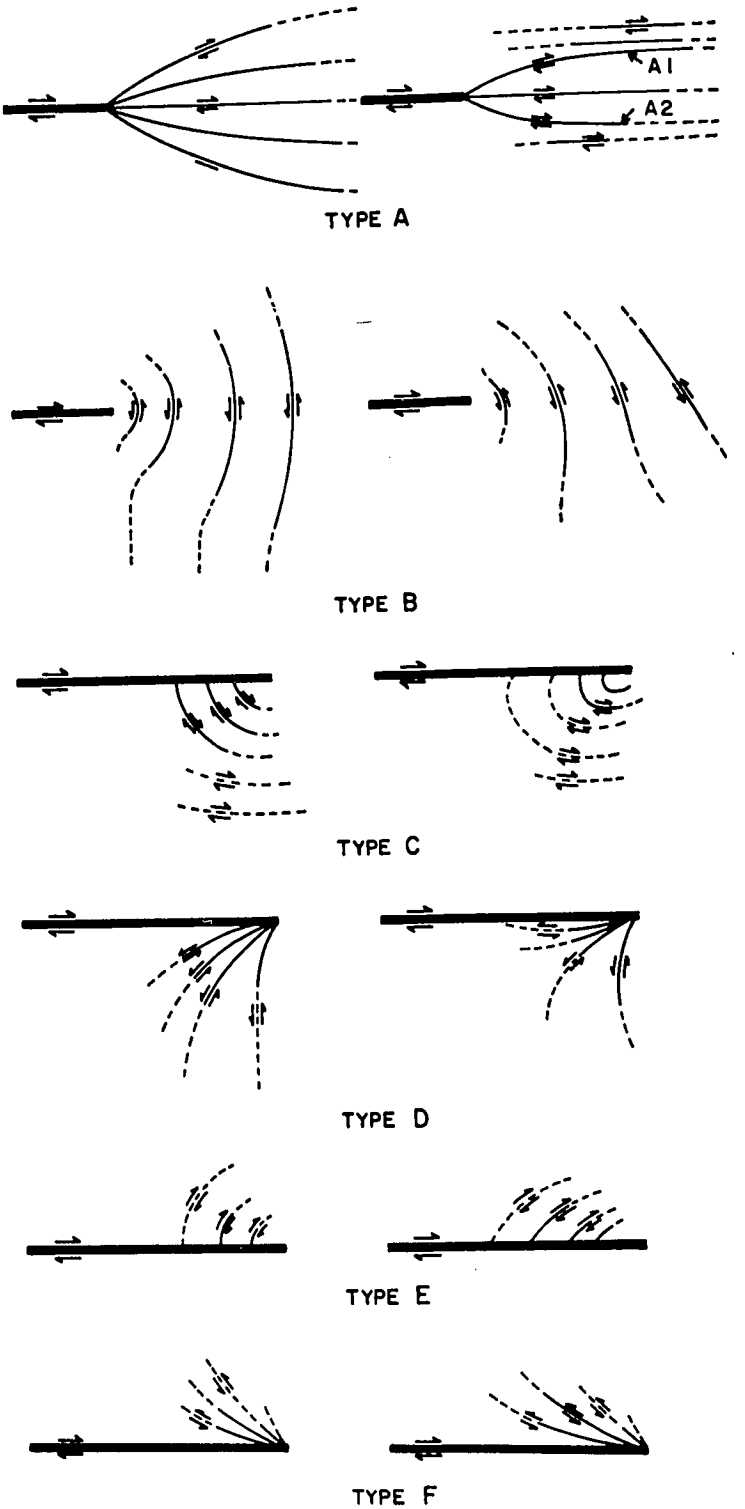

Figure 16. Modes of secondary faulting as deduced by Chinnery (1966b). Right hand patterns result from uniaxial compression, and left hand patterns result under conditions of pure shear.

the strong north-south dextral faults found in the Bridger Mountains to the west (McMannis, 1955). Whether the secondary faulting present within the area was generated as the result of movement along the Lake Basin lineament or the Nye-Bowler lineament or both cannot at this time be ascertained due principally to the lack of detailed structural data outside the Big Timber igneous complex. Although the writer has not attempted any mapping outside the areas shown in Plate I, in traverses through the bench lands many gentle folds were observed. In the area south and east of Plate I extensive faulting is present and is probably related to the faulting present within the area of Plate I.

If these secondary faults present within the area are the result of movement along one of the Lewis and Clark lineaments and if these megashears are surface manifestations of the basement complex, it is not difficult to visualize these secondary faults extending through the basement complex and tapping the mantle as the principal source for the magma. Therefore, it is the writer's opinion that all the igneous events occurred within the Big Timber igneous complex during north-south movements caused by lateral displacement along one of the Lewis and Clark megashears.

PETROGRAPHY

General

Due to the great variety of rocks present within the Big Timber igneous complex and the necessity of collecting large numbers of samples, the systematic collection of the complex has been only partially completed. Because of this incomplete collection and lack of time only a survey of the various rock groups has been made, and a detailed and quantitative petrography of the rocks thus far collected has not been attempted.

The nomenclature used in this paper for the various rock types has been taken from Hatch *et al*. (1961) and Johannsen (1939).

The intrusions comprising the Big Timber igneous complex can be divided into six principal classes: (1) the basic border plutonic phase, (2) the intermediate plutonic phase, (3) the terminal plutonic phase, (4) the basaltic dike phase, (5) the aplitic dike phase, and (6) the porphyritic andesite dike phase.

Contact Relationships

Contact relationships among the plutonic phases within the Big Timber complex are quite varied. The contact of the outer basic phase with the country rocks is well-exposed in

the canyons of Big Timber and Sweetgrass Creeks, but strong shearing, caused by forceful intrusion, has made this contact rather obscure and gradational. Figure 17 excellently shows the contact of the pluton with the metamorphic aureole in the south wall of Big Timber Canyon; Figure 18 shows the contact in a cirque above Pear Lake. These contacts are subvertical, discordant, and usually very ragged along the eastern and western perimeters but flatten to gentle outward dips along the northern and southern borders. The northern and southern contacts, though less steep than those in the east and west, nevertheless show discordant cross-cutting relationships.

The forceful lateral intrusive nature of the intermediate phase of the pluton is shown by the apophyses of dioritic material extending into the metamorphic aureole. These apophyses, frequently extending 0.5 miles outward from the contact, do not cut across relict bedding planes but interlaminate with them, giving the pluton a "cedar tree" appearance similar to that described by Gilbert (1877). A schematic east-west and north-south cross-section through the pluton and its metamorphic aureole is shown in Figure 19.

Hydrous mineral assemblages in the pelitic and quartzofeldspathic country rocks, as described by Weed (1899) and Wolff (1938), indicate that the contact metamorphism occurred at relatively high water pressures. The lenticular and

Top: Figure 17. Contact of pluton with metamorphic aureole, south wall of Big Timber canyon.

Bottom: Figure 18. Contact in cirque headwall above Pear Lake. Note large mass of pyroxenite (A) close to contact (agmatite).

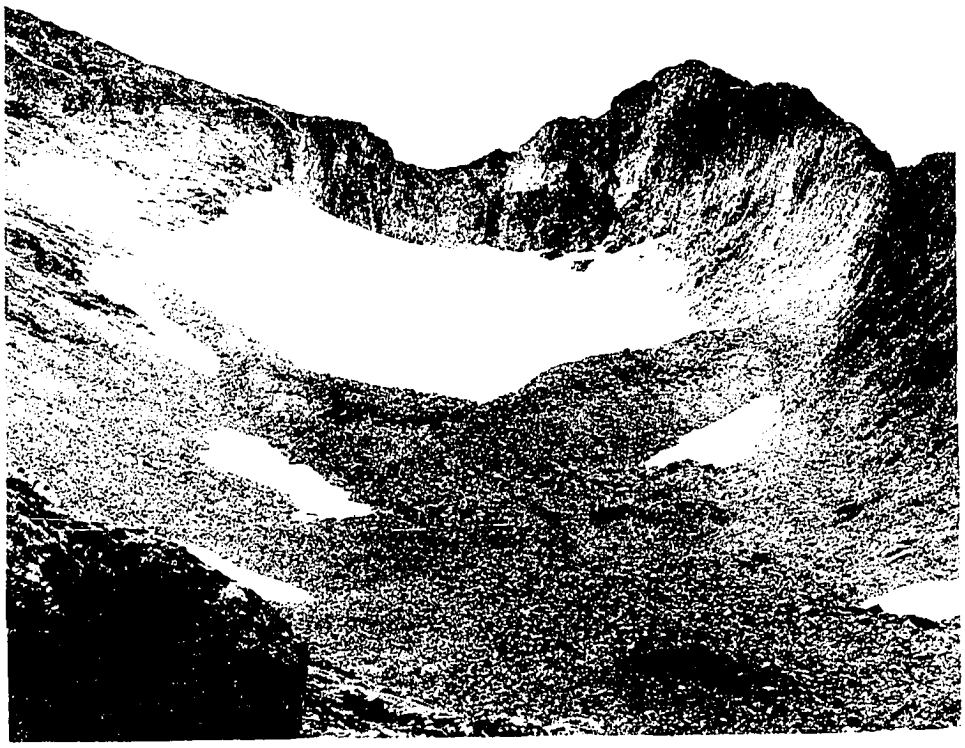

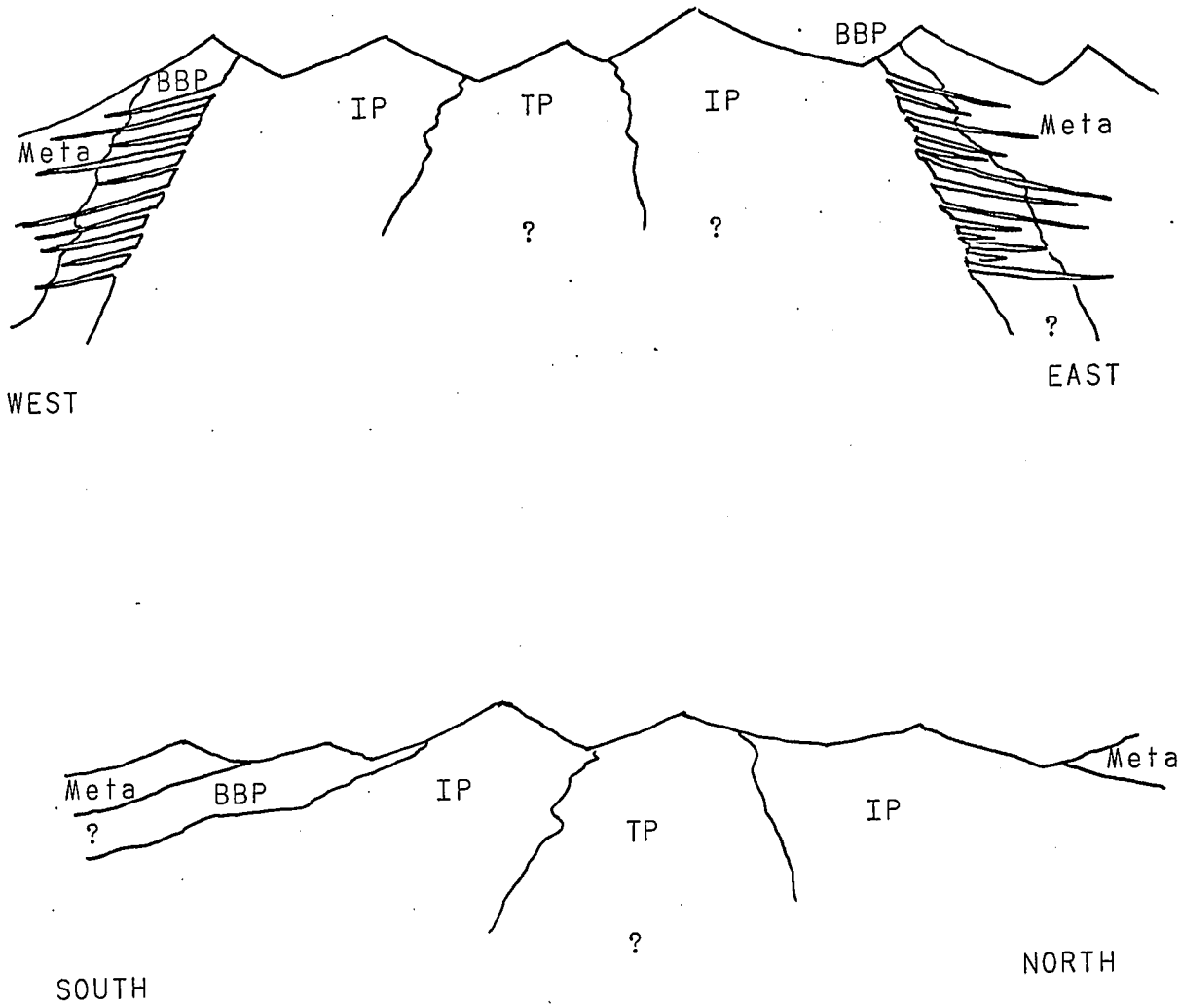

Figure 19. Schematic west-east and south-north cross-section through Big Timber pluton showing relationship among plutonic phases. Dikes not shown.

permeable nature of these country rocks allowed for both the influx of connate water from the sediments into the basic border phase, which shows only slight metasomatism, and also for the escape of magmatic fluids from the intermediate phase. This strong induration of the sediments rendered them very resistant to erosion, resulting in the metamorphic aureole forming the higher peaks within the area.

No evidence has been found of a floor in the deep canyons within the pluton. Therefore, on the basis of the gravity data presented by Kelley (1966) and the discordant field relationships of the pluton with the country rock, this pluton is considered to be a stock rather than a laccolith.

The contact between the outer basic phase and the intermediate plutonic phase shows effects of assimilation by the intermediate phase. Agmatite is present along this contact and varies in size from small fragments as shown in Figures 59 and 60 to extremely large blocks as seen in Figure 18. Well-rounded and "ghost" xenoliths of the early basic phase are well-distributed throughout the outer margins of the intermediate phase.

The contact between the intermediate and the terminal plutonic phases has not been sufficiently investigated to enable one to draw definite conclusions as to its character,

since valley train and colluvial material hide the contact from view. The great difference in grain size, from very coarse in the intermediate phase to fine in the terminal phase, suggests that the contact is very abrupt.

The basaltic dikes, whose trend is schematically shown in Figure 20, transect all the plutonic igneous phases. The contacts of the basaltic dikes show only slightly chilled margins even in the more coarse-grained varieties. Contact between the basalt and the igneous phases is usually very straight, indicating that the basalt has filled tension fractures and that syntectonism was probably proceeding at the time of intrusion.

The aplitic dike phase transects both the earlier plutonic phases and the basaltic phase as shown in Figure 21 and thoroughly net-veins the plutonic phases and the metamorphic aureole as shown in Figures 22 and 23. Although the geometric relations among the various net-veins and sheets as shown in Figure 24 have not been quantitatively studied, net-veining, sensu lato, of the plutonic phases and metamorphic aureole is quite extensive. The type of net-veining described by Windley (1965) has not been found within the Big Timber igneous complex. The determination of whether or not these veins and sheets have been intruded dilatantly as the result of cooling contraction will require much additional study. Several features found in other net-

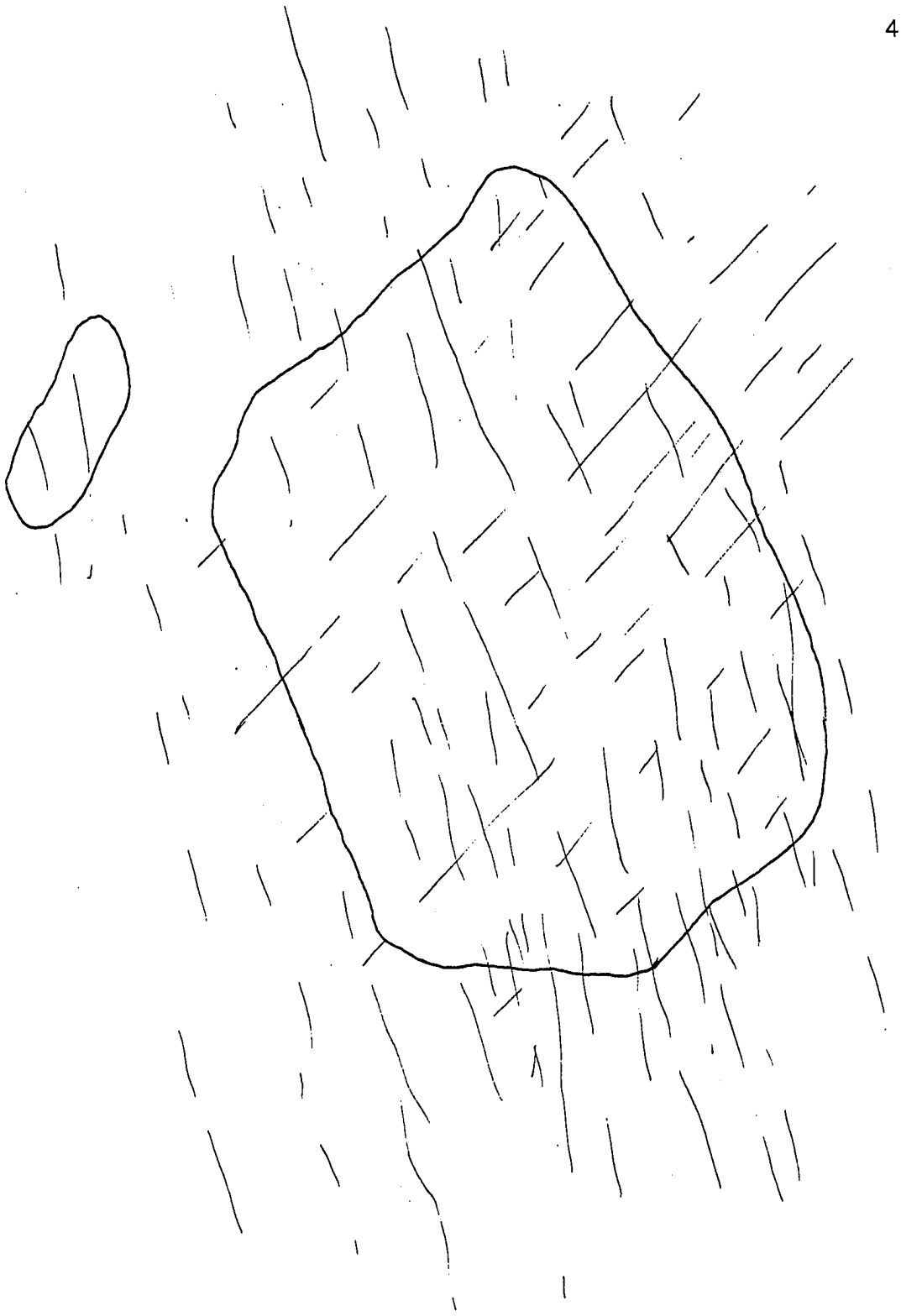

Figure 20. Schematic Map Showing Predominant Dike Trends. Basaltic dikes have a northeast to southwest trend while the andesitic dikes have a north-south trend.

Top: Figure 21. Aplitic dike cutting basaltic dike.

Bottom: Figure 22. Aplitic dike net-veining metamorphic aureole above Pear Lake.

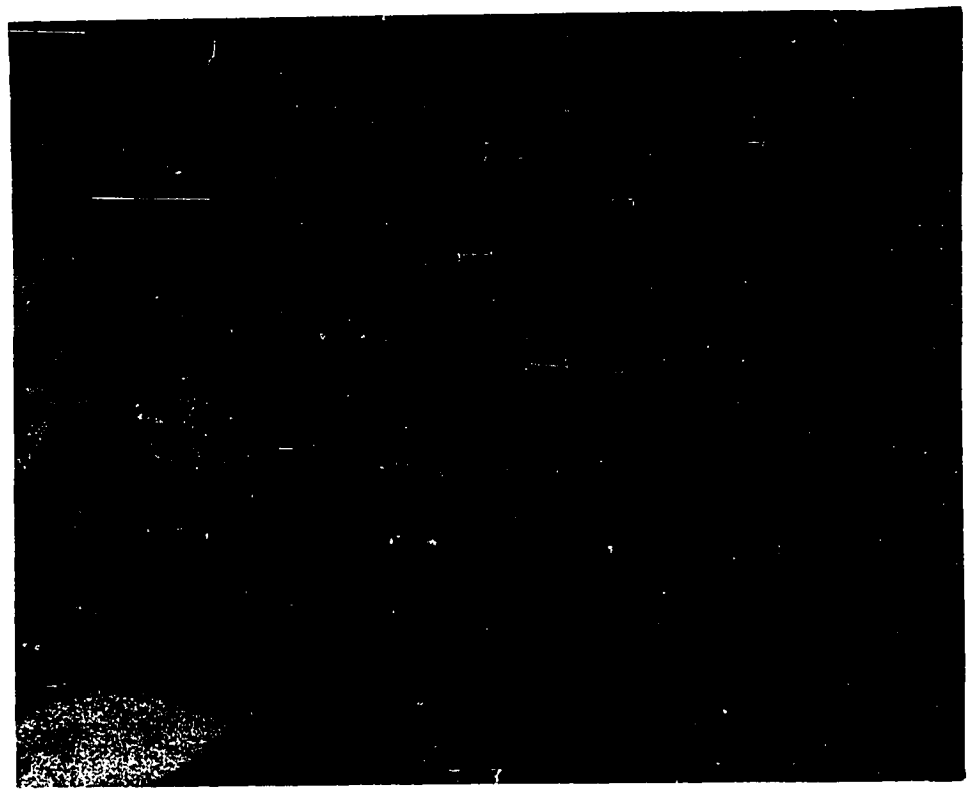

Top: Figure 23. Sheet and net-veining of plutonic rocks by aplite. Photograph taken on the south face of Granite Peak.

Bottom: Figure 24. View of Crazy Peak with fault cutting through Peak at A, showing net-veining by aplite within metamorphic aureole at B.

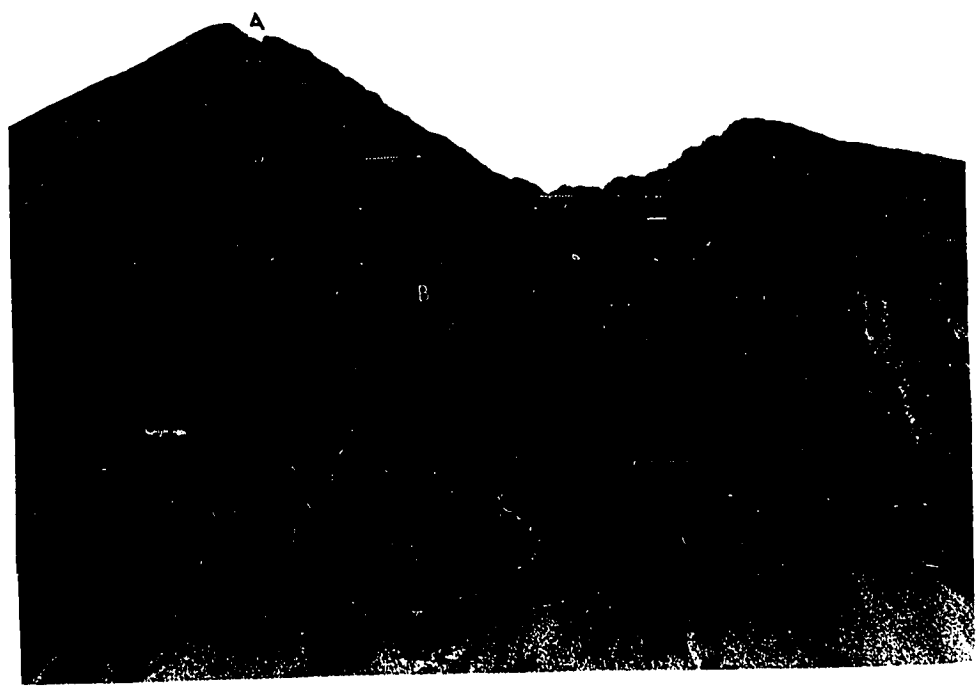

veined dioritic bodies appear to be lacking within the Big Timber pluton; in particular to be noted is a general absence of pillowing of earlier basic material as described by Chapman (1962), Elwell et al. (1962), Reynolds (1954), Wells (1954), and Windley (1965). Although all other net-veined complexes appear to show strong geometric relationships that can be attributed to cooling contraction, within the Big Timber complex no such apparent geometric relationship has been found.

Porphyritic andesite dikes terminated the igneous phases of the Big Timber complex. These were intruded syntectonically with a series of high-angle normal and strike slip faults to which the dikes are parallel and are shown in Figures 25 and 26. These dikes, which cross-cut all previous igneous intrusions within the area, including the metamorphic aureole, end north and south of the area in unmetamorphosed sediments (Davis, 1965 and Simms, 1966). No detailed study has been made of the behavior of these dikes as they cut the metamorphic aureole. All the dikes show very narrow chilled margins, and the faulting associated with them accounts for their linearity and allows them to be seen for long distances.

Top: Figure 25. Vertical andesitic dike cutting both plutonic rocks (foreground) and metamorphic aureole (distant peak).

Bottom: Figure 26. Andesitic dikes following the north-south grain within the pluton.

Basic Border Phase

The early basic plutonic phase, located contiguous to the contact zone around the southern end of the pluton, has rock types varying from pyroxenites to meladiorites with local occurrences of augitites and hornblendites. Grain size is large (5-8 mm.) with phenocrysts of hornblende occasionally exceeding 20 mm. in diameter. Reconnaissance and systematic collecting in the northern half of the pluton have revealed no rocks having similar basic affinities.

The textures of the rocks of this phase of igneous intrusion are shown in Figures 27 through 34; they vary from hypautomorphic- to xenomorphic-granular. All the rocks within this phase show a lack of layering and in many instances show stringers of later or residual magmatic fluids, crystallizing quartz, potassic and sodic feldspars as seen in Figure 29. The pyroxenes and early plagioclases are of about equal size and show no preferred orientation.

The most important textural relations are those which indicate that some of the more pyroxenitic rocks of this phase are aggregates of cumulus crystals. These aggregates were formed by the accumulation of discrete crystals either from sinking through a less dense contemporary melt, in situ or at depth, or from a plastering of the early-formed crystals against the walls of the magma chamber by magmatic currents. In view of the fact that layering has not been

Top: Figure 27. Photomacrograph of sample AX13. Porphyritic hornblende gabbro. 3X)

Bottom: Figure 28. Photomacrograph of sample A273. Hypersthene, augite-hornblende-pyroxenite. (3X)

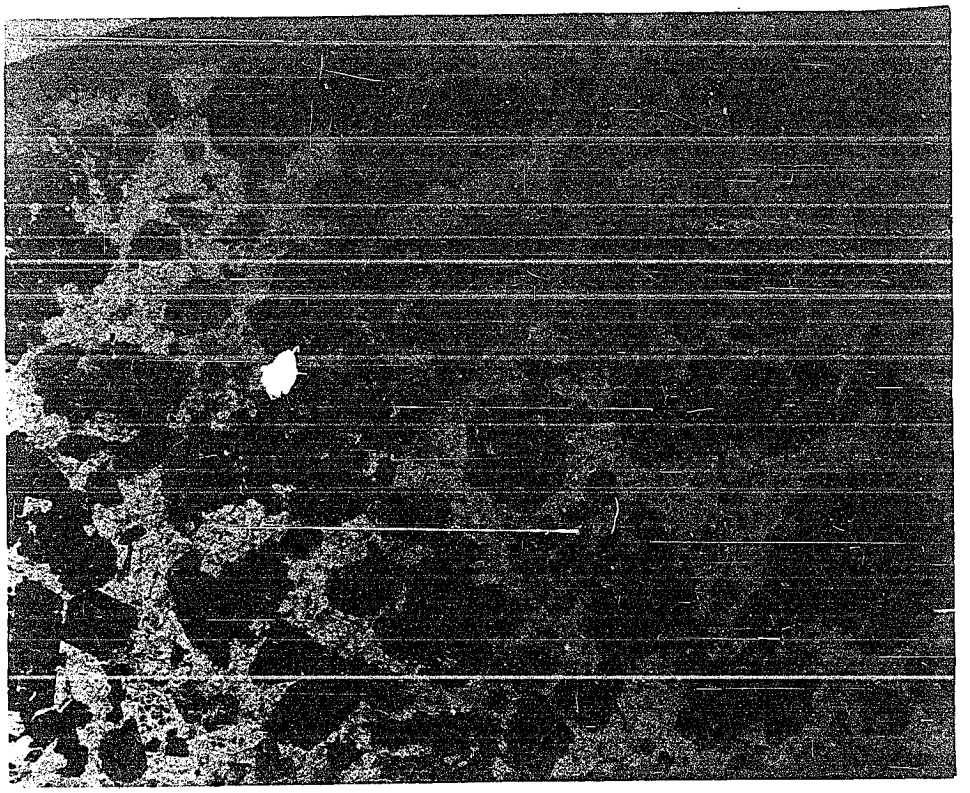

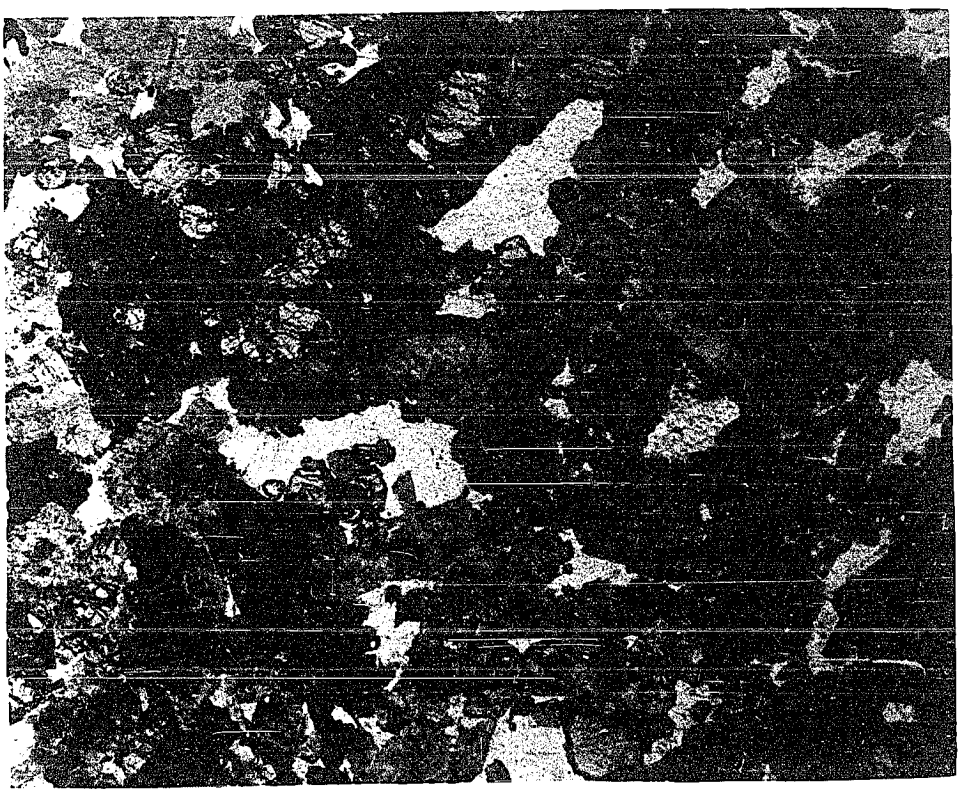

Top: Figure 29. Photomacrograph of sample A563. Hypersthene-bearing, augite-hornblende-gabbro. Note fine grained interstitial sodic plagioclase and small blebs of quartz. (3X)

Bottom: Figure 30. Photomacrograph of sample A573. Porphyritic hornblende-meladiorite. (3X)

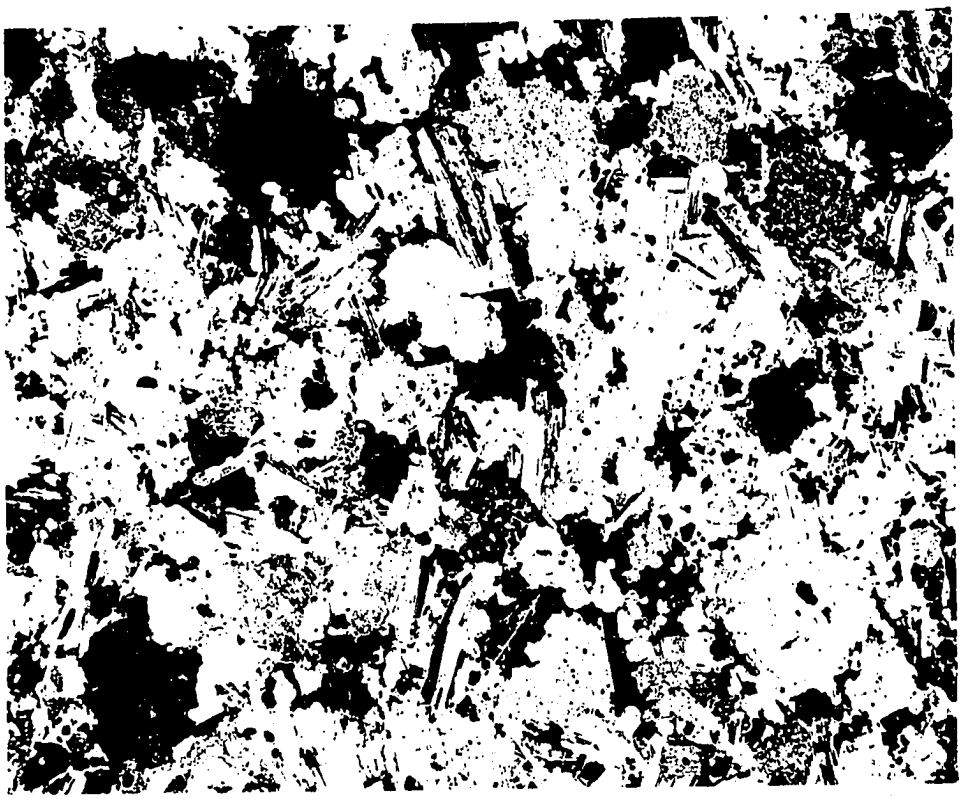

Top: Figure 32. Photomacrograph of sample A253. Porphyritic hornblende-meladiorite. (3X)

Bottom: Figure 31. Photomacrograph of sample A453. Biotite-augite-hornblende gabbro. (3X)

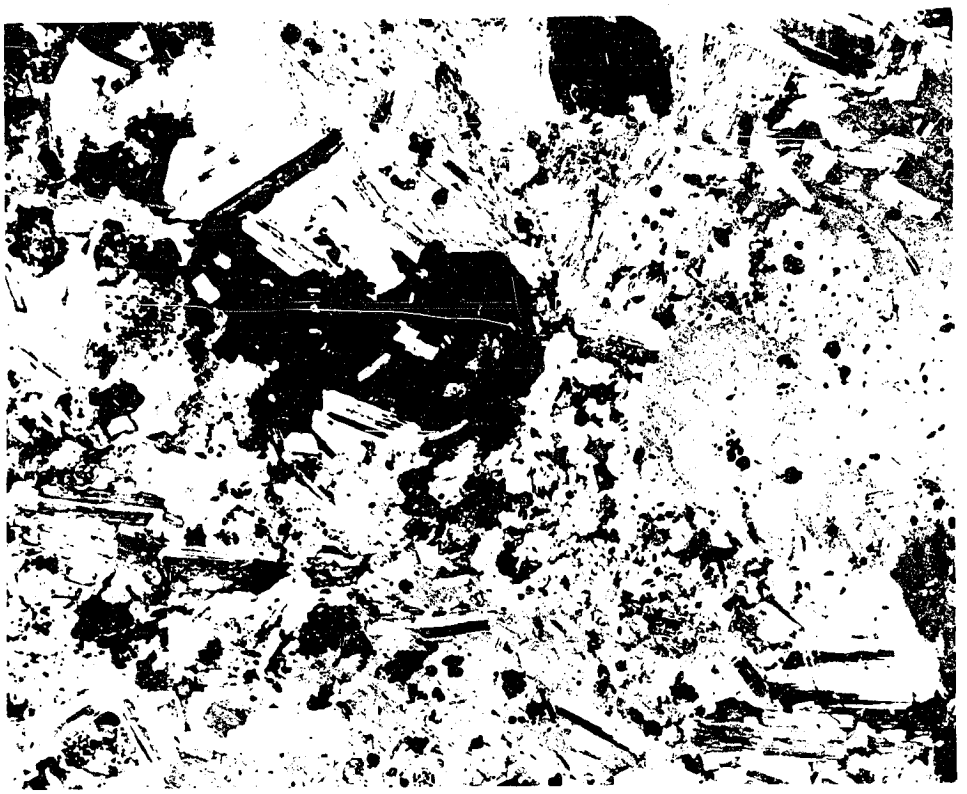

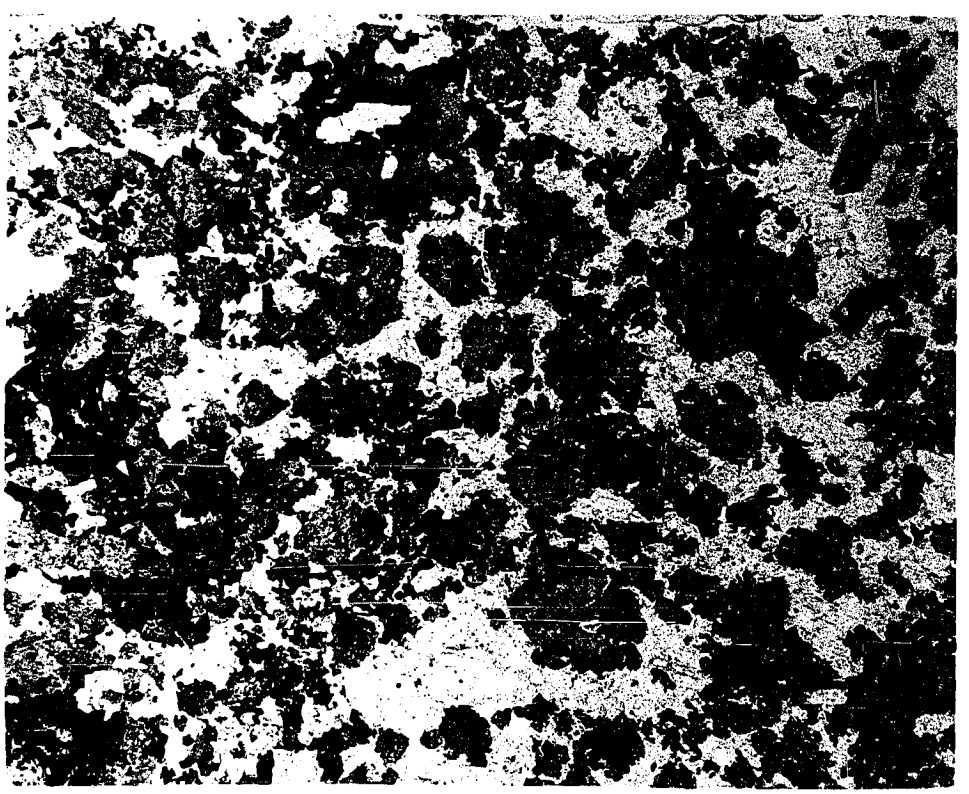

Top: Figure 33. Photomacrograph of sample A483. Porphyritic augite gabbro showing euhedral augite in varying degrees of alteration.

Bottom: Figure 34. Photomacrograph of sample A253. Porphyritic hornblende meladiorite.

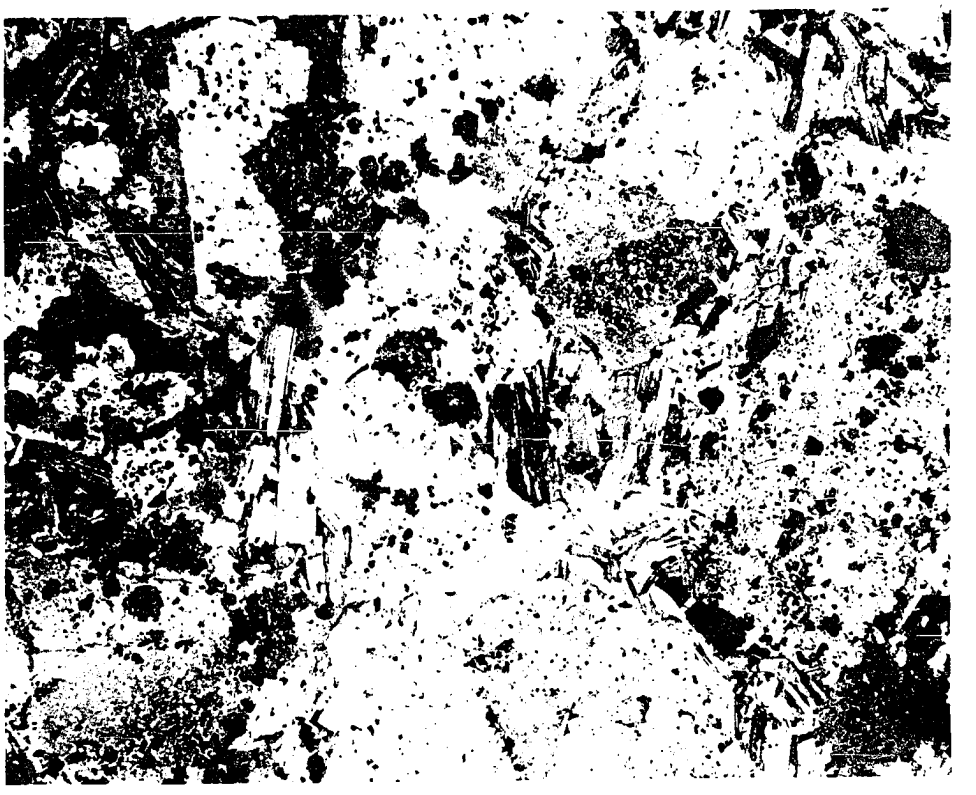

observed in these basic rocks and that the plagioclases show protoclasis, it is this writer's opinion that this phase initially crystallized at depth and was intruded as a crystal mush.

Protoclasis or cataclasis is present in most of the rocks. Many of the plagioclases show lenticular, bent and/or crushed lamellae, suggesting significant post- or syncrystallization strain. Granulation of the mineral phases in distinct shear planes is not uncommon. Whether this protoclasis or cataclasis is directly related to the crystallization of the basic border phase or is associated with later magmatic injection has not been determined.

The mineralogy of this phase has not been complicated to any great extent by secondary metasomatism. Microscopic examination generally reveals an ortho- and clinopyroxene and plagioclase with subordinate amounts of olivine, magnetite, hornblende, biotite, and apatite. The plagioclase, usually subhedral, shows good twinning, usually of the albite law with occasional carlsbad twins. All calcic plagioclases show strong oscillatory zoning, probably reflecting strong magmatic currents operative during the time of crystallization. The orthopyroxenes vary from bronzites to hypersthene, and all are feebly pleochroic from pale green to pale pink. The clinopyroxenes are principally diallagite, ferro- and titanaugite. Birefringence is very strong in the titanaugites.

Hornblende occurs both as primary poikilitic phenocrysts, with inclusions of magnetite and plagioclase and also as an alteration product of the pyroxenes; it shows varying shades of pleochroism from pale green to deep brown and in many instances is pseudomorphous after pyroxene.

Olivine has not been found in essential quantities and usually occurs as well-rounded inclusions in the orthopyroxene. Magnetite is ubiquitous, occurring principally as reaction products of later magmatic fluids with the early-formed olivine and augite. Accessories of apatite, secondary chlorite and a minor amount of sericite are present. Leucoxene occurs as small scattered blebs in many of the samples.

Uralitization (typical tremolite-actinolite feathery intergrowths) of the pyroxenes is common in the later meladioritic rocks. The alteration of olivine to iddingsite, magnetite, and a small amount of hematite has also been noted in the gabbroic rocks.

Normal gabbroic textures are more typical in the later stages of the early basic phase. This contrast in texture may indicate a cessation of the accumulative mechanism which was operative in the formation of the earlier xenomorphic pyroxenitic rocks of this phase.

Intermediate Plutonic Phase

The intermediate plutonic igneous phase consists of rocks varying from mela- to leucodioritic with local developments of quartz diorite. Grain size varies from medium to very coarse (in excess of 10 mm.). These rocks constitute the most extensive igneous event within the Big Timber igneous complex.

Textures throughout this phase show great variety, from hypautomorphic-granular to a minor amount of xenomorphic-granular rocks. Sporadic instances of granulation, as shown in Figure 32, have been found and are generally associated with post-igneous faulting. Parallel to subparallel textures, although present, are not in great abundance. Layering is the most conspicuous textural variant present, and although it is not always present, it is not uncommon. Figures 35 and 36 show the two most prominent types of layering present. Figure 36 shows current layering by magmatic fluids of the "cut-and-fill" type. These layers are generally alternations of hornblende and/or biotite crystals and layers composed almost wholly of plagioclase laths.

Synneusis, senso stricto, (Vogt, 1921) is present in many of the rocks as is shown in Figure 36. Although the cause for synneusis is not clear, this "swimming together" of mafic crystals of hornblende and/or biotite is considered by Vogt to have occurred very rapidly. In other plutons

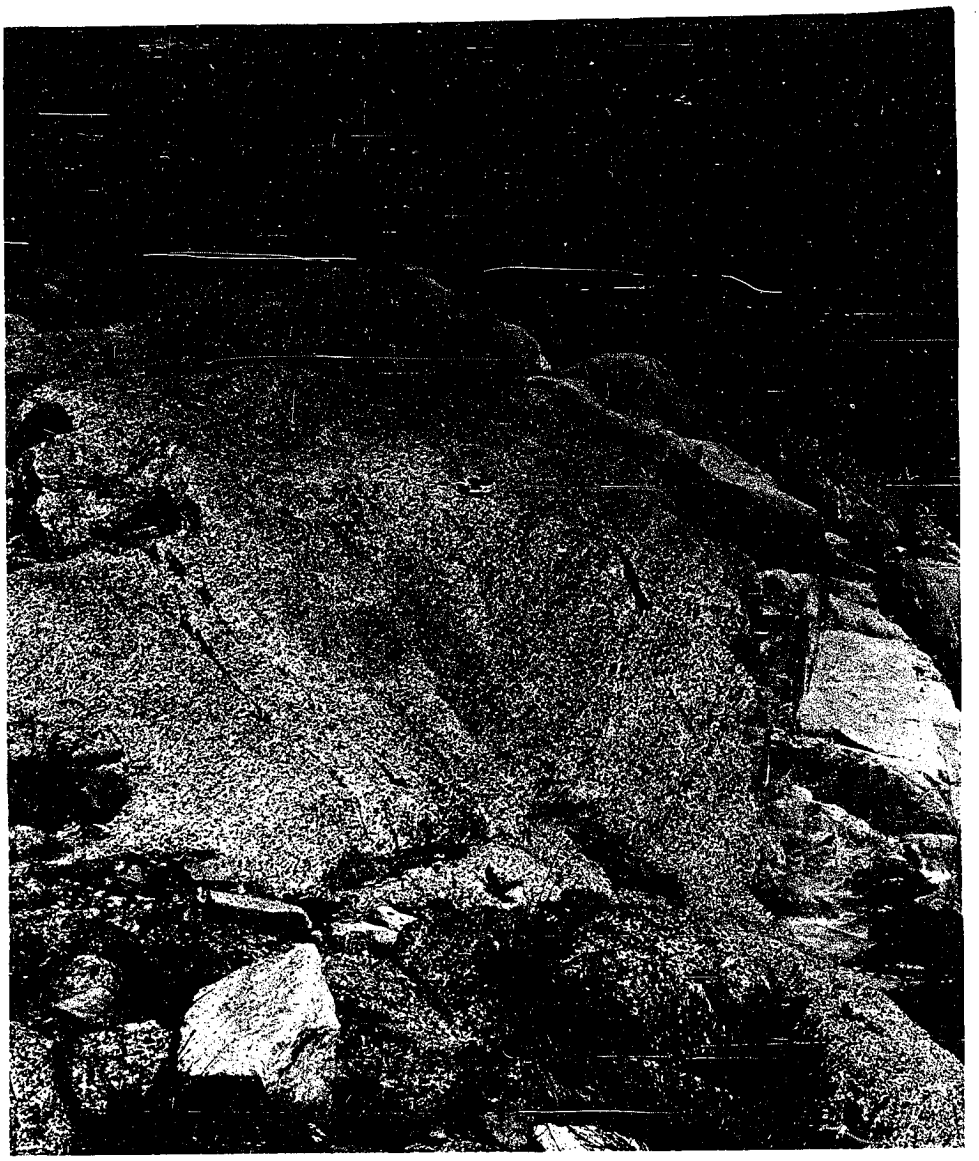

Figure 35. Flow lamination in intermediate phase, paralleling Brunton. Note basaltic dike.

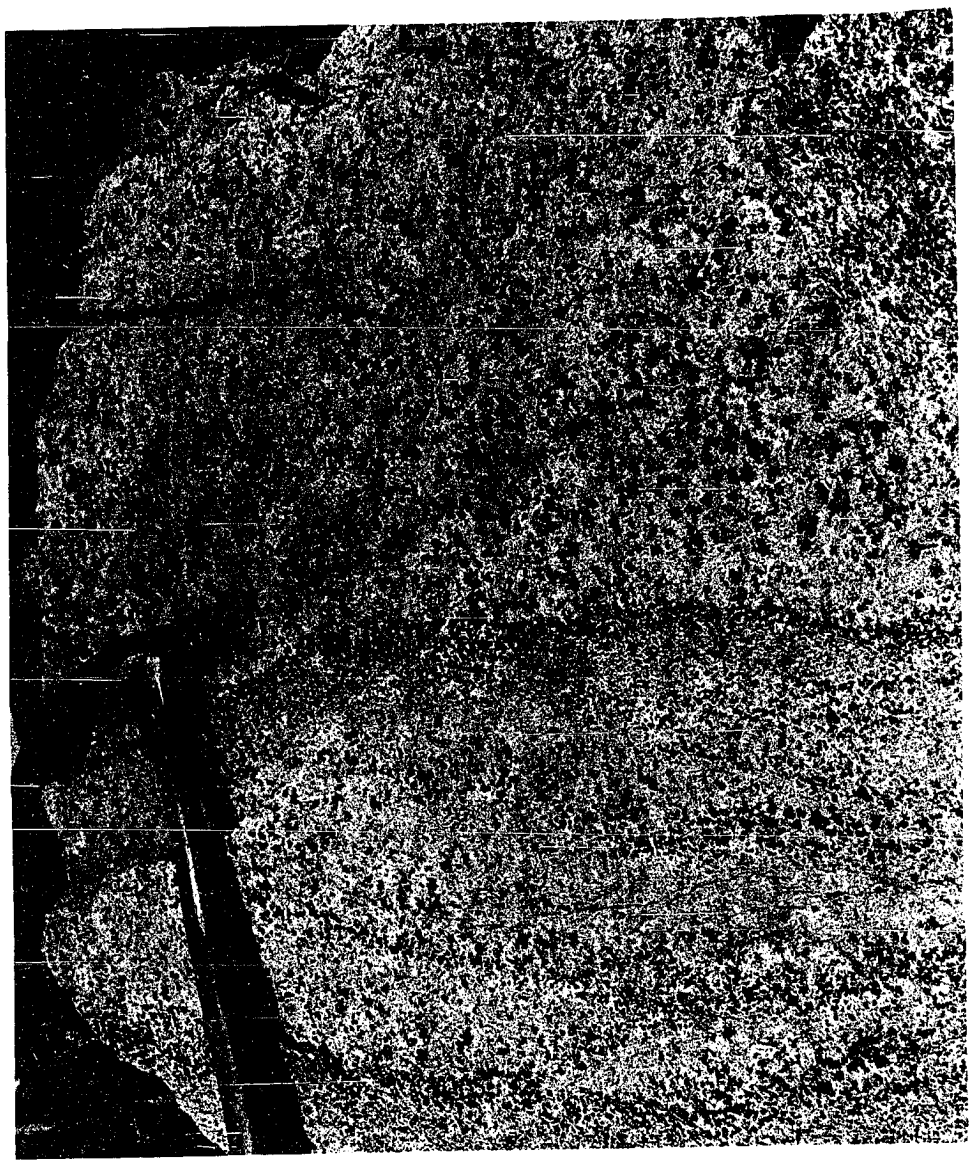

Figure 36. Outcrop of intermediate phase, showing flow layering (bottom) of "cut-and-fill" type and syneusis (top).

Windley (1965) considers the synneusis present in the diorite to be of a secondary nature, since the crystals of hornblende contain inclusions of plagioclase. Although most of the hornblendes present within this intermediate phase of the Big Timber complex show good euhedral outlines and are commonly poikilitic, this does not preclude the secondary nature of the amphibole. All the plagioclase present in association with the synneusis textures are generally subhedral.

Microscopic examination of these rocks (See Figures 37 through 48) show them to contain essential plagioclase, hornblende, clinopyroxene, and biotite with accessory quartz, potassium feldspar, orthopyroxene, magnetite, apatite and uralite. No olivine has been found.

The plagioclases show strong albite twinning and occasional oscillatory zoning (xenocrysts?). Plagioclase laths frequently show parallel textures as seen in Figures 40, 45, and 48. After prolonged etching with hydrofluoric acid and staining with sodium cobaltinitrite, it can readily be observed that cloudy plagioclases are heavily sericitized (See Figure 38).

Euhedral and subhedral hornblende show weak pale green to deep brownish-red pleochroism and are the most common mafic constituent of the intermediate phase. Wolff (1938) optically determined the brown variety to be basaltic hornblende. However, in many instances hornblendes show a dark

Top: Figure 37. Photomacrograph of sample A033. Hornblende-diorite showing granulation and slight metasomatism. (3X)

Bottom: Figure 38. Photomacrograph of sample A533. Hornblende-biotite-diorite showing fault. (3X)

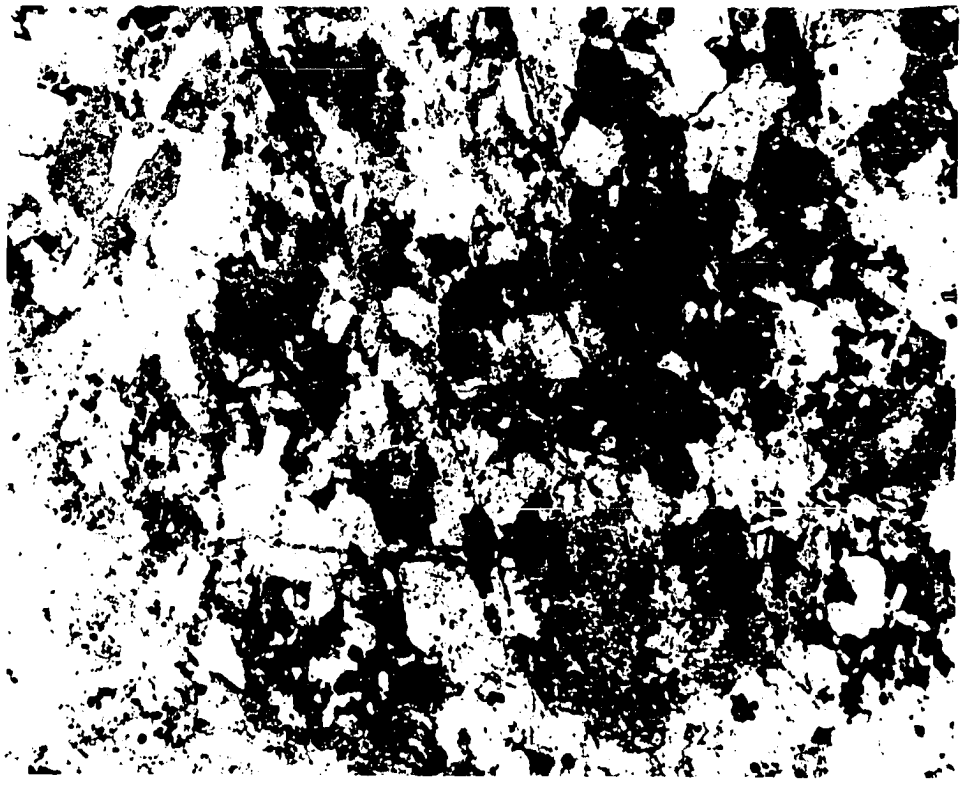

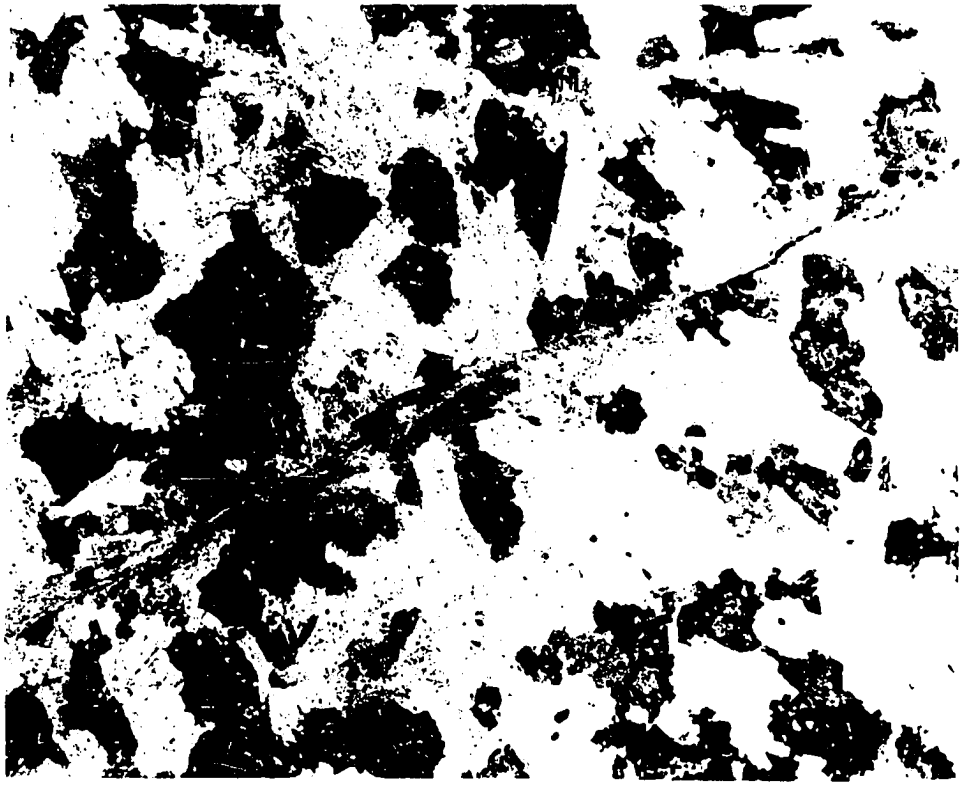

Top: Figure 39. Photomacrograph of sample A353. Biotite-diorite showing subparallel structure.

Bottom: Figure 40. Photomacrograph of sample A333. Augite-bearing hornblende-diorite showing parallel structure.

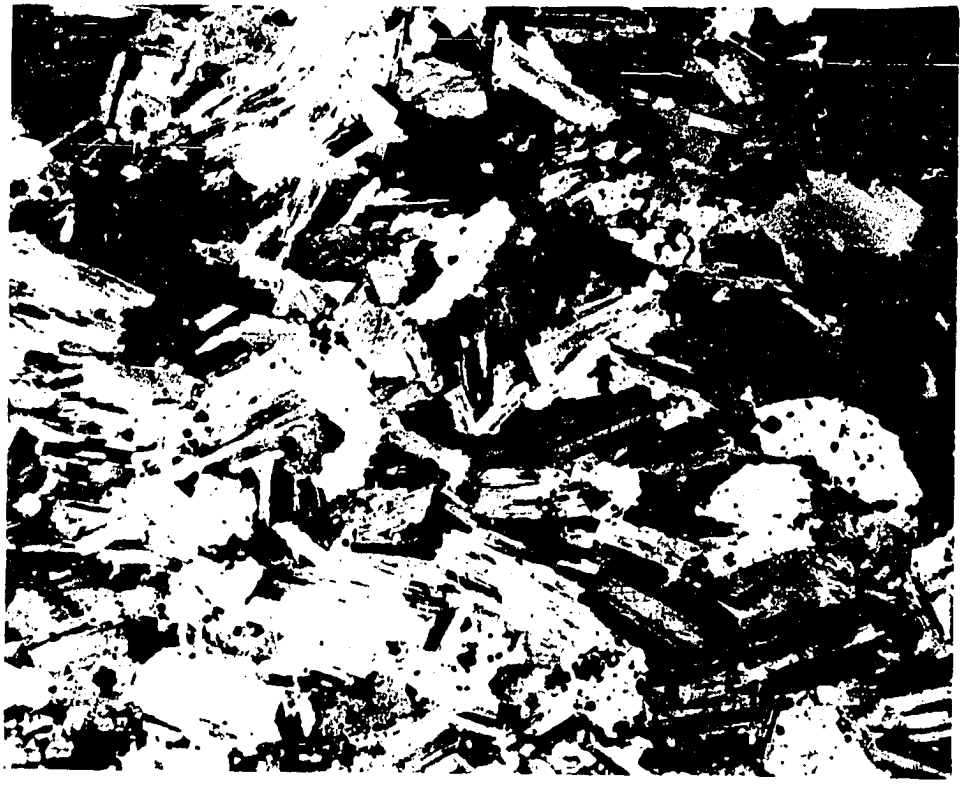

Top: Figure 41. Photomacrograph of sample A563. Porphyritic hornblende-diorite showing extremely poikilitic hornblende.

Bottom: Figure 42. Photomacrograph of sample A353. Biotite-hornblende diorite.

Top: Figure 43. Photomacrograph of sample A393. Augite-diorite showing scattering of magnetite crystals and reaction rims around augites. (3X)

Bottom: Figure 44. Photomacrograph of sample A473. Biotite-diorite showing finer grained intermediate phase. (3X)

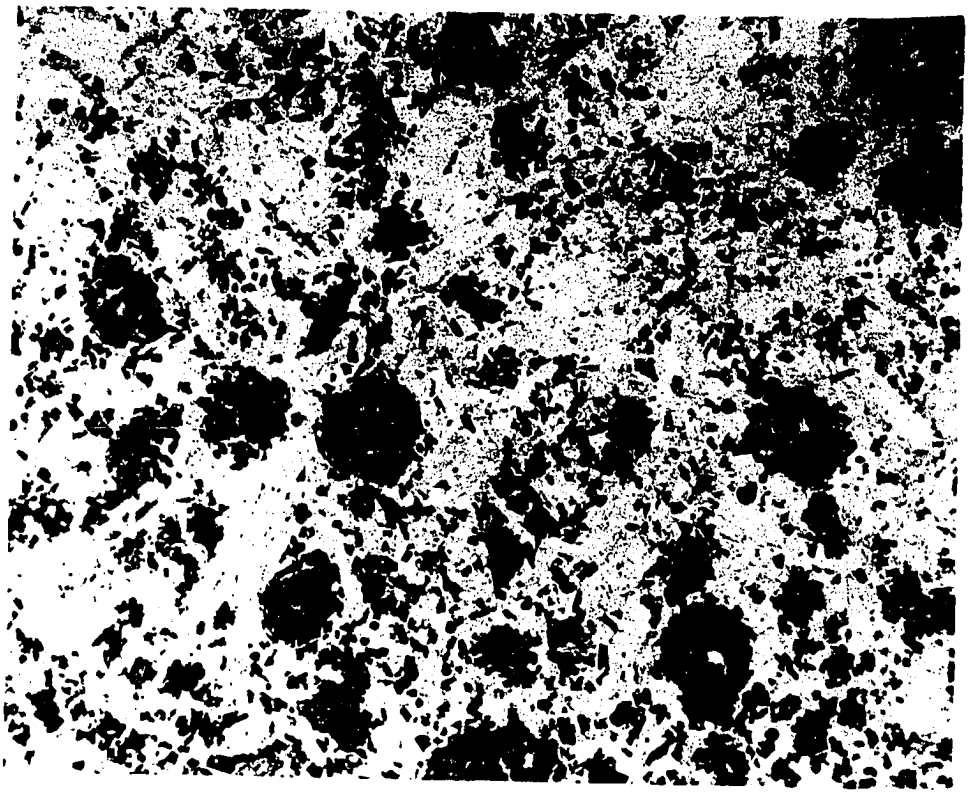

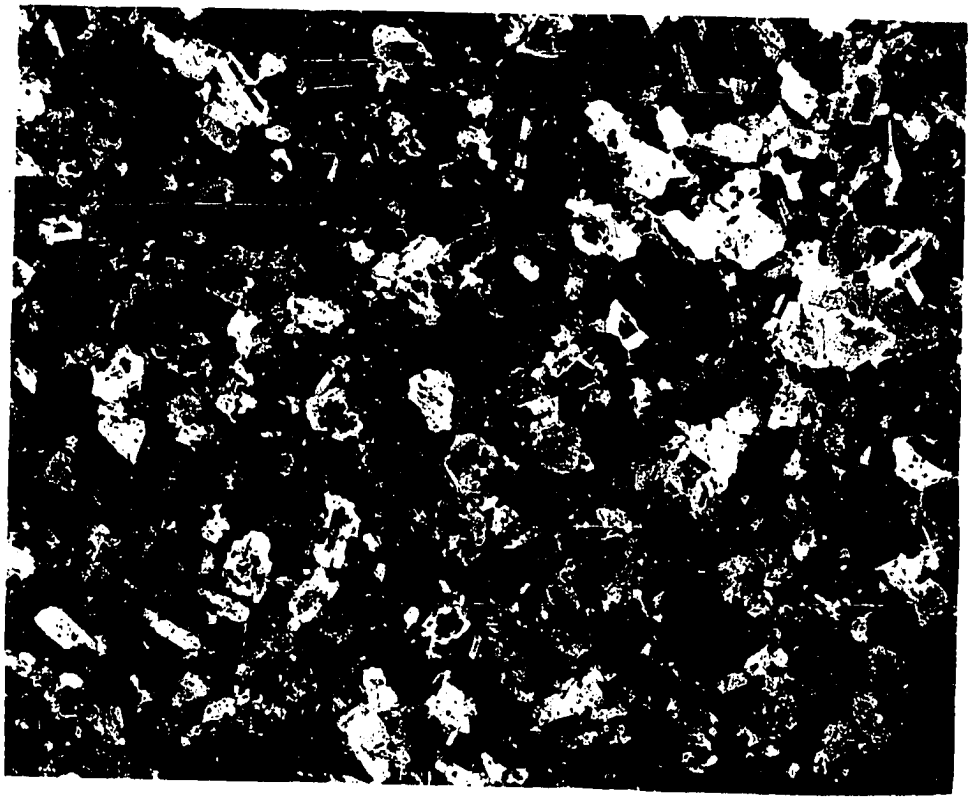

Top: Figure 46. Photomacrograph of sample A523. Biotite-hornblende diorite showing subparallel structure and a concentration of magnetite crystals resulting from replacement of augite. (3X)

Bottom: Figure 45. Photomacrograph of sample A463. Hornblende-diorite showing subparallel structure. Note slight clouding of plagioclases. (3X)

Top: Figure 47. Photomacrograph of sample A413. Biotite-diorite showing replacement of earlier pyroxene by magnetite.

Bottom: Figure 48. Photomacrograph of sample A463. Hornblende-biotite-diorite showing subparallel structures.

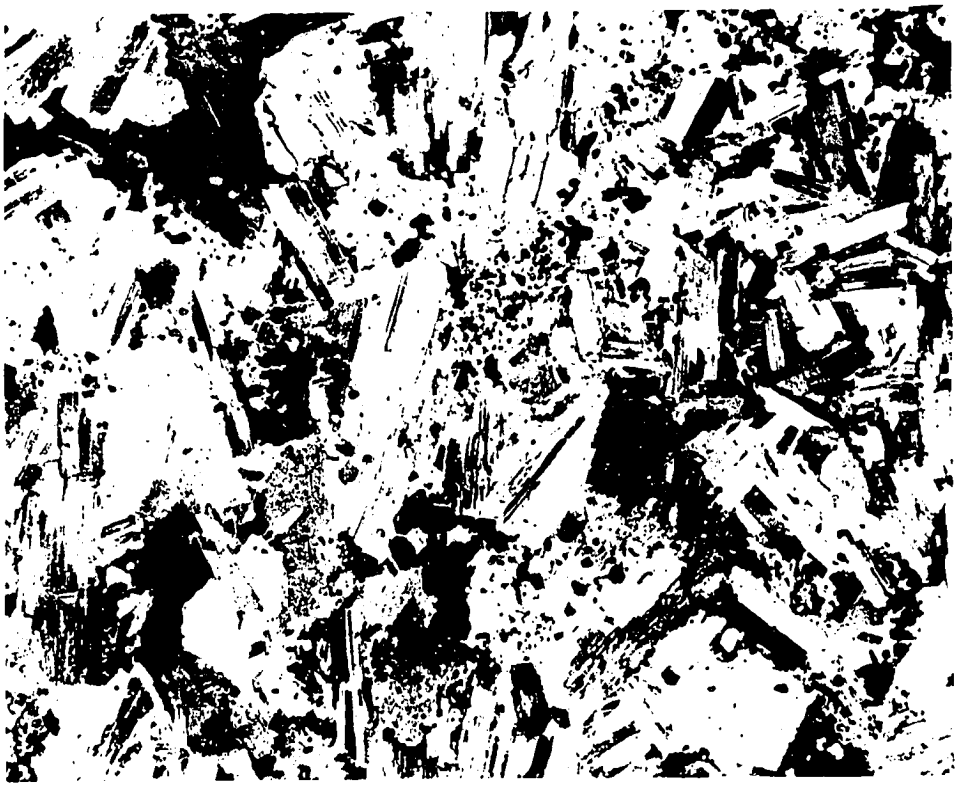

brown core mantled with progressively more green hornblende and on the periphery become very pale green and show weak pleochroism. Similar hornblendes have been found by Deer (1935) in the Carsphairn igneous complex of Scotland. Since there are no reported instances of common hornblende and basaltic hornblende occurring within the same rock, the writer believes the brown variety to be an iron-rich species of the common hornblende group. Chemical analysis and quantitative optical data will be required to determine the variety or varieties of hornblende present.

Biotite occurs as randomly scattered flakes throughout this phase. Both primary, showing occasional strain, and secondary biotite, replacing hornblende and pyroxene, are present.

The clinopyroxene, when found, as in Figures 41, 42, and 44, shows alteration to biotite, magnetite, and hornblende, indicating high iron (and titanium?) content. Some of the clinopyroxene shows good diallage exsolution. Fresh orthopyroxene has not been found. Uralitization of enclosed grains of hypersthene are often completely uralitized. Magnetite occurs both as a primary euhedral phase and as a secondary replacement of clinopyroxene, as shown in Figures 40 and 43. It is usually scattered throughout the rocks as tiny crystals.

Quartz and potassium feldspar are present in minor amounts as interstitial blebs. In local occurrences quartz exceeds 10% of the modal constituents, and the rocks grade into a quartz-diorite. Potassium feldspar occurs only as an accessory (less than 2%). Apatite appears as euhedral crystals in all the other mineral phases.

Terminal Plutonic Phase

The terminal plutonic phase has been the most poorly studied of the three phases of stock intrusion, principally due to the manner in which the systematic collecting has been conducted (See Plate I in pocket). Only three samples of this phase have been collected, chemically analyzed, and studied in thin section.

All these rocks contain essential quartz and sodic-plagioclase with varying amounts of potassium feldspar. The texture is hypautomorphic-equigranular with grain size of 1 to 3 mm., as seen in Figures 49 and 50. Biotite and hornblende, the only primary mafic constituents, are principally accessory minerals with much appearing to be of xenolithic or xenocrystic origin.

The abrupt change in grain size from the intermediate phase to the terminal phase may indicate that the latter phase could be associated with the later aplitic phase. Insufficient field work has prevented the establishment of this relationship.

Top: Figure 49. Photomacrograph of sample A034. Micro-granodiorite from terminal plutonic phase. (3X)

Bottom: Figure 50. Photomacrograph of sample A044. Tonalite from terminal plutonic phase. (3X)

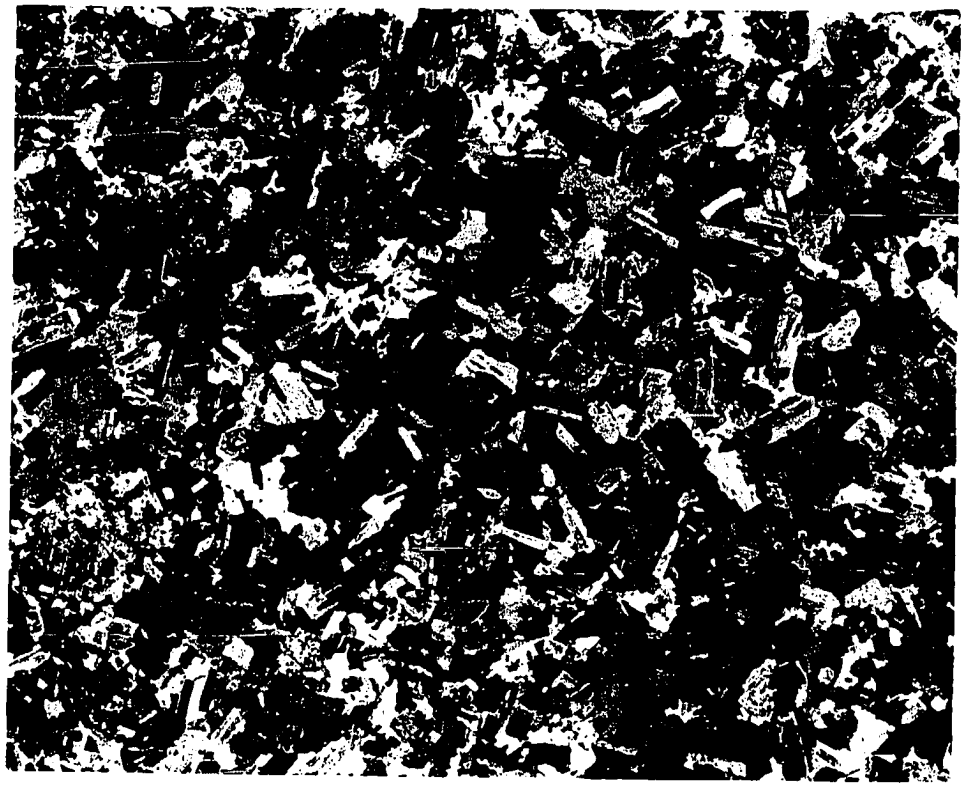

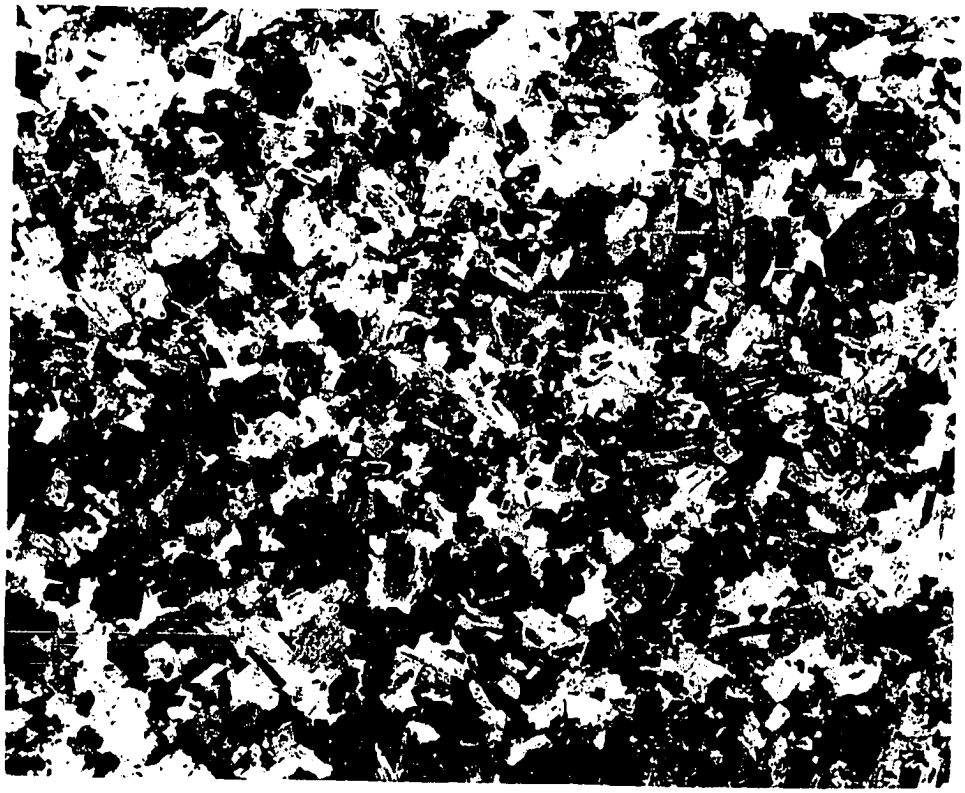

Basaltic Dike Phase

The basaltic dike phase was intruded shortly after the intrusion of the plutonic phases. These dikes are few in number and have a general directional trend of 70° azimuth. A schematic map showing the trends of the dikes within the area mapped is presented as Figure 19. It has been found that these dikes transect both the plutonic phases and the metamorphic aureole, but their extent into the unmetamorphosed sediments has not been determined.

Although only one of the dikes has been analyzed chemically, several have been examined microscopically. Microscopic and chemical examination indicate that all the dikes have alkaline basalt affinities. No olivine has been found. The analyzed sample (C063), hornblende spessartite, shows long euhedral laths of basaltic hornblende in a pilotaxitic groundmass of intermediate plagioclase and hornblende. Iddings (Wolff, 1938) collected a picrite basalt near the head of Big Timber Creek, but the writer has not found rocks having a similar composition.

Other basalts within the area show similar pilotaxitic texture, as seen in Figure 51; still others display hyalopilitic and strong flow textures as shown in Figure 52. Xenoliths of feldspathic quartzite have been found in two basalts, one from the upper drainage of Big Timber Creek, shown in Figure 53, and the other from the canyon of Sweetgrass Creek.

Top: Figure 51. Photomacrograph of sample C034. Basalt from Sweetgrass Canyon. (3X)

Bottom: Figure 52. Photomacrograph of sample C173. Flow structure in basalt from upper Big Timber Creek. Note late quartzo-feldspathic stringers.

Top: Figure 53. Photomacrograph of sample C243. Quartzo-feldspathic xenolith in basalt from headwaters of Big Timber Creek. (3X)

Bottom: Figure 54. Photomacrograph of sample C142. Multiple dikes of aplite in basalt. (3X)

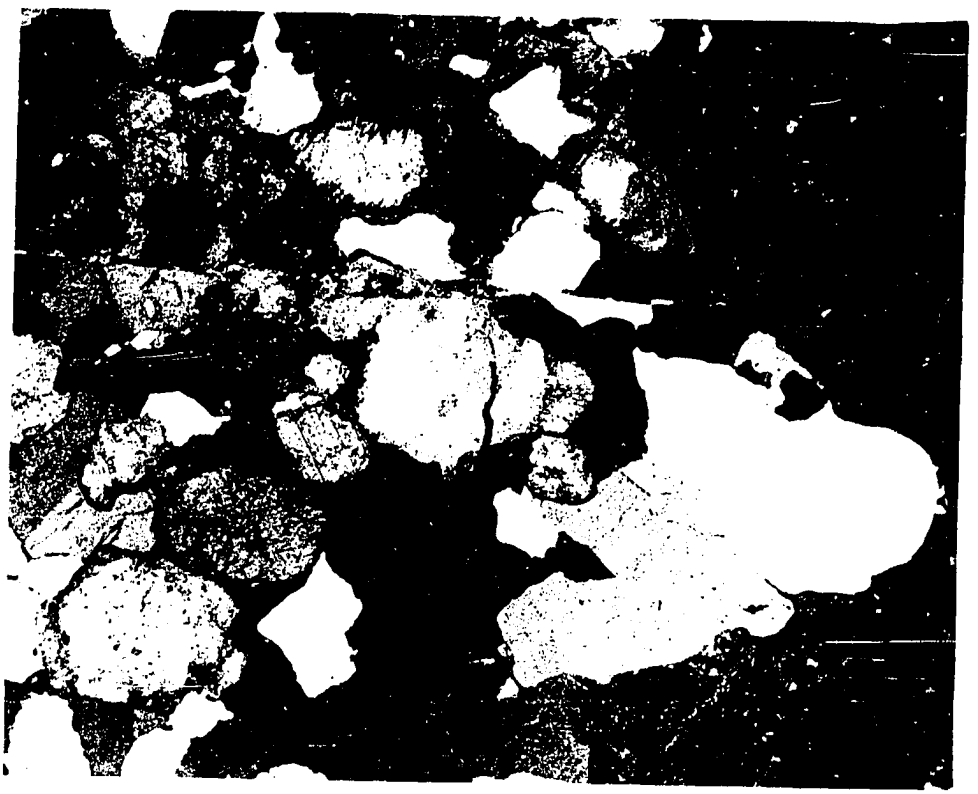

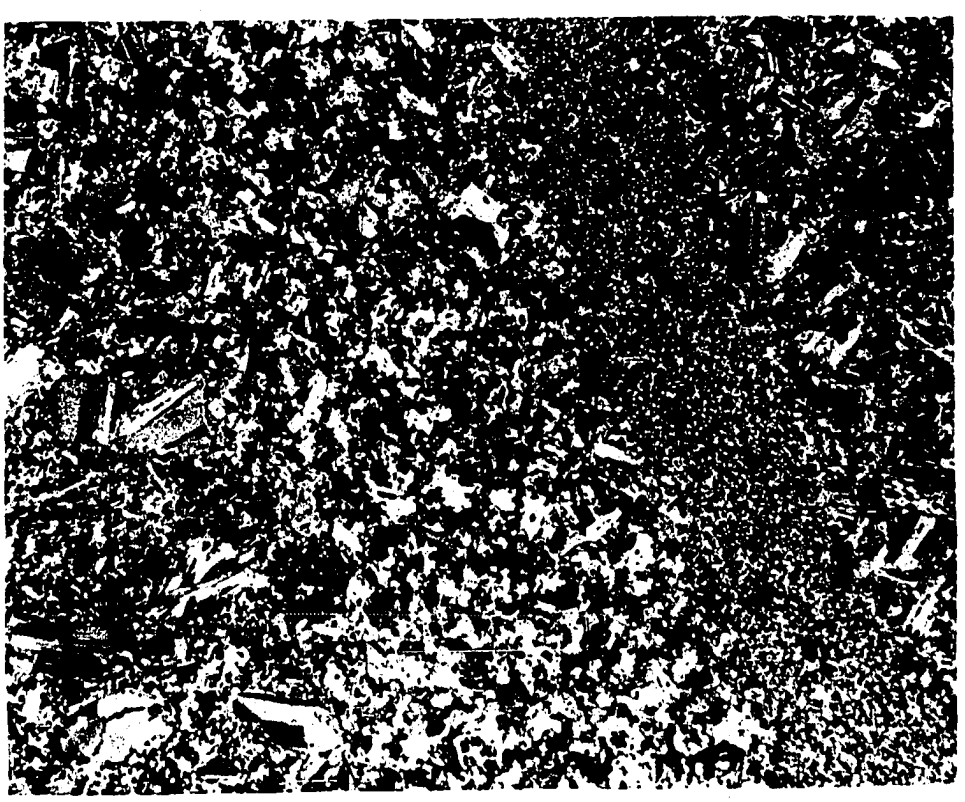

Aplitic Igneous Dike Phase

The aplitic dike phase post-dates both the plutonic igneous and basaltic dike phases. These dikes vary in composition from granodioritic to alaskitic. In hand specimen the colors vary from a pinkish-buff colored rock to almost wholly white (alaskites). The grains, of medium size in the mafic varieties, become increasingly fine in the alaskitic varieties.

The initial intrusion of the aplitic dikes shows medium grain size and an enrichment of mafic constituents. Later alaskitic aplitic dikes, fine in grain size and depleted in mafic minerals, cross-cut the earlier, more mafic and coarser-grained granodioritic aplites. Multiple intrusions of aplites are common and can be seen in Figure 54. No pegmatite has been found or reported by other workers in the area.

The principal minerals of the aplites are quartz and microcline with subordinate amounts of plagioclase and occasional biotite. Only minor amounts of magnetite and apatite are present.

Although Windley (1965) and Chapman (1962) have shown a definite geometric relationship between aplite dikes and particular fracture patterns, this writer has made no such investigation.

The granodioritic aplite commonly shows significant amounts of biotite and altered hornblende which gives the rocks a speckled appearance similar to many microgranites. Frequently the saccharoidal texture present in most of the other aplites of the area is absent from these more mafic varieties.

Microscopically the textures of the aplitic dikes vary from xenomorphic-granular to panallotriomorphic-granular with a grain size of less than 3 mm. Their constituent minerals are essentially quartz, potassium feldspar and plagioclase with subordinate biotite and hornblende.

Plagioclase forms subhedral to anhedral grains and tends to form minerals of the largest grain size. These frequently have irregular, indented grain boundaries where they have been penetrated and replaced by quartz and microcline (?). Relict crystals of plagioclase are situated within the potassium feldspar and are frequently optically continuous. The potassium feldspar is believed to be microcline but very infrequently shows the typical cross-hatch twinning. Quartz occurs with anhedral outline and with only slight strain shadows. Biotites occur as primary flakes and as secondary alteration of hornblende. The alaskitic aplites are composed essentially of quartz and potassium feldspar with varying amounts of sodic feldspar.

Andesitic Dike Phase

The andesitic dike phase contains a wide variety of rock types due to the variation among the types of phenocrysts present in the rock. This dike phase shows strong chemical affinities as opposed to the wide chemical variance of the dikes and sills of the northern part of the Crazy Mountain basin (Simms, 1966).

All the rocks in this phase are porphyritic with phenocrysts of hornblende, andesine plagioclase, biotite, and augite. No attempt has been made to affix any of the particular sophisticated rock names which abound in the geological literature to these rocks.

Textural variations within this group are particularly striking. Generally the rocks are porphyritic with a pilotaxitic groundmass, with trachytic and microlitic textures also being common, as shown in Figures 55 through 58. Plagioclase (ca. An_{25}) occurs both as euhedral and subhedral phenocrysts and as laths in the groundmass. When flow texture is present, these groundmass laths show a preferred orientation parallel to flow. Albite twinning is common, and occasional mild zoning is also present. Figure 56 shows twinning plagioclase with a border of secondary sodic feldspar. Potassium feldspar is a minor constituent and has been found only in the matrix as small blebs (revealed by staining).

Top: Figure 55. Photomacrograph of sample C133. Flow texture in andesite. (3X)

Bottom: Figure 56. Photomacrograph of sample C143. Porphyritic hornblende andesite collected in Big Timber Canyon. Note sodic rim around plagioclases.

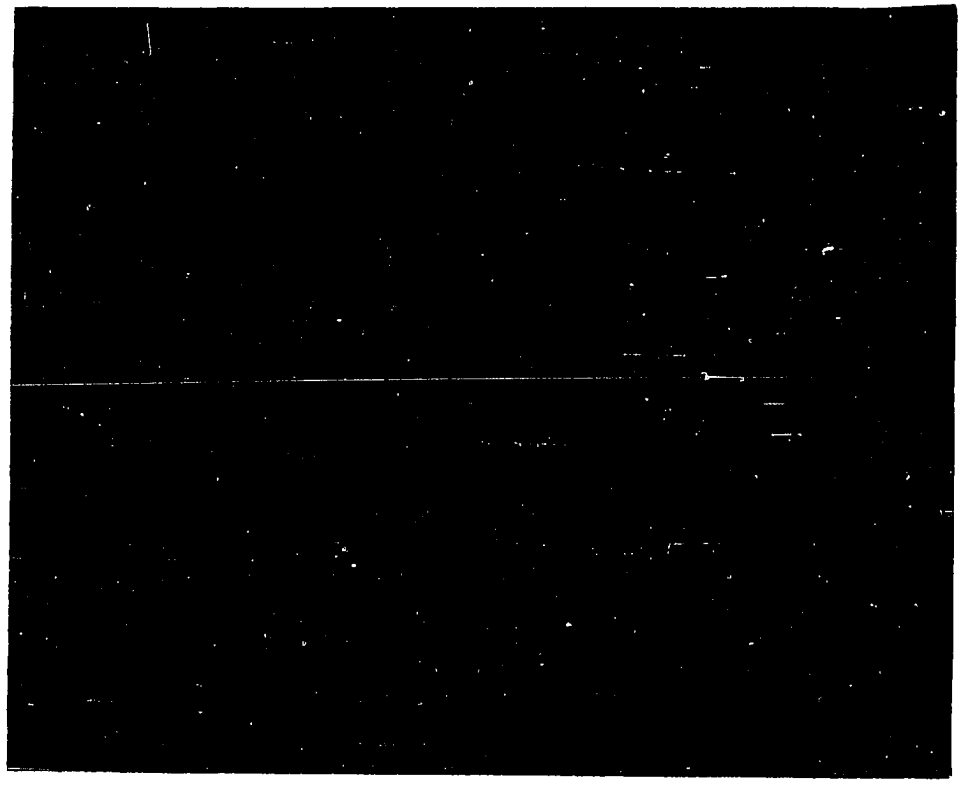

Top: Figure 57. Photomacrograph of sample C073. Porphyritic oligoclase-andesite showing pelotaxitic groundmass. Collected in Big Timber Canyon.

Bottom: Figure 58. Photomacrograph of sample C233. Porphyritic hornblende andesite showing "syneusis" of magnetite.

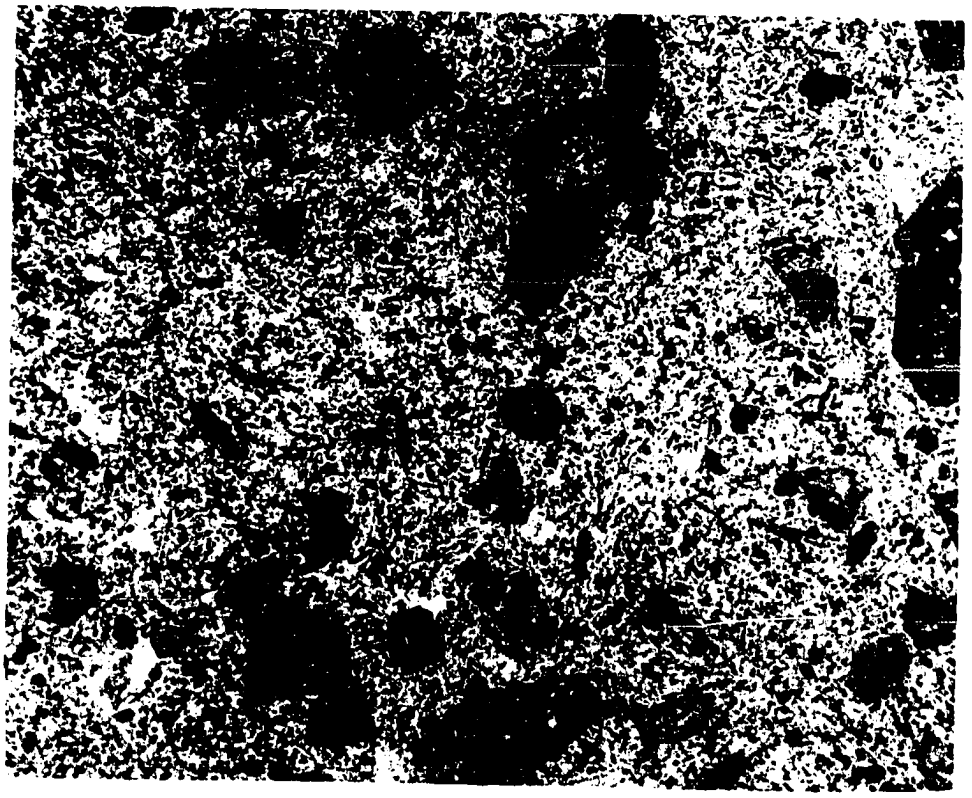

The most common mafic constituent is hornblende, which varies from pale green to dark brown. This hornblende is usually found in long euhedral, frequently poikilitic laths, as seen in Figures 56 and 58, but is also found as interlaminated laths with plagioclase in the groundmass. Rarely does the phenocrystic hornblende show any preferred orientation with the flow texture present in the mesotasis.

Biotite occurs as small primary and alteration flakes throughout this group, while magnetite occurs as small crystals, frequently showing euhedral outlines as seen in Figure 56. Reaction of the magma with enclosed xenoliths frequently resulted in an aggregation of the magnetite into clusters as seen in Figure 57.

All the dikes in this group show parallel intrusive relationships, having been intruded syntectonically with strong north-south faulting seen in Figures 25 and 26. Conchoidal fractures within this dike group indicate that movement has taken place either after or during the intrusion. This same fracturing has been reported in the Sweetgrass Hills by Kemp and Billingsley (1921).

ASSIMILATION OF COUNTRY ROCKS

Recognizable inclusions of country rock in the Big Timber igneous complex are few considering the size of the intrusion. No significant amounts of country rock have been found either near the contact or in the highest exposures within the pluton. The general paucity of accidental xenoliths, sensu stricto, indicates either that few were ever present in the Big Timber magma series or that, if any are present, they have been sufficiently modified so as to escape recognition. Walker and Poldervaart (1949) were still able to recognize inclusions of country rock in the Karroo dolerites, even though a large amount of metasomatism had taken place. Less extreme assimilation is thought by Turner and Verhoogen (1960, p. 150) to cause the formation of abundant hypersthene. Hypersthene is present in the early basic phase of the Big Timber complex but not in large quantities. Turner and Verhoogen argue that even though basaltic magma has sufficient heat to melt the sedimentary sequence into which it is intruded, the appearance of unusual mineral phases need not occur, if the sediments are quartzo-feldspathic. They continue:

> Lime, alumina, and silica are all major constituents of, and hence must be readily soluble in, basaltic magma. Presumably considerable additional amounts of any one could be accomodated by redistribution of ions among the

> ionic groups comprising the liquid magma. This might subsequently be reflected only in differences in composition of pyroxene, olivine, and plagioclase, or in the relative proportions of these minerals, as compared with those in the uncontaminated basalt.

Since no particular mineral appears to be present in unusually large quantities to the exclusion of other minerals, it is the opinion of the writer that assimilation of the country rock into which the stock was intruded was minor, if not entirely lacking, in the formation of the rock series present.

AGMATITE

Agmatite is found in various localities in the southern half of the pluton. It consists of elements of the early basic phase enclosed in later intermediate phase material. There is not a large amount of agmatite present, but it does occur regularly close to the contact of the early basic phase with the intermediate phase, as is shown by Plate I in pocket.

Contact relationships between the early basic phase and the intermediate phase are, for the most part, obscure due to intermingling of the two phases and partial resorption of the earlier phase. Figures 59 and 60 show examples of agmatite found near the shore of Thunder Lake. Other examples of this agmatite are found in the transition zone between the earlier basic phase and the later intermediate phase. The angularity of the agmatitic fragments indicates complete consolidation prior to the introduction of the later intermediate phase.

Relationships between the matrix and fragments vary between two extremes. Some of the agmatite is characterized by a network of thin leucocratic veins completely enclosing very fresh, angular mafic fragments which often are so little disturbed by the veins that they can be fitted together in jigsaw-puzzle fashion. This type of agmatite is similar to the "net-veining" found by other investigators

Top: Figure 59. Agmatitic zone between the basic border and intermediate phases exposed near the south shore of Thunder Lake.

Bottom: Figure 60. Agmatite showing extreme fragmentation and stringers of leucodiorite penetrating fragments of gabbroic rock.

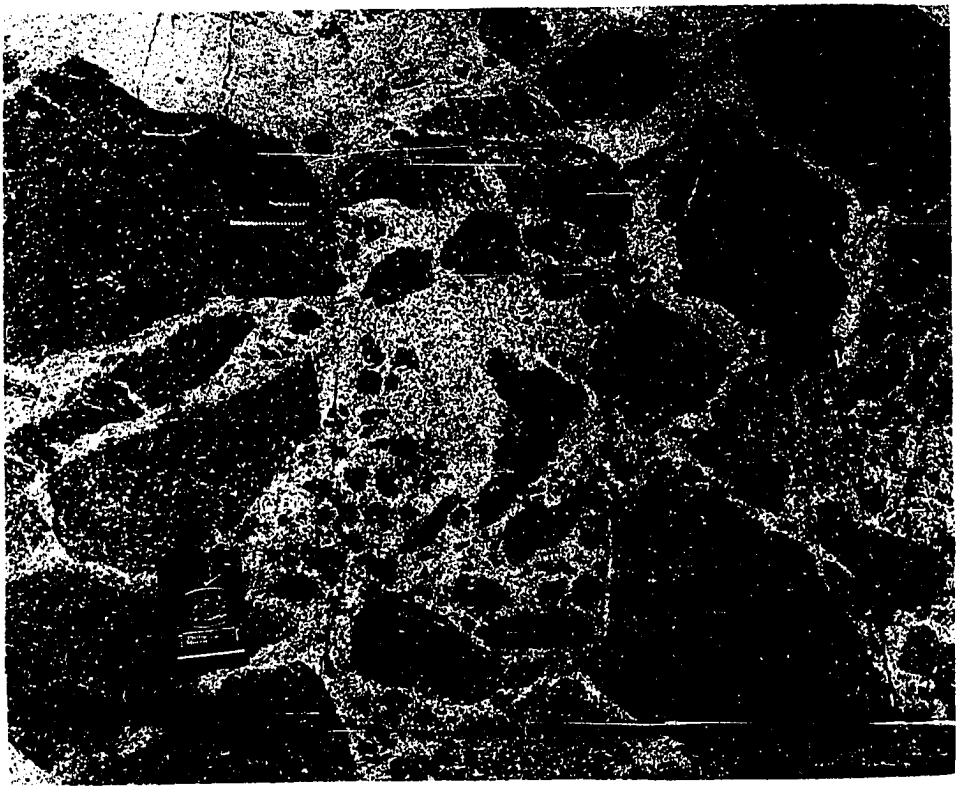

(Reynolds, 1954, plate 2B) around some of the basic intrusive complexes in Scotland. The other type of agmatite found probably should not be called agmatite, *sensu stricto*; although the type of fragmentation is similar to that of agmatite, it lacks angularity. This latter type of fragmental material is composed principally of leucocratic rock types in a subordinate amount of well-rounded fragments. These fragments have lost all evidence of their interrelationship, are poor- to well-rounded, sometimes well-embayed, and, for the most part, partially assimilated by the leucocratic matrix, with the textures and grain size of the different fragments in a single exposure varying greatly. Thus, these fragments should more properly be called cognate xenoliths (Weggman, 1938).

Most of the mafic fragments are gabbroic in which the original textures and minerals vary from no apparent change to a high degree of uralitization of the mafic constituents. The dioritic matrix of the agmatite is usually lithologically homogeneous between adjacent sharply enclosed fragments and is composed of varying amounts of plagioclase, hornblende, and biotites and subordinate amounts of potassium feldspar and quartz. The matrix of agmatite varies in composition from mela- to leucodiorite. Insufficient field time prevented the evaluation of the agmatite on a vertical basis.

CHEMISTRY

Due to the increasing importance of quantitative data in petrogenetic interpretation, the writer has determined the major elements in fifty-three rocks systematically collected within the Big Timber igneous complex. These analyses along with computed normative, ionic weight percent, and equivalent cationic data are presented in Tables I, II, III, and IV. Analyses of the plutonic phases, given in Tables I and II, are divided into three groups: (1) the early basic phase, (2) the intermediate phase, and (3) the terminal phase. Tables III and IV present the same data for the dike phases of the complex which are also broken into three groups: (1) the aplitic phase, (2) the basaltic phase, and (3) the andesitic phase. Sample numbers are the same as those shown on Plate I (map in pocket).

There has been no attempt to present the chemical data as related to its geographical variation, because over fifty percent of the area has not as yet been systematically collected.

Gross Chemical Variation

In inspecting Table I and comparing it with the averages of igneous rocks presented by Nockolds (1954), it can be seen that the basic border phase differs only slightly in average composition from pyroxenites and gabbros, generally lying

TABL

Chemical Analysis of Plutonic R

Weight %

	Early Basic Phase													
Sample No.	A243	A573	A263	A253	A453	A543	A473	A124	A533	A463	A083	A293	A144	A133	A183
SiO_2	49.76	48.52	48.46	49.33	50.16	50.19	51.44	51.75	52.13	52.29	52.55	52.56	52.74	52.77	52.86
TiO_2	2.33	2.14	1.69	1.74	1.98	2.01	1.71	1.46	1.36	1.38	1.63	1.50	1.39	1.72	1.81
Al_2O_3	18.03	16.42	18.24	13.77	11.79	18.68	16.67	16.57	15.80	19.81	15.10	15.92	16.15	16.74	16.79
Fe_2O_3	5.49	3.61	4.44	3.99	4.54	3.15	3.58	3.29	2.98	2.29	2.19	3.27	1.90	3.20	2.70
FeO	9.48	9.50	7.76	8.40	8.73	6.25	6.28	6.63	5.99	4.64	6.69	6.25	6.92	6.52	6.21
MnO	.21	.23	.19	.22	.12	.21	.14	.09	.12	.12	.18	.17	.11	.17	.15
MgO	6.96	5.89	12.59	8.35	7.42	4.05	5.00	4.72	5.88	3.31	6.41	5.66	6.55	4.79	4.31
CaO	11.18	10.75	10.35	9.30	10.27	9.79	8.32	8.22	8.53	8.63	7.89	8.04	7.69	8.27	8.58
Na_2O	2.32	2.58	1.95	2.74	2.33	3.50	3.28	3.70	3.45	4.33	3.92	3.77	3.63	3.47	3.82
K_2O	.78	1.10	1.19	1.35	1.84	1.13	2.48	1.74	2.00	1.51	1.53	2.13	2.18	1.42	1.27
P_2O_5	.81	1.03	.87	.71	.74	.38	.63	.81	.89	.77	.83	.58	.61	.64	.62
H_2O	.11	.15	.13	.15	.21	.15	.21	.16	.18	.18	.21	.17	.11	.19	.21
Total	100.48	99.92	99.66	100.05	100.13	100.19	99.54	99.14	99.31	99.26	99.13	100.02	99.98	99.90	99.33
Total Fe as FeO	12.25	10.99	9.04	10.18	9.84	11.64	10.39	10.74	10.09	11.20	8.98	10.43	9.16	10.73	10.25
Total Fe as Fe_2O_3	16.01	14.15	13.05	13.32	14.23	10.10	10.45	10.69	9.74	7.45	9.62	10.22	9.59	10.45	9.60
													Normative Minerals r		
Q	.00	.00	.00	.00	.73	.38	.00	.41	.00	.00	.00	.00	.00	3.28	2.65
Or	4.59	6.51	7.06	7.99	10.88	6.67	14.75	10.39	11.92	9.01	9.14	12.61	12.90	8.42	7.57
Ab	19.56	21.88	16.58	23.21	19.73	29.60	27.94	31.63	29.45	36.98	33.53	31.95	30.75	29.44	32.61
An	28.19	30.04	15.75	21.31	16.29	32.45	23.05	23.71	21.91	30.44	19.29	20.26	21.36	25.98	25.14
Wo	9.32	7.24	12.82	8.64	12.67	4.56	6.17	5.29	6.47	3.42	6.40	6.79	5.53	4.76	5.90
En	5.71	3.94	9.19	5.52	7.93	2.72	3.90	3.12	4.18	2.08	3.99	4.33	3.36	2.87	3.50
Fs	3.89	3.05	2.48	2.56	3.96	1.60	1.88	1.91	1.86	1.15	2.03	2.03	1.86	1.63	2.10
En	5.85	3.75	12.77	9.67	10.56	7.36	7.72	8.76	10.55	5.13	10.01	6.80	6.69	9.10	7.33
Fs	3.17	2.91	3.45	4.49	5.28	4.34	3.72	5.37	4.69	2.84	5.09	3.19	3.71	5.19	4.41
Fo	4.00	4.91	6.69	3.94	.00	.00	.84	.00	.03	.78	1.49	2.09	4.40	.00	.00
Fa	2.39	4.19	1.99	2.02	.00	.00	.34	.00	.02	.48	.84	1.08	2.69	.00	.00
Mt	7.93	5.25	6.47	5.79	6.59	4.57	5.23	4.82	4.36	3.35	3.21	4.75	2.76	4.65	3.95
Il	4.45	4.07	2.84	3.31	3.76	3.82	3.27	2.80	2.61	2.65	3.13	2.85	2.64	3.28	3.47
Ap	1.76	2.26	1.91	1.55	1.62	1.92	1.39	1.79	1.96	1.70	1.83	1.27	1.33	1.40	1.37
H_2O	.11	.15	.13	.15	.21	.15	.21	.16	.18	.18	.21	.17	.11	.19	.21
Normative Plagioclase	An_{28}	An_{30}	An_{16}	An_{21}	An_{16}	An_{32}	An_{23}	An_{24}	An_{22}	An_{30}	An_{19}	An_{20}	An_{21}	An_{26}	An_{25}

Notes:
1. Sample locations are shown on map in pocket.
2. Non-classical analytical methods employed; principally absorption and flame spectrophotometric and volumetric.
3. Analyses performed on samples dried for 4 hours at 110°C.
4. Analyses were performed at the Geology Laboratory, University of Cincinnati.
5. John Tappe, analyst.

Sample No.	Name
A243	olivine-bearing, uralite-porphyritic hornblende-meladiorite
A573	uralite-hornblende-meladiorite
A263	olivine-bearing, augite-hypersthene-meladiorite
A253	olivine-bearing, biotite-porphyritic hornblende-meladiorite
A453	uralite-hypersthene-hornblende-meladiorite
A543	biotite-hornblende-diorite
A473	uralite-biotite-porphyritic hornblende-diorite
A124	biotite-meladiorite
A533	hypersthene-biotite-augite-hornblende-diorite
A463	biotite-augite-hornblende-diorite
A083	uralite-augite-diorite
A293	uralite-dialiagite-biotite-diorite

TABLE I

utonic Rocks of the Big Timber Stock

Weight % Oxides

	Intermediate Phase											Terminal Phase		
A183	A123	A213	A093	A154	A423	A353	A393	A114	A134	A203	A104	A014	A024	A044	A034
52.86	52.96	53.06	53.11	53.53	53.86	54.02	54.33	55.11	55.26	55.45	56.17	58.32	69.19	69.19	66.44
1.81	1.57	1.64	1.39	1.20	1.56	1.47	1.46	1.40	1.36	1.46	1.15	1.27	.65	.72	.62
16.79	16.27	17.01	12.76	19.08	17.15	19.02	18.19	16.27	17.71	17.91	15.94	16.29	15.48	15.92	14.98
2.70	4.18	3.27	2.12	2.01	3.47	3.05	4.15	1.93	2.92	2.26	1.98	2.44	1.46	1.21	1.46
6.21	5.57	5.64	7.14	6.86	5.14	4.31	4.47	6.41	5.61	4.98	5.40	4.37	2.20	2.52	2.08
.15	.16	.15	.17	.14	.10	.13	.11	.12	.13	.14	.11	.09	.06	.05	.06
4.31	4.58	3.80	7.99	6.79	6.03	3.50	3.16	4.49	3.52	3.13	4.79	2.34	2.00	1.92	1.74
8.58	7.90	6.56	8.92	8.06	7.13	7.24	6.91	7.21	6.49	7.18	6.10	6.09	3.51	3.39	3.55
3.82	3.55	4.18	3.14	3.45	4.13	4.47	4.04	4.09	4.07	4.07	4.13	4.27	4.56	4.69	4.46
1.27	2.10	2.13	1.77	1.57	1.78	2.11	1.80	2.72	2.27	2.41	2.63	2.80	3.14	3.14	3.68
.62	.68	.97	.67	.56	.56	.53	.63	.43	.53	.63	.62	.55	.51	.43	.43
.21	.20	.18	.20	.16	.20	.15	.14	.13	.21	.17	.17	.20	.21	.17	.21
99.33	99.72	99.39	99.38	100.21	101.09	99.90	99.39	100.31	100.06	99.77	99.19	99.83	98.97	99.31	99.52
10.25	11.50	11.28	7.86	9.15	11.17	11.50	12.33	9.25	10.88	10.31	9.15	9.77	8.42	8.37	8.20
9.60	10.36	9.44	10.05	9.62	9.18	7.74	9.12	9.04	9.15	7.79	7.97	7.29	3.90	4.01	3.76

nerals recalculated to 100%

2.65	3.02	1.69	.00	.20	.25	.62	5.85	.00	3.64	3.59	2.51	7.09	17.22	16.30	18.45
7.57	12.47	12.69	10.55	9.27	10.43	12.50	10.72	16.04	13.43	14.30	15.69	16.61	18.79	18.72	20.71
32.61	30.18	35.65	26.79	29.18	34.64	37.92	34.44	34.54	34.49	34.57	35.29	36.26	32.07	39.69	38.00
25.14	22.36	23.73	15.62	23.19	22.74	25.66	26.38	17.97	23.38	23.58	17.36	17.08	12.65	13.41	10.65
5.90	5.43	1.39	10.45	5.69	3.78	3.01	1.85	6.35	2.40	3.53	3.98	5.84	.81	.42	1.85
3.50	3.61	.84	6.65	3.44	2.70	2.02	1.28	3.54	1.37	2.04	2.42	3.29	.54	.26	1.23
2.10	1.42	.47	3.13	1.87	.75	.76	.42	2.56	.92	1.34	1.34	2.30	.20	.14	.48
7.33	7.85	8.69	13.03	13.46	12.19	6.72	6.65	6.49	7.41	5.79	9.63	2.56	4.50	4.56	3.13
4.41	3.08	4.80	6.14	7.34	3.39	2.54	2.17	4.69	4.97	3.81	5.31	1.79	1.69	2.42	1.23
.00	.00	.00	.27	.00	.00	.00	.00	.80	.00	.00	.00	.00	.00	.00	.00
.00	.00	.00	.14	.00	.00	.00	.00	.63	.00	.00	.00	.00	.00	.00	.00
3.95	6.09	4.78	3.10	2.91	4.99	4.29	6.06	2.79	4.24	3.29	2.90	3.55	2.14	1.77	2.13
3.47	3.00	3.14	2.66	2.28	2.94	2.80	2.79	2.65	2.59	2.78	2.21	2.42	1.25	1.38	1.19
1.37	1.49	2.14	1.48	1.22	1.21	1.16	1.39	.94	1.16	1.38	1.37	1.21	1.13	.95	.95
.21	.20	.18	.20	.16	.20	.15	.14	.13	.21	.17	.17	.20	.21	.17	.21
An_{46}	An_{43}	An_{46}	An_{37}	An_{46}	An_{46}	An_{46}	An_{43}	An_{36}	An_{46}	An_{41}	An_{33}	An_{32}	An_{36}	An_{36}	An_{28}

blende-	A144	biotite-hornblende-diorite
	A133	biotite-augite-diorite
lende-	A183	hypersthene-biotite-diorite
	A123	biotite-hornblende-diorite
e	A213	quartz-bearing, hornblende-biotite-diorite
te	A093	hypersthene-augite-hornblende-meladiorite
	A154	biotite-hornblende-diorite
	A423	xenolithic hypersthene-biotite-diorite
	A353	quartz-bearing, biotite-hornblende-diorite
	A393	quartz-bearing, hypersthene-augite-biotite-diorite
	A114	biotite-hornblende-diorite
	A134	biotite-meladiorite
	A203	biotite-augite-hornblende-diorite
	A104	biotite-diorite
	A014	biotite-hornblende-tonalite
	A024	tonalite
	A044	granodiorite
	A034	granodiorite

TABLE II

Chemical Analysis of the Plutonic Rocks of

% Ionic

Early Basic Phase

Sample No.	A243	A573	A263	A253	A453	A543	A473	A124	A533	A463	A083	A293	A133	A144	A183
Si^{4+}	21.39	21.74	22.65	23.06	23.44	23.46	24.04	24.19	24.36	24.44	24.56	24.56	24.66	24.65	24.7
Ti^{4+}	1.40	1.28	.89	1.04	1.18	1.20	1.02	.87	.81	.82	.97	.89	1.03	.83	1.0
Al^{3+}	7.95	8.68	5.41	7.28	6.23	9.99	8.71	8.76	8.36	10.48	7.99	8.42	8.85	8.54	8.8
Fe^{3+}	4.09	2.69	3.31	2.97	3.38	2.35	2.67	2.45	2.22	1.70	1.63	2.43	2.38	1.41	2.0
Fe^{2+}	7.36	7.38	6.03	6.52	6.78	4.85	4.88	5.15	4.65	3.60	5.20	4.85	5.06	5.37	4.8
Mn^{2+}	.16	.17	.14	.17	.09	.16	.10	.06	.09	.09	.13	.13	.13	.08	.1
Mg^{2+}	4.19	3.55	7.59	5.03	4.47	2.44	3.01	2.84	3.54	1.99	3.86	3.41	2.88	3.95	2.5
Ca^{2+}	7.99	7.68	7.40	6.65	7.34	7.00	5.95	5.87	6.10	6.17	5.64	5.75	5.91	5.49	6.1
Na^{2+}	1.72	1.91	1.44	2.03	1.72	2.59	2.43	2.74	2.55	3.21	2.90	2.79	2.57	2.69	2.8
K^{1+}	.64	.91	.98	1.12	1.52	.93	2.05	1.44	1.66	1.25	1.27	1.76	1.17	1.80	1.0
P^{5+}	.45	.58	.49	.40	.41	.49	.35	.45	.50	.43	.46	.32	.36	.34	.3
O^{-2}	43.07	43.29	43.28	43.74	43.49	44.68	44.27	44.25	44.42	45.02	44.46	44.64	44.83	44.76	44.7
$Fe^{2+} + Fe^{3+}$	11.46	10.07	9.34	9.50	10.17	7.20	7.55	7.60	6.87	5.31	6.83	7.29	7.45	6.79	6.8

% Cationic recalcula

Si^{4+}	46.83	48.18	51.01	51.38	51.76	52.35	54.06	54.63	55.21	55.70	55.84	55.18	55.16	55.65	55.6
Ti^{4+}	3.19	2.94	2.08	2.41	2.71	2.78	2.38	2.04	1.91	1.95	2.30	2.09	2.39	1.95	2.5
Al^{3+}	13.05	14.43	9.14	12.16	10.32	16.70	14.68	14.84	14.19	17.90	13.61	14.18	14.84	14.45	15.0
Fe^{3+}	6.99	4.65	5.82	5.17	5.83	4.09	4.68	4.32	3.93	3.03	2.89	4.27	4.16	2.49	3.5
Fe^{2+}	11.60	11.76	9.76	10.46	10.77	7.79	7.89	8.36	7.58	5.91	8.50	7.84	8.15	8.73	7.8
Mn^{2+}	.25	.28	.23	.27	.14	.25	.17	.11	.15	.15	.22	.21	.20	.13	.1
Mg^{2+}	4.77	4.09	8.89	5.83	5.13	2.83	3.52	3.34	4.17	2.36	4.56	3.98	3.35	4.63	3.0
Ca^{2+}	10.67	10.38	10.16	9.03	9.88	9.52	8.15	8.09	8.42	8.57	7.81	7.87	8.06	7.56	8.4
Na^{1+}	1.22	1.37	1.05	1.47	1.23	1.88	1.77	2.01	1.88	2.37	2.14	2.04	1.87	1.97	2.0
K^{1+}	.62	.89	.98	1.10	1.48	.92	2.04	1.43	1.66	1.26	1.27	1.75	1.16	1.80	1.0
P^{5+}	.75	.97	.83	.67	.69	.83	.60	.78	.86	.75	.80	.55	.61	.58	.5

Notes:
1. Sample locations are shown on map in pocket. For sample descriptions see Table I.
2. Non-classical analytical methods employed; principally absorption and flame spectrophotometric and volumetric.
3. Analyses performed on samples dried for 4 hours at 110°C.
4. Analyses were performed at the Geology Laboratory, University of Cincinnati.
5. John Toppe, analyst.

of the Big Timber Stock

	Intermediate Phase											Terminal Phase		
3	A123	A213	A093	A154	A423	A353	A393	A114	A134	A203	A104	A0	A244	A034
71	24.75	21.80	24.82	25.02	25.17	25.25	25.39	25.76	25.82	25.91	26.25	27.26	30.47	30.47	31.07
08	.94	.98	.83	.71	.93	.88	.87	.83	.81	.87	.68	.76	.38	.43	.37
88	8.61	9.42	6.75	8.40	9.06	10.06	9.62	8.61	9.37	9.47	8.43	8.62	8.19	8.42	7.92
01	3.11	2.43	1.58	1.49	2.58	2.20	3.09	1.44	2.17	1.68	1.47	1.82	1.08	.90	1.08
82	4.32	4.38	5.55	5.33	3.99	3.35	3.47	4.98	4.36	3.87	4.19	3.39	1.71	1.95	1.61
11	.12	.11	.13	.10	.07	.10	.08	.09	.10	.10	.08	.06	.04	.03	.04
59	2.76	2.29	4.81	4.09	3.63	2.11	1.90	2.70	2.12	1.88	2.88	1.41	1.20	1.15	1.04
13	5.65	4.69	6.37	5.76	5.09	5.17	4.94	5.15	4.64	5.13	4.36	4.92	2.51	2.42	2.52
83	2.63	3.10	2.32	2.55	3.06	3.31	2.99	3.03	3.01	3.01	3.06	3.16	3.38	3.44	3.30
05	1.74	1.76	1.46	1.30	1.47	1.75	1.49	2.25	1.88	2.00	2.18	2.32	2.60	2.60	2.88
34	.38	.54	.37	.31	.31	.29	.35	.24	.29	.35	.34	.30	.28	.24	.24
71	44.66	44.83	44.32	45.08	45.65	45.39	45.14	45.18	45.44	45.44	45.19	45.75	47.07	47.19	47.38
84	7.44	6.82	7.13	6.83	6.58	5.55	6.57	6.42	6.53	5.55	5.67	5.21	2.79	2.86	2.70

lated to 100%

69	55.48	56.01	56.22	56.30	56.22	57.08	57.20	57.79	57.93	58.43	59.79	61.32	69.64	69.39	70.51
53	2.18	2.30	1.95	1.67	2.16	2.06	2.04	1.95	1.89	2.04	1.62	1.77	.92	1.01	.87
00	14.46	15.95	11.46	14.17	15.17	17.05	16.24	14.47	15.75	16.01	14.39	14.53	14.03	14.37	13.48
54	5.45	4.30	2.79	2.63	4.51	3.88	5.44	2.52	3.81	2.96	2.62	3.19	1.94	1.60	1.92
82	6.97	7.11	9.03	8.62	6.41	5.44	5.62	8.03	7.03	6.27	6.87	5.49	2.81	3.20	2.63
18	.19	.18	.21	.17	.12	.16	.13	.14	.16	.17	.13	.11	.07	.06	.07
04	3.21	2.69	5.67	4.79	4.22	2.48	2.23	3.15	2.47	2.21	3.42	1.65	1.43	1.37	1.23
43	7.71	6.45	8.80	7.90	6.94	7.13	6.78	7.05	6.34	7.05	6.05	6.75	3.49	3.36	3.49
07	1.91	2.27	1.71	1.87	2.22	2.43	2.19	2.21	2.20	2.21	2.26	2.31	2.51	2.55	2.44
04	1.72	1.76	1.46	1.29	1.45	1.74	1.48	2.23	1.86	1.99	2.19	2.30	2.62	2.62	2.89
59	.65	.93	.64	.53	.53	.51	.60	.41	.50	.60	.60	.52	.49	.41	.41

TABLE III

Chemical Analysis of Dike Rocks of the

Weight % Oxides

	Aplitic Phase										Basalt
Sample No.	B432	B422	B462	B332	B222	B402	B292	B312	B193	B262	B203	C063
SiO_2	62.69	64.85	66.18	66.46	67.82	68.12	68.55	69.38	70.61	72.07	76.84	50.17
TiO_2	.84	.70	.65	.56	.52	.57	.41	.47	.35	.32	.10	2.29
Al_2O_3	17.16	16.12	15.93	16.12	16.76	14.78	15.45	14.54	14.93	13.03	12.29	15.05
Fe_2O_3	2.15	1.74	1.57	1.43	.87	.83	1.12	1.07	1.17	.99	.00	4.40
FeO	2.53	2.40	2.11	1.83	1.89	2.36	1.24	1.38	1.02	.79	.72	6.56
MnO	.08	.07	.08	.05	.04	.04	.05	.07	.00	.02	.00	.31
MgO	1.60	1.83	.94	.99	.59	2.21	1.75	1.03	.42	.42	.00	6.18
CaO	2.68	2.11	2.10	2.42	2.02	2.03	2.02	1.92	1.74	1.06	.22	7.85
Na_2O	5.14	4.70	5.24	4.79	4.84	4.47	4.63	4.28	4.03	3.84	4.13	3.27
K_2O	3.89	3.73	4.12	3.68	4.75	3.40	3.54	4.29	4.31	5.38	4.20	2.23
P_2O_5	.39	.56	.37	.56	.28	.56	.39	.37	.43	.33	.23	.71
H_2O	.18	.20	.17	.18	.12	.14	.21	.18	.18	.12	.19	.18
Total	99.53	99.01	99.46	99.07	100.50	99.51	99.16	99.98	99.19	99.22	98.92	99.18
Total Fe as FeO	9.87	8.99	8.73	8.68	8.41	7.48	8.07	7.61	7.33	7.23	5.33	11.17
Total Fe as Fe_2O_3	4.96	4.40	3.87	3.46	2.99	3.45	2.49	2.60	2.31	1.83	.71	11.68

Normative Minerals recalcul

	Q	9.80	16.73	14.45	18.88	16.84	21.76	22.78	23.18	27.54	27.27	36.80	.00
	Or	23.14	22.31	24.52	21.99	27.96	20.22	19.95	25.66	25.72	32.08	25.14	13.31
	Ab	43.77	40.25	44.65	40.98	40.80	38.06	39.59	36.65	34.44	32.79	35.39	27.95
Di	An	11.07	7.26	7.83	8.81	8.34	6.82	7.81	7.44	6.16	3.35	-.25	20.00
Di	Wo	.00	.00	.20	.00	.00	.00	.00	.00	.00	.00	.00	6.27
Di	En	.00	.00	.11	.00	.00	.00	.00	.00	.00	.00	.00	4.31
	Fs	.00	.00	.08	.00	.00	.00	.00	.00	.00	.00	.00	1.46
Hy	En	4.51	4.61	2.25	2.49	1.46	5.54	4.40	2.60	1.06	1.06	.00	9.28
Hy	Fs	1.64	1.97	1.59	1.36	1.96	2.80	.78	1.02	.33	.14	1.17	3.14
	Fo	.00	.00	.00	.00	.00	.00	.00	.00	.00	.00	.00	1.37
	Fa	.00	.00	.00	.00	.00	.00	.00	.00	.00	.00	.00	.51
	Mt	3.14	2.55	2.29	2.10	1.26	1.21	1.64	1.57	1.71	1.45	.00	6.44
	Il	1.61	1.35	1.24	1.08	.98	1.09	.79	.90	.67	.61	.19	4.39
	Ap	.86	1.24	.81	1.24	.61	1.23	.86	.82	.95	.73	.51	1.57
	H_2O	.18	.20	.17	.18	.12	.14	.21	.18	.18	.12	.19	.18
	Others	.46	1.74	.00	1.08	.59	1.27	1.40	.16	1.41	.53	1.06	.00
	Normative Plagioclase	An_{20}	An_{18}	An_{18}	An_{18}	An_{17}	An_{18}	An_{11}	An_{17}	An_{18}	An_{9}	An_{9}	An_{41}

Notes: 1. Sample locations are shown on map in pocket.

2. Non-classical analytical methods employed; principally absorption and flame spectrophotometric and volumetric.

3. Analyses performed on samples dried for 4 hours at 110°C.

4. Analyses were performed at the Geology Laboratory, University of Cincinnati.

5. John Tappe, analyst.

Sample No.	Name
B432	micro-granodiorite
B422	porphyritic micro-granodiorite
B462	micro-granodiorite
B332	granodioritic aplite
B222	granodioritic aplite
B402	dacite
B292	porphyritic-ada
B312	micro-adamellit
B193	adamellitic apl
B262	granodioritic a
B203	alaskitic aplit

TABLE III

e Rocks of the Big Timber Stock

ight % Oxides

Basalt	Andesitic Phase									
C063	C162	C023	C013	C073	C083	C093	C033	C113	C093	C043	C103
50.17	55.67	55.85	56.04	56.13	57.41	58.02	58.69	58.89	59.33	60.04	60.27
2.29	1.48	1.29	1.35	1.47	1.55	1.22	1.27	1.09	1.19	1.02	1.16
15.05	16.47	17.74	17.46	17.90	16.28	16.02	18.37	17.59	16.12	17.05	17.24
4.40	.31	2.38	2.28	2.79	3.21	2.74	.34	2.59	2.59	2.56	1.68
6.56	6.32	5.07	5.31	4.44	5.20	3.68	6.04	2.98	3.43	3.46	3.23
.31	.09	.21	.21	.26	.23	.19	.16	.23	.21	.21	.19
6.18	3.63	3.18	2.68	2.52	3.24	4.46	4.58	1.98	2.68	1.89	1.78
7.83	6.56	5.80	5.54	6.49	5.88	5.99	5.54	4.64	5.02	4.48	5.79
3.27	4.45	4.14	4.13	4.18	4.10	3.85	3.78	4.62	4.05	4.47	4.77
2.23	2.83	2.48	2.85	2.79	2.78	2.85	2.98	3.18	3.34	3.32	3.86
.71	.64	.72	.77	.67	.76	.56	.45	.78	.85	.67	.87
.18	.23	.29	.27	.19	.21	.17	.21	.25	.23	.22	.26
99.18	98.68	99.15	98.89	99.83	99.86	99.75	99.41	98.82	99.04	99.37	99.10
11.17	7.72	10.35	10.13	10.84	10.55	9.24	7.25	10.50	9.84	10.22	9.43
11.68	7.71	8.01	8.18	7.72	8.99	6.82	7.03	5.90	6.40	6.42	5.27

nerals recalculated to 100%

.00	.00	4.89	5.02	4.81	6.27	7.22	5.56	8.29	10.20	9.73	7.93
13.31	16.99	14.82	17.08	16.55	16.48	16.91	17.75	19.06	19.97	19.79	23.08
27.95	38.24	35.43	35.43	35.49	34.81	32.71	32.24	39.66	34.68	38.14	40.83
20.00	16.87	22.76	20.97	21.92	17.87	18.09	16.30	18.12	16.13	16.74	13.85
6.27	5.16	.86	.96	2.69	2.89	3.53	3.65	.24	1.67	.71	.00
4.31	2.53	.48	.49	1.58	1.52	2.35	1.97	.16	1.12	.42	.00
1.46	2.54	.34	.44	.98	1.29	.65	1.56	.06	.43	.26	.00
9.28	5.91	7.53	6.28	4.72	4.08	8.60	9.53	4.84	5.64	4.33	4.48
3.14	5.93	5.33	5.67	2.94	3.48	2.19	7.53	1.93	2.18	2.71	3.02
1.37	.52	.00	.00	.00	.00	.00	.00	.00	.00	.00	.00
.51	.57	.00	.00	.00	.00	.00	.00	.00	.00	.00	.00
6.44	.46	3.49	4.35	4.06	4.67	3.99	.50	3.81	3.80	3.74	3.81
4.39	2.86	2.48	2.60	2.80	2.97	2.33	2.43	2.10	2.29	1.95	2.23
1.57	1.42	1.59	1.71	1.47	1.67	1.23	.99	1.73	1.88	1.48	1.52
.18	.23	.29	.27	.19	.21	.17	.21	.25	.23	.22	.26
.00	.00	.00	.00	.00	.00	.00	.00	.00	.00	.00	.20
An_{41}	An_{31}	An_{30}	An_{37}	An_{38}	An_{34}	An_{36}	An_{34}	An_{31}	An_{32}	An_{34}	An_{33}

porphyritic-adamellitic aplite
icro-adamellite
damellitic aplite
granodioritic aplite
leskitic aplite

C063 augite-bearing, hornblende-spessartite
C162 uralite-augite-andesite
C023 augite-biotite-microdiorite
C013 porphyritic oligoclase-augite-andesite
C073 porphyritic andesite
C083 uralite-augite-hornblende-andesite
C093 augite-hypersthene-kersantite
C033 augite-uralite-kersantite
C113 augite-andesite
C093 hornblende-andesite
C043 hornblende-andesite
C103 hornblende-andesite

TABLE

Chemical Analysis of Dike Rocks

% Ioni

Aplitic Phase

Basalt

Sample No.	B432	B422	B462	B332	B222	B402	B292	B312	B193	B262	B203	C063
Si^{4+}	29.30	30.31	30.93	31.06	31.70	31.84	32.04	32.43	33.00	33.69	35.92	23.45
Ti^{4+}	.50	.41	.38	.33	.31	.34	.24	.28	.20	.19	.05	1.37
Al^{3+}	9.08	8.53	8.43	8.53	8.86	7.82	8.17	7.69	7.90	7.34	6.50	7.96
Fe^{3+}	1.60	1.29	1.17	1.06	.64	.61	.83	.79	.87	.73	.00	3.28
Fe^{2+}	1.96	1.86	1.64	1.42	1.46	1.83	.96	1.07	.79	.61	.55	5.09
Mn^{2+}	.06	.05	.06	.03	.03	.03	.03	.05	.00	.01	.00	.24
Mg^{2+}	1.08	1.10	.56	.59	.35	1.33	1.05	.62	.25	.25	.00	3.72
Ca^{2+}	1.91	1.50	1.50	1.73	1.44	1.45	1.44	1.37	1.24	.75	.15	5.60
Na^{2+}	3.81	3.48	3.88	3.55	3.59	3.31	3.43	3.17	2.98	2.84	3.06	2.42
K^{1+}	3.22	3.09	3.42	3.05	3.94	2.82	2.77	3.56	3.57	4.46	3.48	1.85
P^{5+}	.21	.31	.20	.31	.15	.31	.21	.20	.24	.18	.12	.40
O^{-2}	46.74	47.01	47.24	47.35	47.97	47.77	47.92	47.70	48.09	48.11	49.03	43.76
$Fe^{2+} + Fe^{3+}$	3.57	3.16	2.81	2.48	2.11	2.45	1.79	1.87	1.66	1.35	.55	8.38

% Cationic recalcu

Si^{4+}	66.74	69.26	70.41	70.93	71.48	72.33	73.26	73.96	74.97	76.47	81.65	52.69
Ti^{4+}	1.18	.99	.91	.79	.72	.80	.58	.66	.49	.45	.14	3.19
Al^{3+}	15.49	14.60	14.37	14.59	14.98	13.31	14.00	13.15	13.45	12.49	11.08	13.41
Fe^{3+}	2.85	2.31	2.08	1.90	1.14	1.09	1.49	1.42	1.54	1.30	.00	5.75
Fe^{2+}	3.22	3.06	2.68	2.33	2.38	2.99	1.58	1.75	1.29	1.00	.91	8.23
Mn^{2+}	.10	.08	.10	.06	.04	.05	.06	.08	.00	.02	.00	.38
Mg^{2+}	1.28	1.31	.67	.70	.41	1.57	1.25	.73	.29	.29	.00	4.35
Ca^{2+}	2.66	2.10	2.08	2.40	1.98	2.01	2.01	1.90	1.72	1.04	.21	7.66
Na^{1+}	2.82	2.58	2.87	2.63	2.63	2.44	2.55	2.35	2.20	2.10	2.26	1.77
K^{1+}	3.24	3.12	3.43	3.07	3.92	2.82	2.79	3.58	3.58	4.47	3.49	1.83
P^{5+}	.37	.54	.36	.54	.26	.54	.38	.36	.41	.32	.22	.68

Notes:
1. Sample locations are shown on map in pocket. For sample descriptions see Table III.
2. Non-classical analytical methods employed; principally absorption and flame spectrophotometric and volumetric.
3. Analyses performed on samples dried for 4 hours at 110°C.
4. Analyses were performed at the Geology Laboratory, University of Cincinnati.
5. John Tappe, analyst.

TABLE IV

s of Dike Rocks of the Big Timber Stock

% Ionic

	Basalt	Andesitic Phase										
3203	C063	C162	C023	C013	C073	C083	C053	C033	C113	C093	C043	C103
5.92	23.45	26.02	26.10	26.19	26.23	26.83	27.12	27.43	27.52	27.73	28.06	28.17
.05	1.37	.88	.77	.80	.88	.93	.73	.76	.65	.71	.61	.69
6.50	7.96	8.71	9.38	9.24	9.47	8.61	8.47	8.13	9.30	8.53	9.01	9.12
.00	3.28	.23	1.77	1.70	2.08	2.39	2.04	.25	1.93	1.93	1.91	1.25
.55	5.09	4.91	3.94	4.12	3.45	4.04	2.86	4.69	2.31	2.66	2.68	2.51
.00	.24	.06	.16	.16	.20	.17	.14	.12	.17	.16	.16	.14
.00	3.72	2.18	1.91	1.61	1.51	1.35	2.68	2.76	1.19	1.61	1.13	1.07
.15	5.60	4.69	4.14	3.96	4.64	4.20	4.28	3.96	3.31	3.59	3.20	2.71
3.06	2.42	3.30	3.07	3.06	3.10	3.04	2.85	2.80	3.42	3.00	3.31	3.53
3.48	1.85	2.34	2.05	2.36	2.31	2.30	2.36	2.47	2.63	2.77	2.75	3.20
.12	.40	.36	.40	.43	.37	.42	.31	.25	.43	.47	.37	.49
9.03	43.76	44.94	45.39	45.21	45.54	45.52	45.85	45.75	45.88	45.83	46.12	46.17
.55	8.38	5.14	5.71	5.82	5.53	6.43	4.90	4.94	4.24	4.59	4.59	3.76

ationic recalculated to 100%

1.65	52.69	59.66	59.30	59.54	59.04	59.95	61.34	62.31	62.93	63.03	63.61	64.37
.14	3.19	2.10	1.82	1.90	2.05	2.16	1.71	1.79	1.54	1.68	1.43	1.64
1.08	13.41	14.97	15.98	15.73	15.97	14.42	14.36	13.84	15.94	14.52	15.30	15.62
.00	5.75	.41	3.14	3.01	3.65	4.17	3.60	.44	3.44	3.42	3.37	2.23
.91	8.23	8.09	6.43	6.74	5.58	6.49	4.65	7.66	3.80	4.35	4.38	4.12
.00	.38	.11	.26	.26	.32	.28	.23	.20	.29	.26	.26	.23
.00	4.35	2.60	2.26	1.91	1.77	1.56	3.16	3.26	1.41	1.90	1.34	1.27
.21	7.66	6.55	5.74	5.48	6.36	5.72	5.90	5.48	4.62	4.97	4.42	3.77
2.26	1.77	2.45	2.26	2.26	2.26	2.20	2.09	2.06	2.54	2.21	2.44	2.62
3.49	1.83	2.37	2.06	2.37	2.30	2.27	2.36	2.47	2.66	2.78	2.75	3.23
.22	.68	.62	.69	.74	.64	.72	.54	.43	.76	.82	.64	.85

intermediate between the two. The principal differences are found in the amount of TiO_2 and Al_2O_3 present. In the basic border rocks TiO_2 is found in greater quantities than in most gabbroic rocks; Al_2O_3 falls intermediate between the average ultramafic and gabbroic rocks; and K_2O is significantly higher than in either ultramafic or gabbroic rocks. This latter fact may be explained by the late quartzo-feldspathic interstitial blebs found in many of the rocks of the basic border phase. Since these rocks show similarities to both the ultramafic pyroxenites and to gabbroic rocks, the significant differences in the aforementioned oxides may be explained by the later introduction of intermediate plagioclase through filter pressing (?) or through fractures. This would add additional Al_2O_3, Na_2O, and K_2O to the bulk rock composition.

The intermediate plutonic phase has chemistry similar to the pyroxene-mica-diorites reported by Nockolds (1954). This series of rocks varies from meladiorites to leucodiorites with the principal mafic constituent being hornblende; however, no chemical similarities could be found between this rock group and the hornblende-diorites documented by Nockolds. The higher silica content may be attributed to assimilation at depth of crustal material rich in silica. Silica-rich material has been found in the later basaltic rocks as xenoliths of feldspathic-quartzite, but

no similar xenoliths have been found in the early basic or intermediate plutonic phases. Most dioritic rocks are considered to be hybrids (Johannsen, v.III, 1937, p. 146 and Deer, 1935), caused by the mixing of mafic magma constituents with acidic magma. Flow structures and xenolithic material found in the outer margins of the intermediate phase show some degree of assimilation of more mafic constituents, causing this rock suite to display some signs of hybridization.

The terminal plutonic phase (Table I) shows more extreme alkali and silica enrichment than the other plutonic igneous phases. In spite of the fact that only three samples have been collected, the abrupt increase of silica and alkali over the intermediate phase is apparent. With additional collecting and chemical analysis a relationship may either be confirmed or denied between the terminal plutonic phase and either the intermediate plutonic phase or the aplitic phase.

The only basaltic rock which has been analyzed shows strong chemical similarities to a basalt intermediate between tholeiite and alkali basalts. The analyzed basalt from the Big Timber complex shows higher TiO_2 and lower CaO than normal tholeiite basalts (Yoder and Tilley, 1962) and a large excess of K_2O. This latter excess could be attributed to the introduction of K_2O from xenolithic feldspathic

quartzites, as seen in Figure 53. Additional collecting and chemical analysis will be required to determine whether or not there is a relationship between the basaltic rocks and the other rocks within the complex. At the present time no obvious field or chemical relationship has been detected.

The aplitic dike phase shows chemical variations almost identical to those of the granite clan of Nockolds (1954). Since these rocks are quartzo-feldspathic and contain few mafic constituents, no unusual characteristics have been found in them.

The andesitic dike phase shows a rather broad chemical variation, with samples C033 and C053 being similar to quartz-basalts except for a greater amount of SiO_2. All the other rocks in this group are similar to other oligoclase-andesites (See Figure 70).

Ionic Weight Percent Diagrams

There have been many methods developed for the presentation of chemical data. The writer has chosen to present them using ionic weight percents as described by Green and Poldervaart (1958). This method allows the reader to compare quickly the similarities and differences between the rocks comprising the Big Timber igneous complex and the average rocks as computed by Green and Poldervaart. The ionic weight percents of the elements for the rocks of the Big Timber

complex are presented in Tables II and IV.

Figures 61 through 66 are a series of ionic variation diagrams on which data from the Big Timber igneous complex have been plotted. On these diagrams, which are identical to those of Green and Poldervaart, are shown both Green and Poldervaart's average igneous rock trends and annotated points corresponding to rock samples whose analyses are shown in Tables II and IV. These figures also show the variation of the rocks of the complex with respect to aluminum, iron, magnesium, calcium, sodium, and potassium.

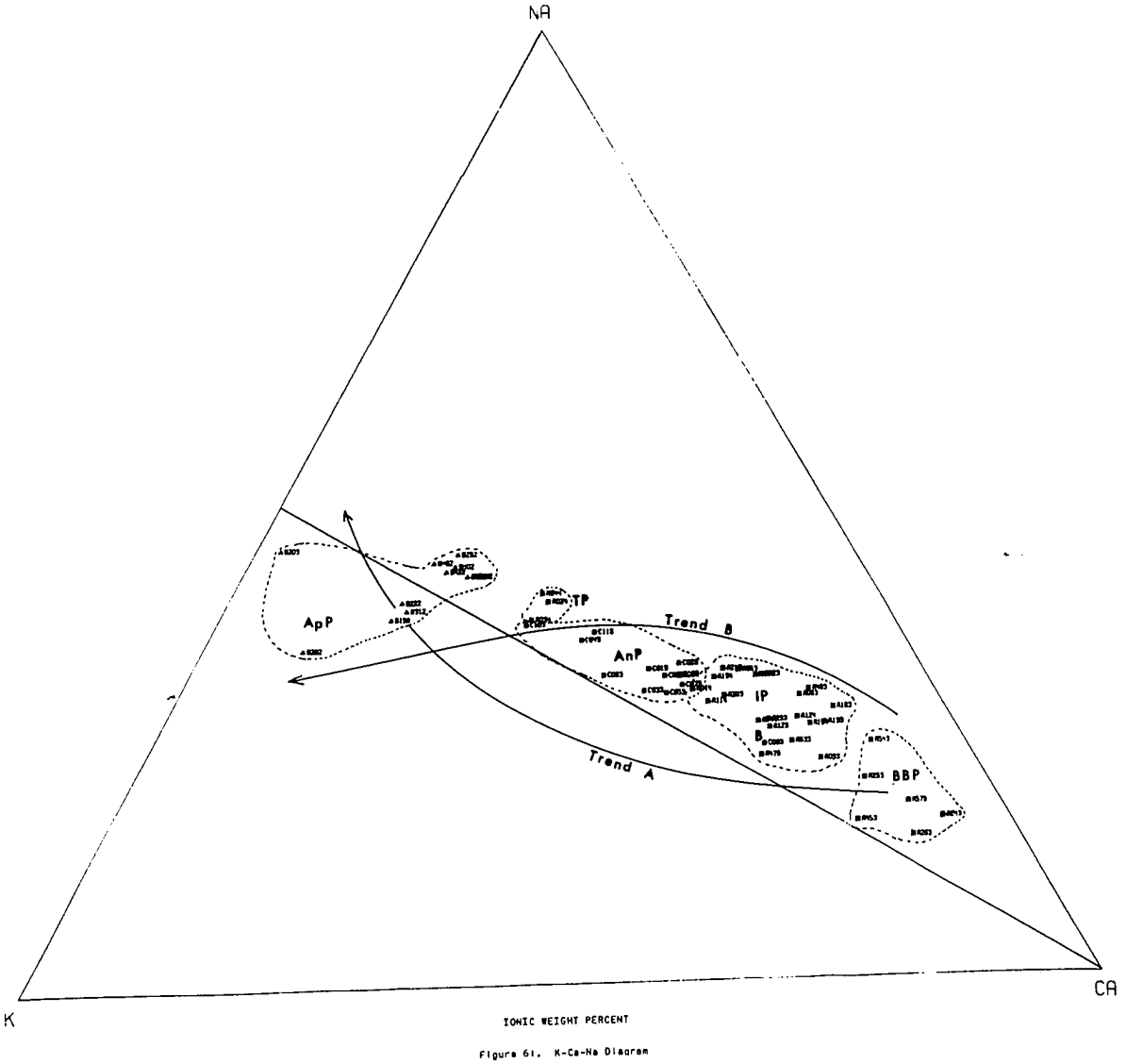

Figure 61. K-Ca-Na Diagram

Trend line(s) from Green and Poldervaart (1958)
(BBP=Basic Border Phase, IP=Intermediate Phase,
TP=Terminal Phase, B=Basalt,
ApP=Aplitic Phase, AnP=Andesitic Phase)
Sample numbers correspond to those on Tables I, II, III, & IV.

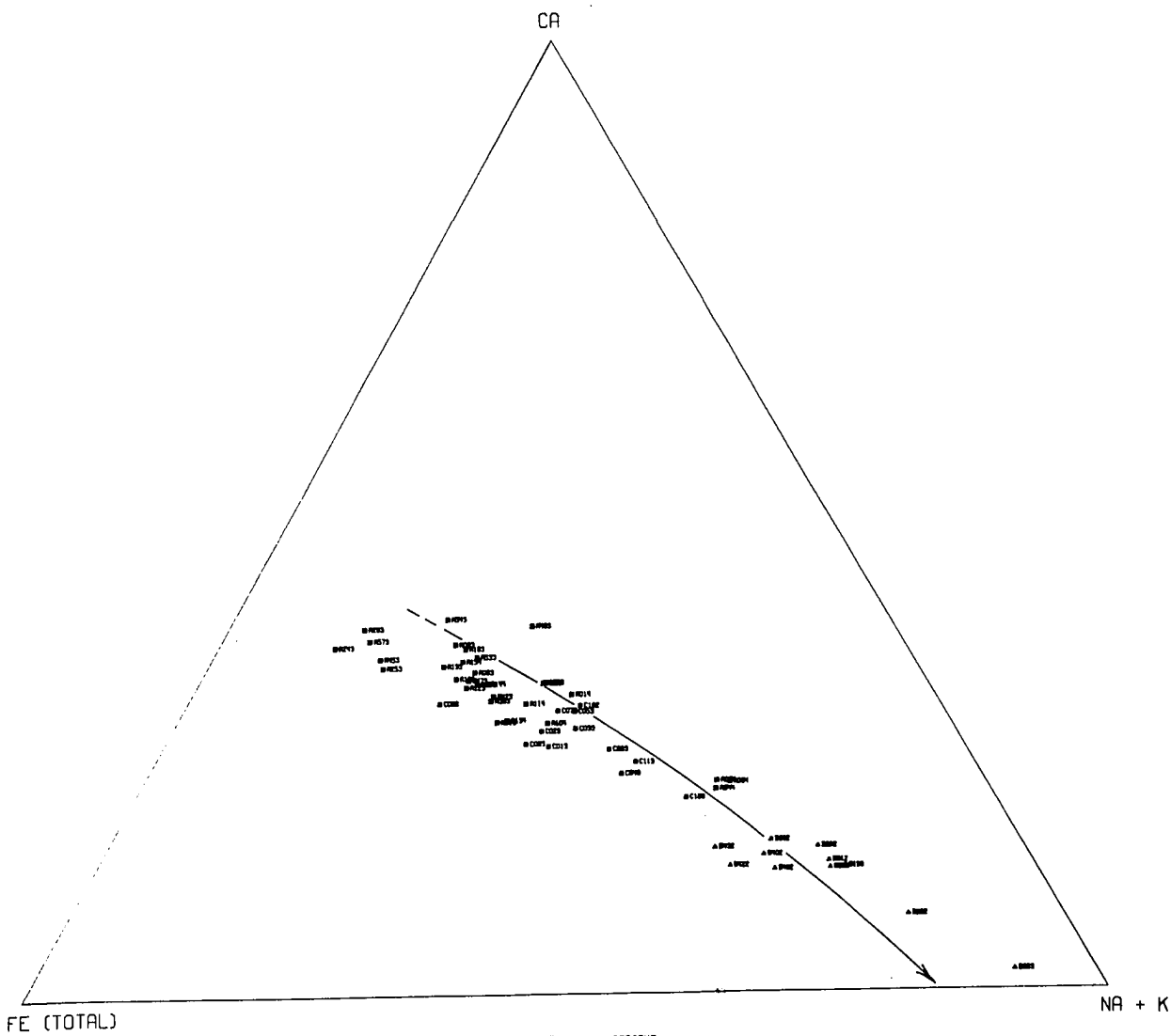

Figure 62. Fe (total)-Na+K-Ca Diagram
For explanation of symbols see Figure 61

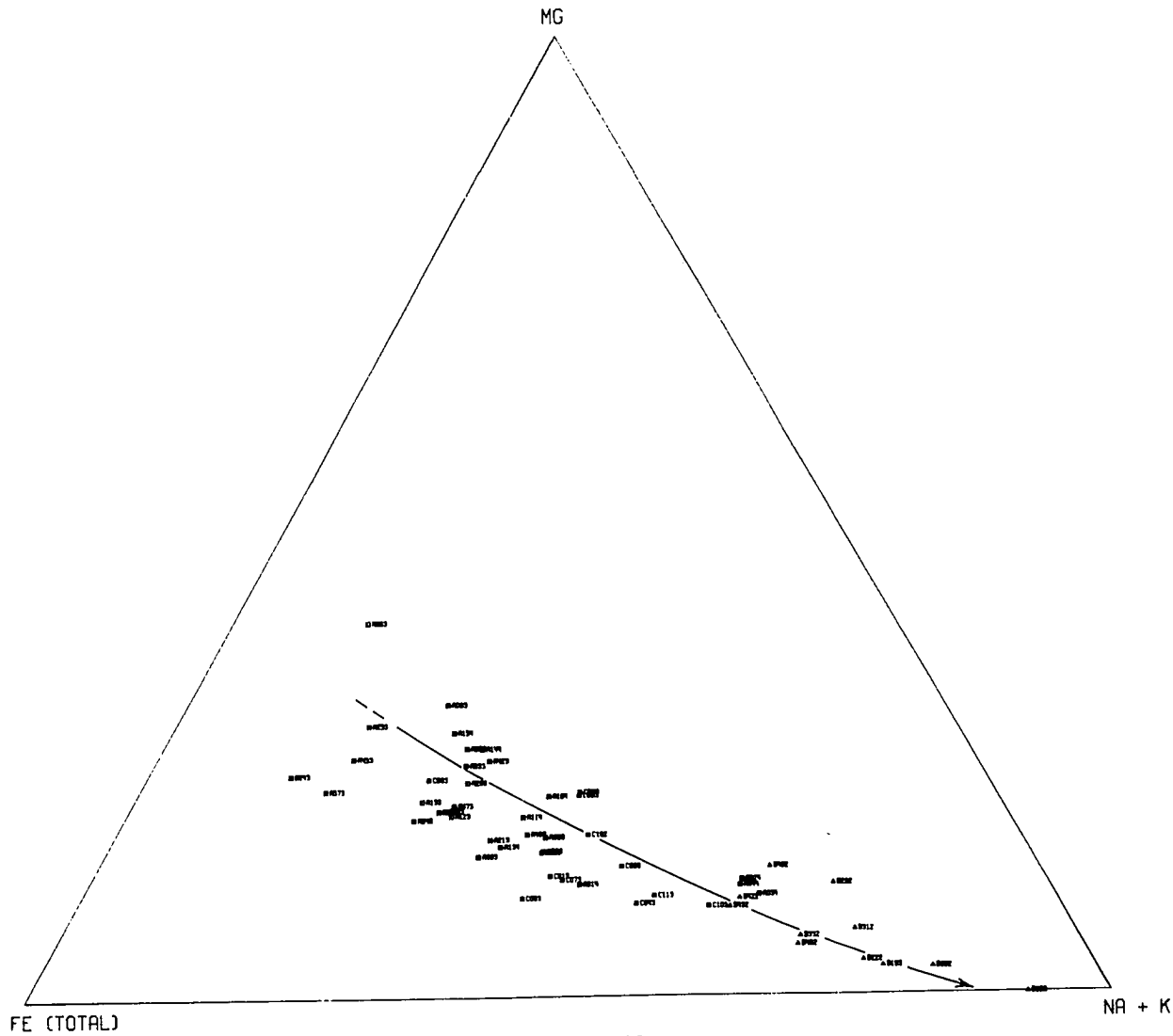

Figure 63. Fe (total)-Na+K-Mg Diagram
For explanation of symbols see Figure 61

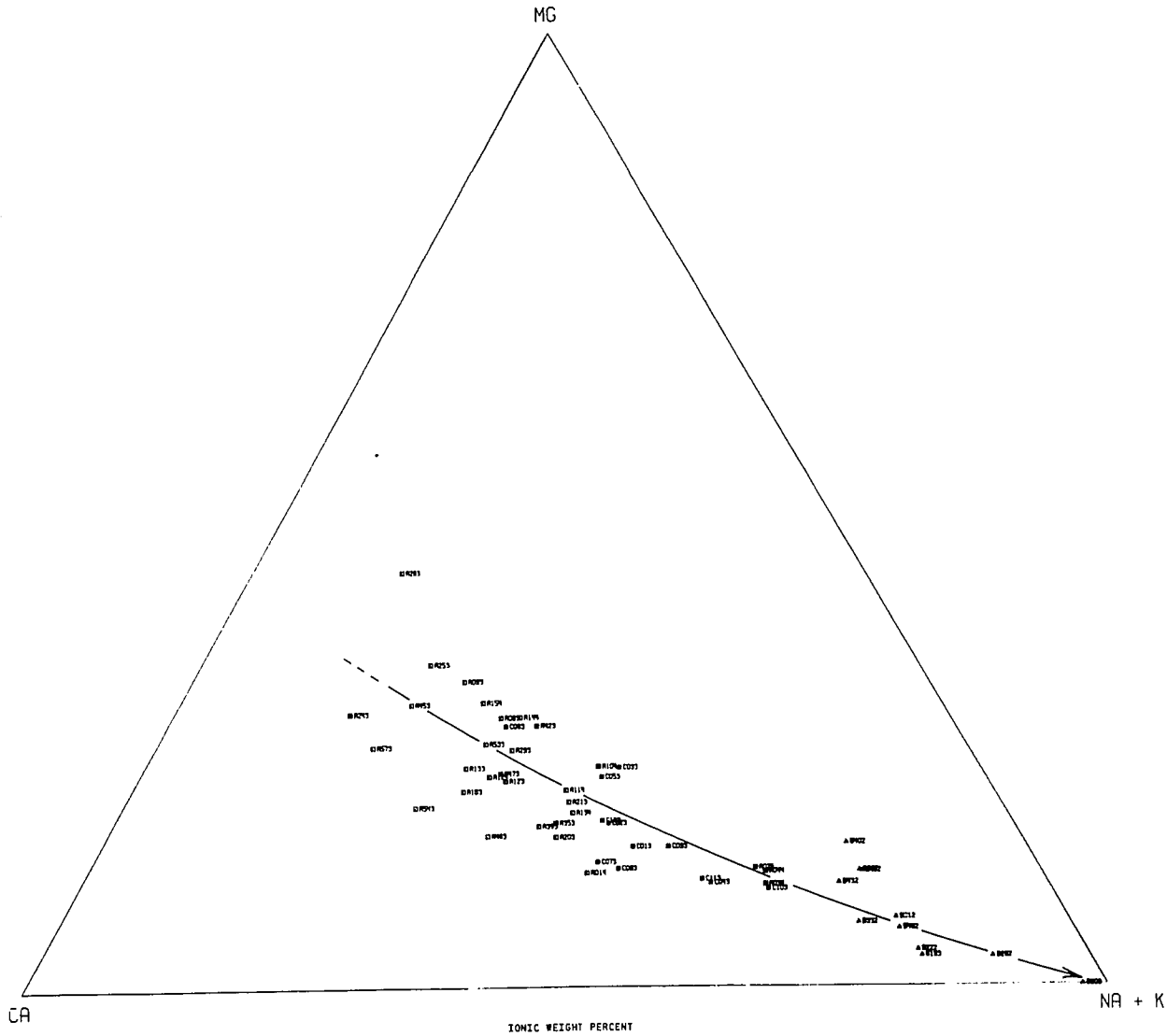

Figure 64. Ca-Na+K-Mg Diagram
For explanation of symbols see Figure 61

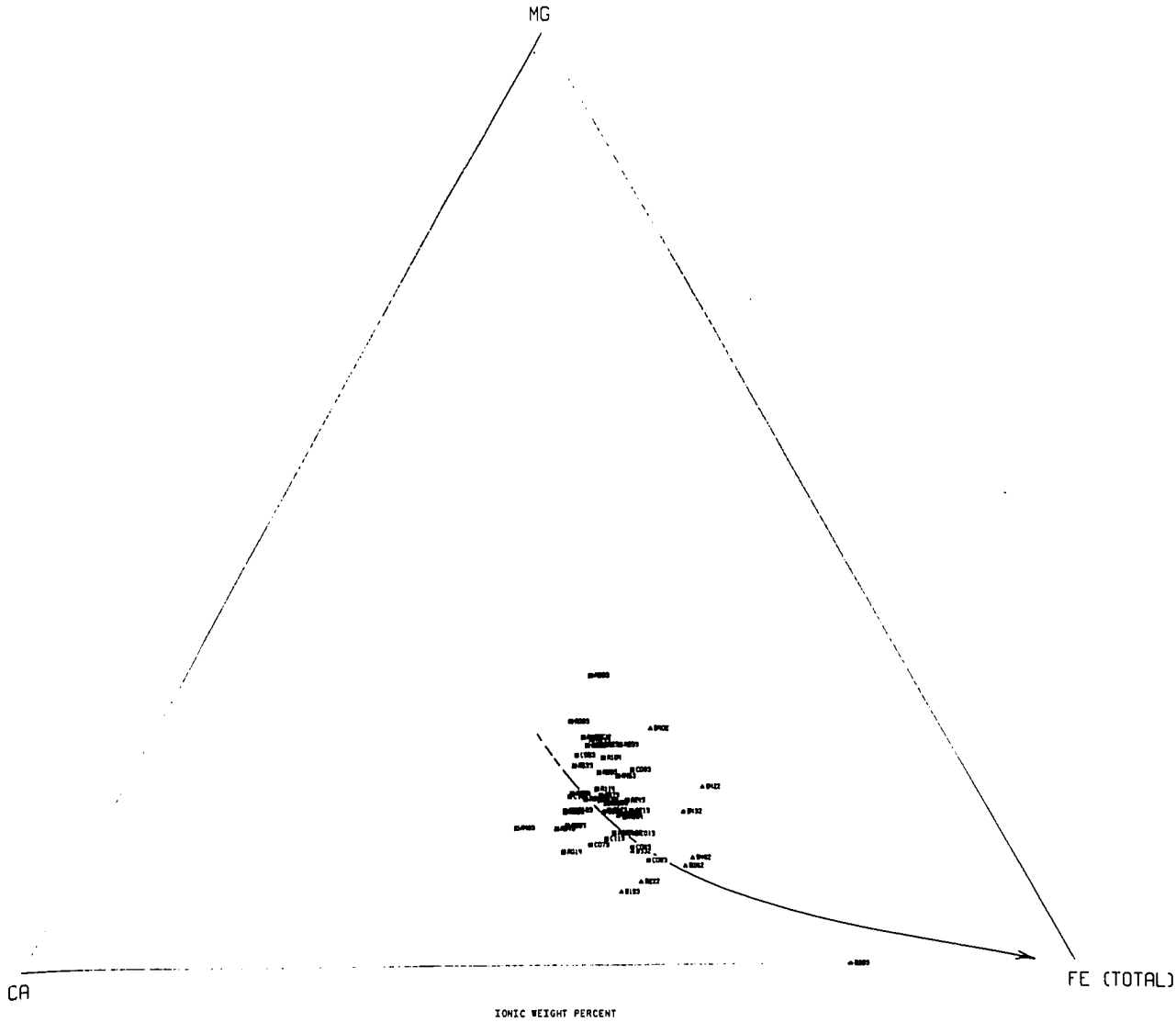

Figure 65. Ca-Fe (total)-Mg Diagram

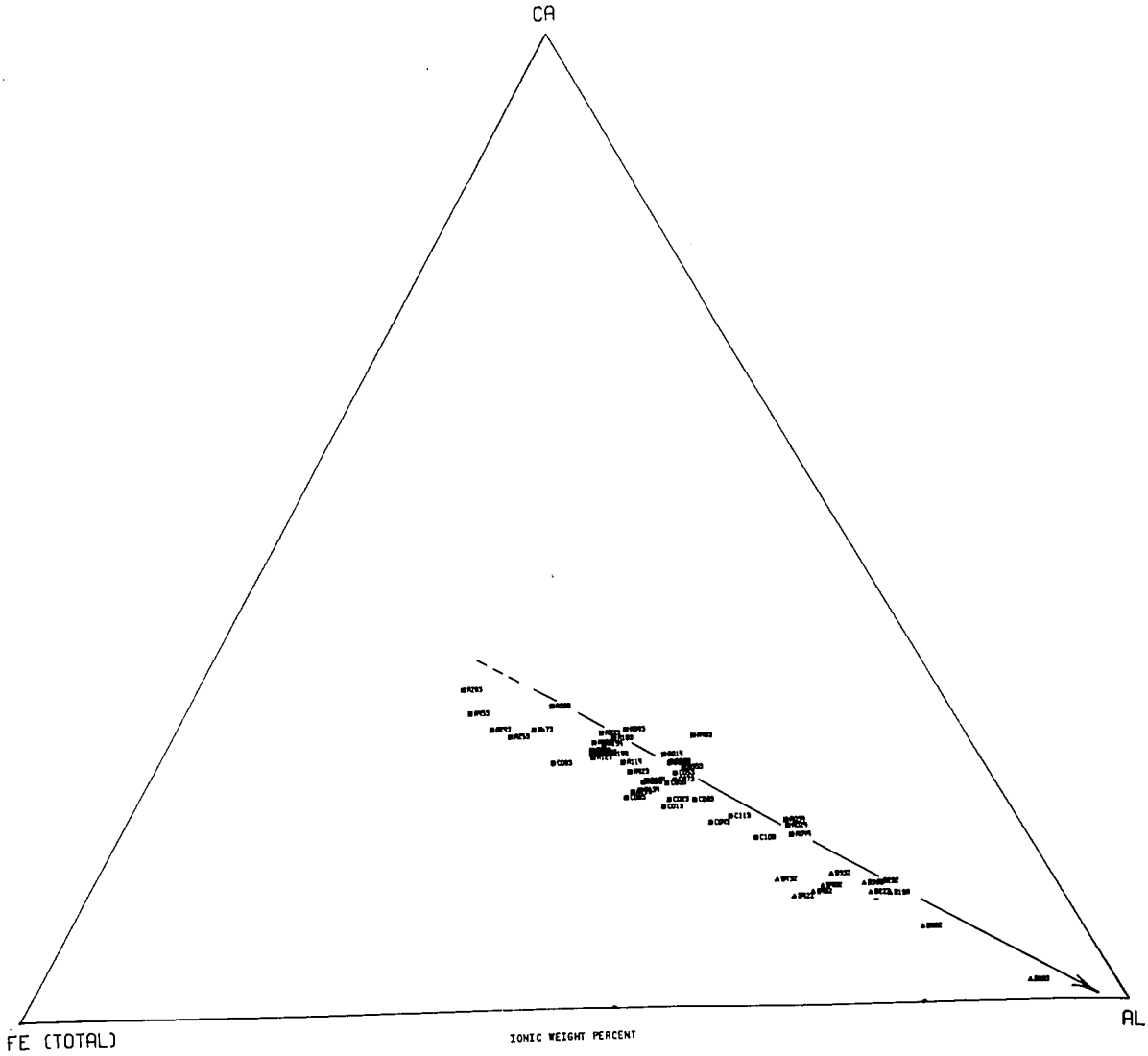

Figure 66. Fe (total)-Al-Ca Diagram
For explanation of symbols see Figure 61

VARIATION DIAGRAMS

Having examined the bulk chemistry of the Big Timber igneous complex, it is now necessary to examine each individual variation diagram in some detail.

Ionic Variation Diagrams

K-Ca-Na Diagram (Figure 61). On this diagram the points for each individual plutonic phase cluster closely together, forming their own individual field; compositely, however, the phases form a trend originating within the basalt field and terminating in the granodiorite field. This trend contains a rather conspicuous gap between the intermediate and terminal phases. The dike phases superpose this overall trend with the aplitic phase showing extreme alkali enrichment in an almost 1:1 ratio at the expense of Ca.

Green and Poldervaart (1958) have shown that when chemical data from all rock types are plotted on this diagram, the points are widely scattered but distributed equally on either side of a line joining the Ca corner with a point midway along the Na-K side of the diagram. From these data two prominent trends are depicted. Trend A in Figure 61 is a series of basalt-latite-trachyte-phonolite rock types typically found in oceanic domains, while Trend B is a series of basalt-andesite-dacite-rhyolite rock types

typically found within the continents. It can be seen in this diagram that the rocks comprising the early basic border phase fall entirely within the Green and Poldervaart basalt field. The intermediate plutonic phase shows rather tight grouping of points, somewhat intermediate between Trends A and B, failing to show the greater sodium enrichment common to continental rocks.

Not shown on this diagram is the trend line for the rocks of the northern part of the Crazy Mountain basin, computed by the writer from the analyses presented by Simms (1966); however, this trend shows initial similarities to the plutonic phases of the Big Timber complex. Since it culminates within the phonolite field, however, it is obvious that different physico-chemical processes were operative in the two areas during emplacement of the "phonolites" and the aplites.

Fe (total)-Na+K-Ca (Figure 62). As in Figure 61 above the points in Figure 62 for each individual plutonic phase cluster closely together. The composite trend shows a 1:1 iron (total) to Ca depletion ratio, trending toward the Na corner. As in Figure 61 there is a conspicuous gap between the intermediate and terminal phases. The andesitic dike phase essentially plots in the gap between the intermediate and terminal phases.

Fe (total)-Na+K-Mg (Figure 63). The points for each individual plutonic phase in Figure 63 show a greater amount of scatter than did those of Figures 61 and 62; however, they can be said to form discrete groups. If the diagrams presented by Poldervaart and Green are used as criteria, the Fe (total)-Na+K-Mg diagram should show the least scatter of all the diagrams presented. However, as noted above, there is a great deal of scatter present in this diagram, a discrepancy which can perhaps be explained by the influx of magnesium into the rocks of the Big Timber igneous complex.[1]

The overall trend of this diagram shows itself to be slightly more iron-rich than the average igneous rock trend. The basic border phase shows an individual trend of iron enrichment at the expense of magnesium (the normal iron enrichments trend). A noticeable gap exists between the basic border phase and the intermediate phase, and a smaller gap than in previous diagrams exists between the intermediate and terminal phases. The andesitic dike phase is slightly superposed over the intermediate phase.

Ca-Na+K-Mg (Figure 64). This diagram shows clustering similar to that in Diagram 63. The overall trend follows the average igneous rock trend of Green and Poldervaart. A

[1] The plotting of data from the northern part of the Crazy Mountain basin shows an even greater degree of scatter about the average igneous rock trend than in the southern area.

less distinct separation than previously noted is shown between the basic border phase and the intermediate phase, but a pronounced separation exists between the intermediate and terminal phases. The basic border phase shows a typical calcium enrichment trend which has been shown by Green and Poldervaart to exist between ultramafic rocks and basic igneous rocks.

Ca-Fe (total)-Mg Diagram (Figure 65). This diagram differs greatly from all those analyzed above due to the fact that it displays a rather concentrated point plot for all rocks of the Big Timber complex (except for the aplites which show a general iron depletion). Because of the tight cluster of all the points no obvious trend is present. A complete overlap and superposition of all rocks is present, indicating the general iron-rich character shown also in Figures 62, 63, and 66.

Fe (total)-Al-Ca Diagram (Figure 66). This figure shows very tight clusters for all the rocks of the plutonic phases of the Big Timber complex. Although the overall trend is a straight line toward the aluminum corner, it does show a slight iron-rich character. Of all the diagrams presented, this one shows the least scatter about the trend line. There is an overlap between the rocks of the basic border phase and those of the intermediate phase and a slight gap between the rocks of the intermediate phase and

terminal phase. The andesitic dike phase partially superposes the intermediate phase and fills in the gap between the intermediate phase and the terminal phase.

Oxide Variation Diagrams

Na_2O-CaO-K_2O Diagram (Figure 67). This diagram is similar to Figure 61 in that it shows the general trend of the igneous rocks of the Big Timber complex away from the CaO corner. This trend reveals the progressive enrichment of the alkalis Na_2O and K_2O in the residual liquid. Also shown is a slight convexity toward the Na_2O corner which is characteristic of calc-alkaline rocks. This diagram, commonly included in other papers in which sufficient chemical data is presented, is reproduced here so that the reader can compare results from other areas.

AMF Diagram (Figure 68). This AMF diagram is also presented for the purpose of comparing the relationship of alkali-magnesium-total iron with rocks from other areas. It can be seen from this diagram that the rocks from the early basic group, slightly enriched in Na_2O and K_2O, still show an initial trend similar to that of the Skaergaard (East Greenland) liquid (the "tholeiite rock series"). On the other hand, those rocks comprising the other phases within the Big Timber complex show an alkali enrichment trend similar to the calc-alkaline trend of Daly (1933) with the exception of a slight enrichment in FeO.

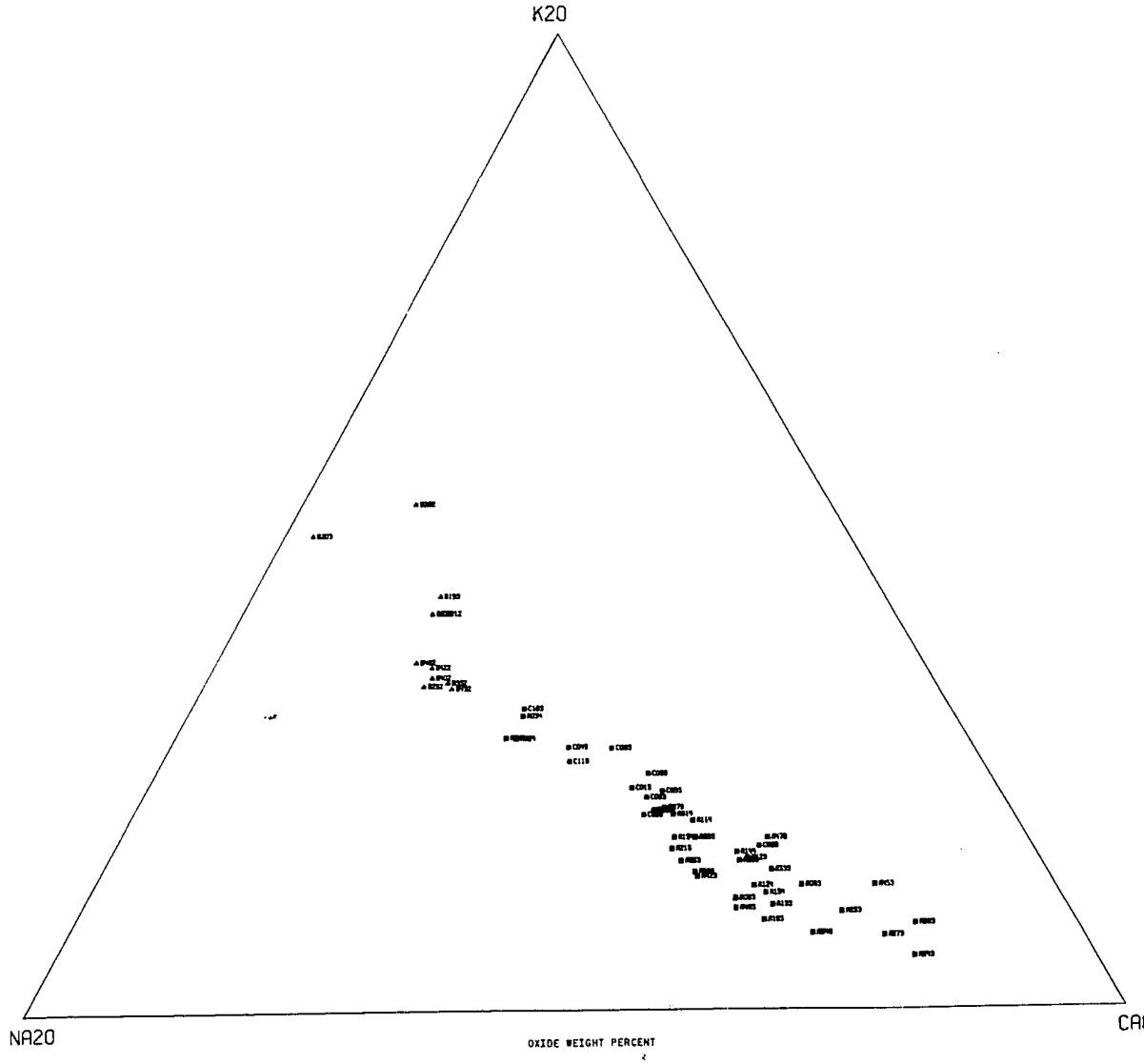

Figure 67. Na_2O-CaO-K_2O Diagram
For explanation of symbols see Figure 61

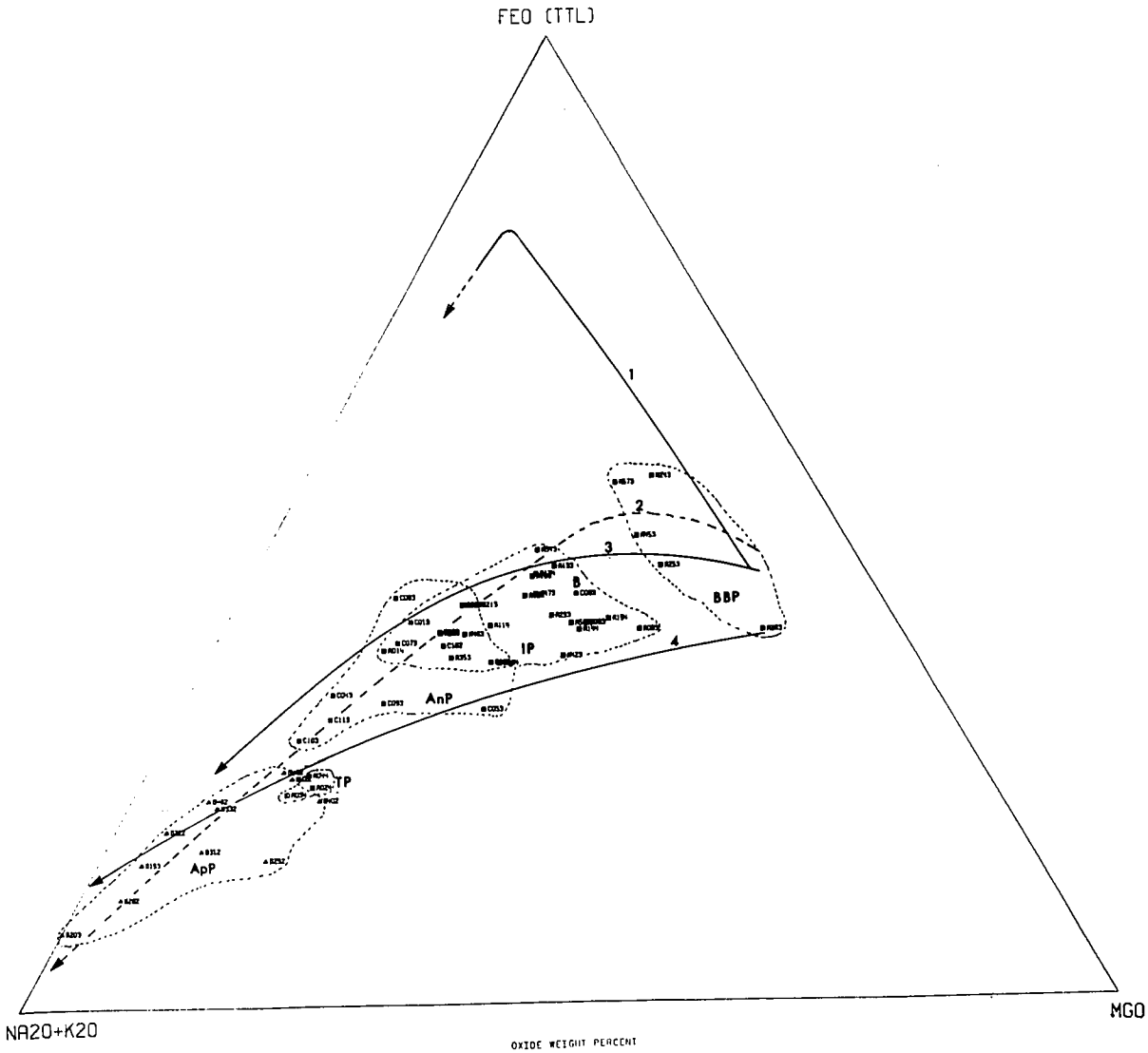

Figure 68. AMF Diagram
For explanation of symbols see figure 61

$Na_2O+K_2O-SiO_2$ Diagram (Figure 69). From the recent work by Kuno (1965) on the fractionation trends of basaltic magmas three distinct magma series were postulated. These three fields of basaltic magmas are shown by the solid lines on Figure 69, a diagram of total alkalis versus SiO_2. From the plot of the rock analyses of the Big Timber complex, it can be seen that all the rocks generally fall into the alkali basalt field. Also shown are trends from the Skaergaard and the Katmai Peninsula (Alaska). It is interesting to note that under Kuno's classification the rocks comprising the Skaergaard are classed as high alumina basalts, while those of the Katmai would be classed as tholeiites.[2]

Murata Diagram (Figure 70). To overcome the possibility of alkalis causing a scattering of points on the diagram, Murata (1960) has provided a new method of plotting the chemical data of rocks with basaltic affinities. This type of plot is shown in Figure 70 in which the effective separation of tholeiites and the alkali basalts is indicated. He concludes (p. 251) from the alignment of the various points for each series with a pyroxene (P) of fixed composition that the "fractional crystallization of clinopyroxene is the general mechanism for converting the tholeiitic magmas into alkalic magmas." From this graphical construction

[2] It is entirely possible that the rocks of the Katmai could have been intruded from depth without any additional influx of alkalis.

Figure 69. Na_2O+K20 Diagram. Fields are those of Kuno (1965). S=Skaergaard, K=Katmai. Sample numbers same as those on Tables I, II, III, and IV.

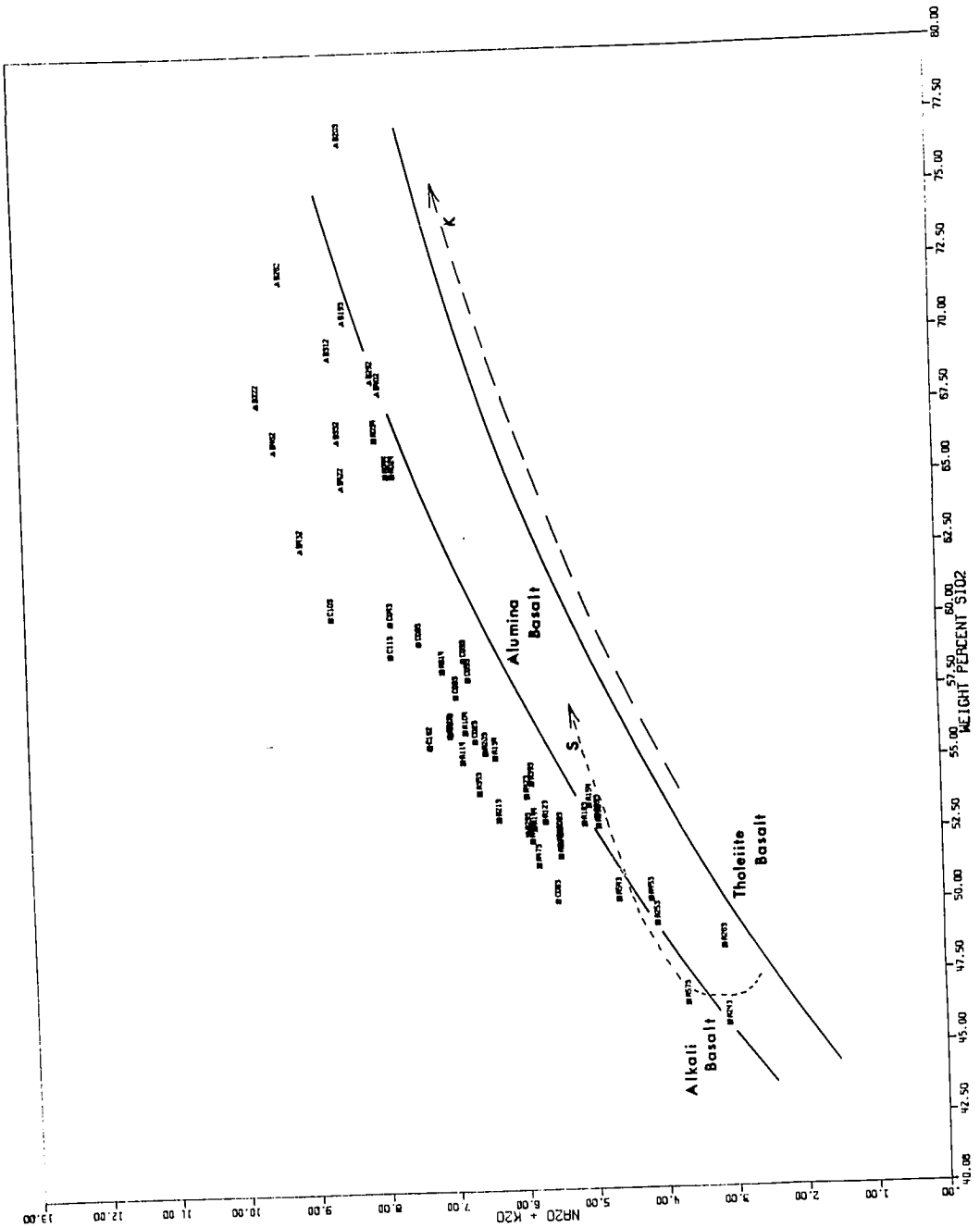

Figure 70. Murata Diagram (MgO-Alumina/Silica) P= Pyroxene. For explanation of symbols see Figure 61.

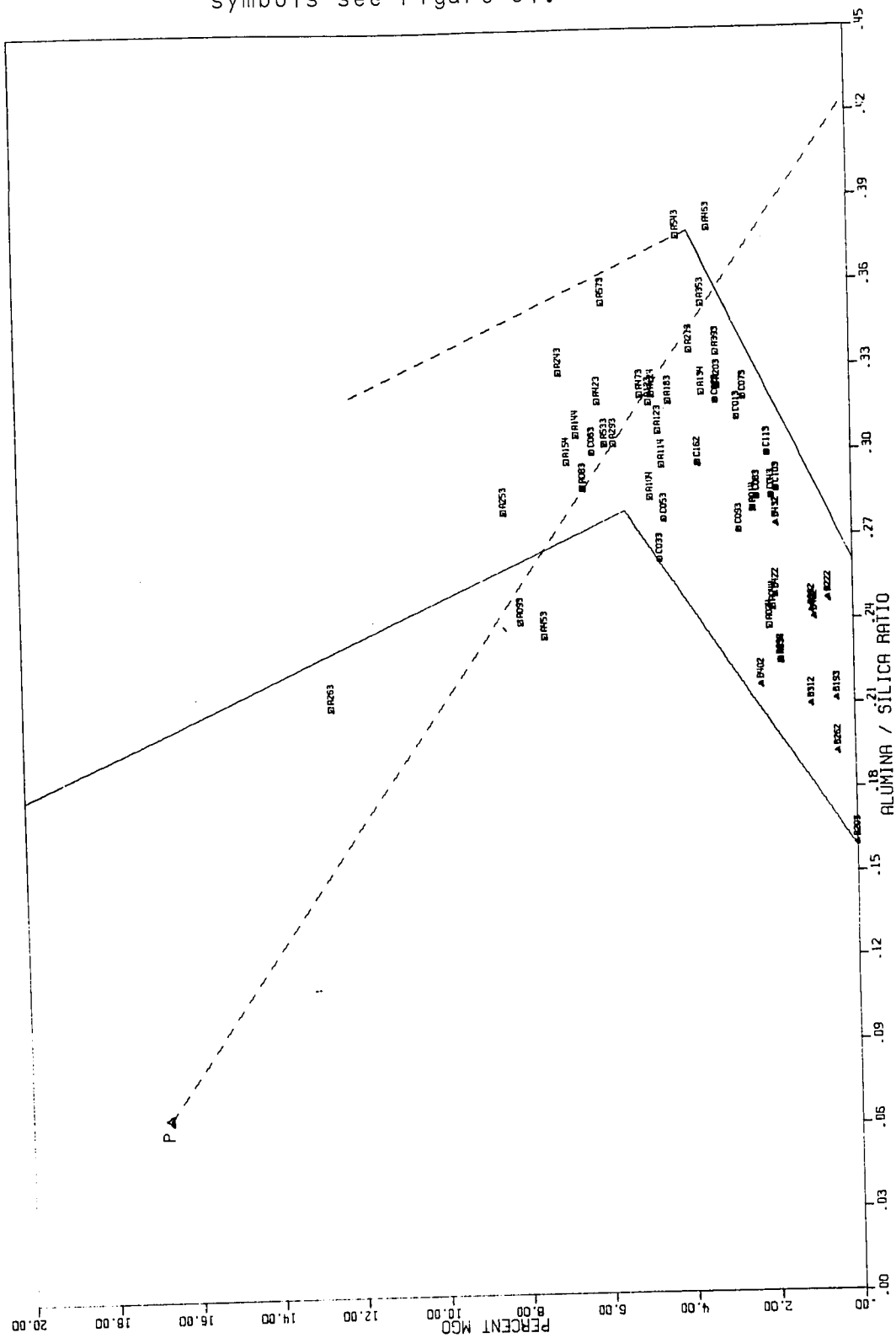

Murata concludes that if an appropriate amount of clinopyroxene is removed from the members of the tholeiitic series, one would plot corresponding points of alkali basalt. The more recent work of Yoder and Tilley (1962, p. 417) shows that with the removal of a clinopyroxene the resulting rock would still have tholeiitic affinities. However, this does not preclude the usefulness of the diagram as representing the bulk rock composition, free from the introduction of bias from the alkalis (See Simms, 1966).

$FeO+Fe_2O_3/FeO+Fe_2O_3+MgO-SiO_2$ Diagram (Figure 71). An extreme amount of scatter with no obvious trend is revealed in this diagram. Here again, magnesium introduced as a variable (See also Figure 65) makes correlation of the data with those of other areas difficult. Generally, however, two trends are present: (1) the early basic phase possesses a negative slope similar to that of the Skaergaard trend, and (2) the intermediate plutonic phase and part of the andesitic dike phase follow a trend similar to that found for the Thingmuli volcano (Iceland (Carmichael, 1964).

$FeO+Fe_2O_3-SiO_2$ Diagram (Figure 72). The differences among the several rock series within the pluton can best be illustrated by comparing total iron as FeO against weight percent silica (Osborn, 1962). This scatter diagram is shown in Figure 72. Comparing this diagram with Figure 73,

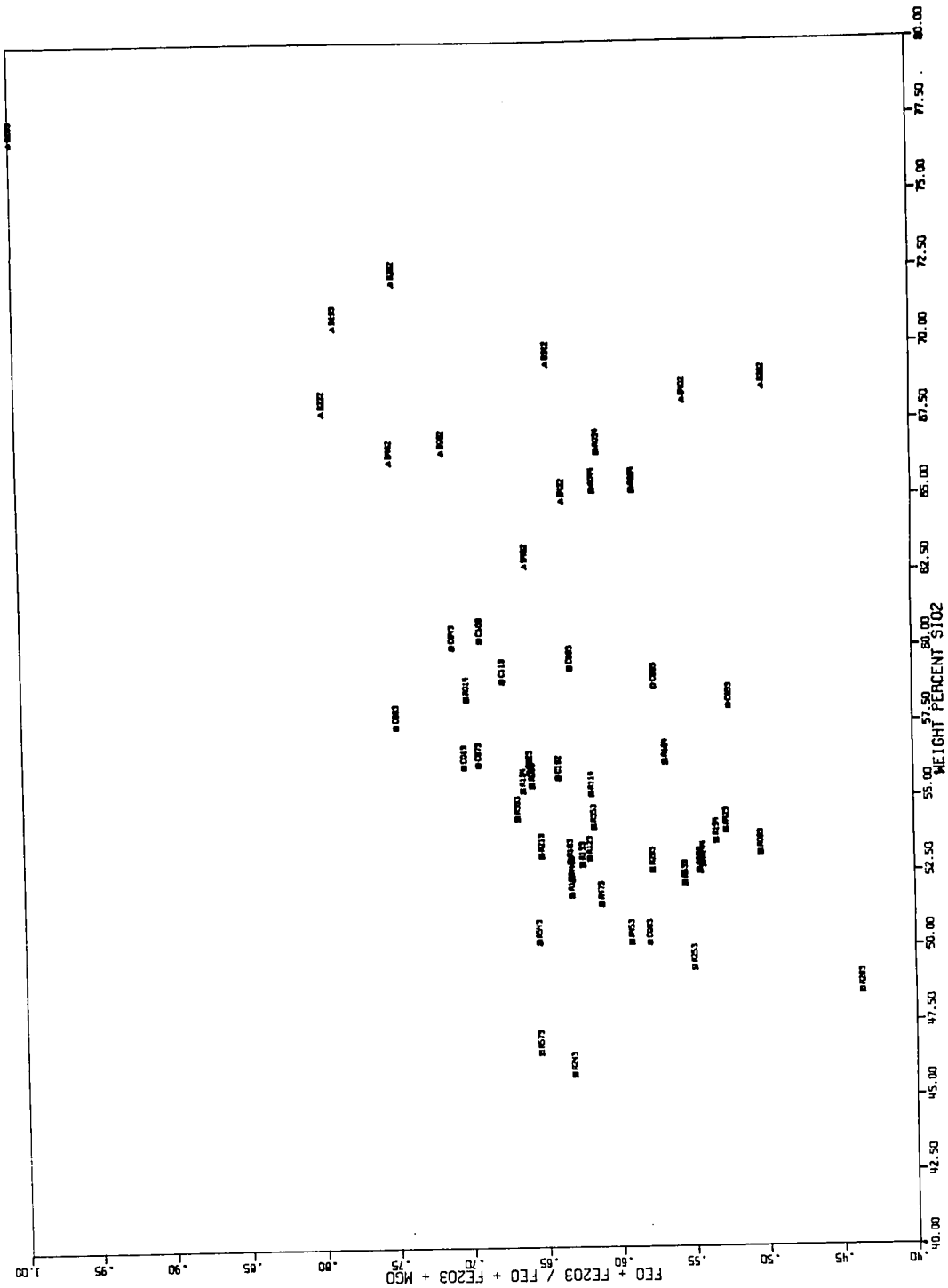

Figure 71. $FeO+Fe_2O_3/FeO+Fe_2O_3+MgO-SiO_2$ Diagram.
For explanation of symbols see Figure 61.

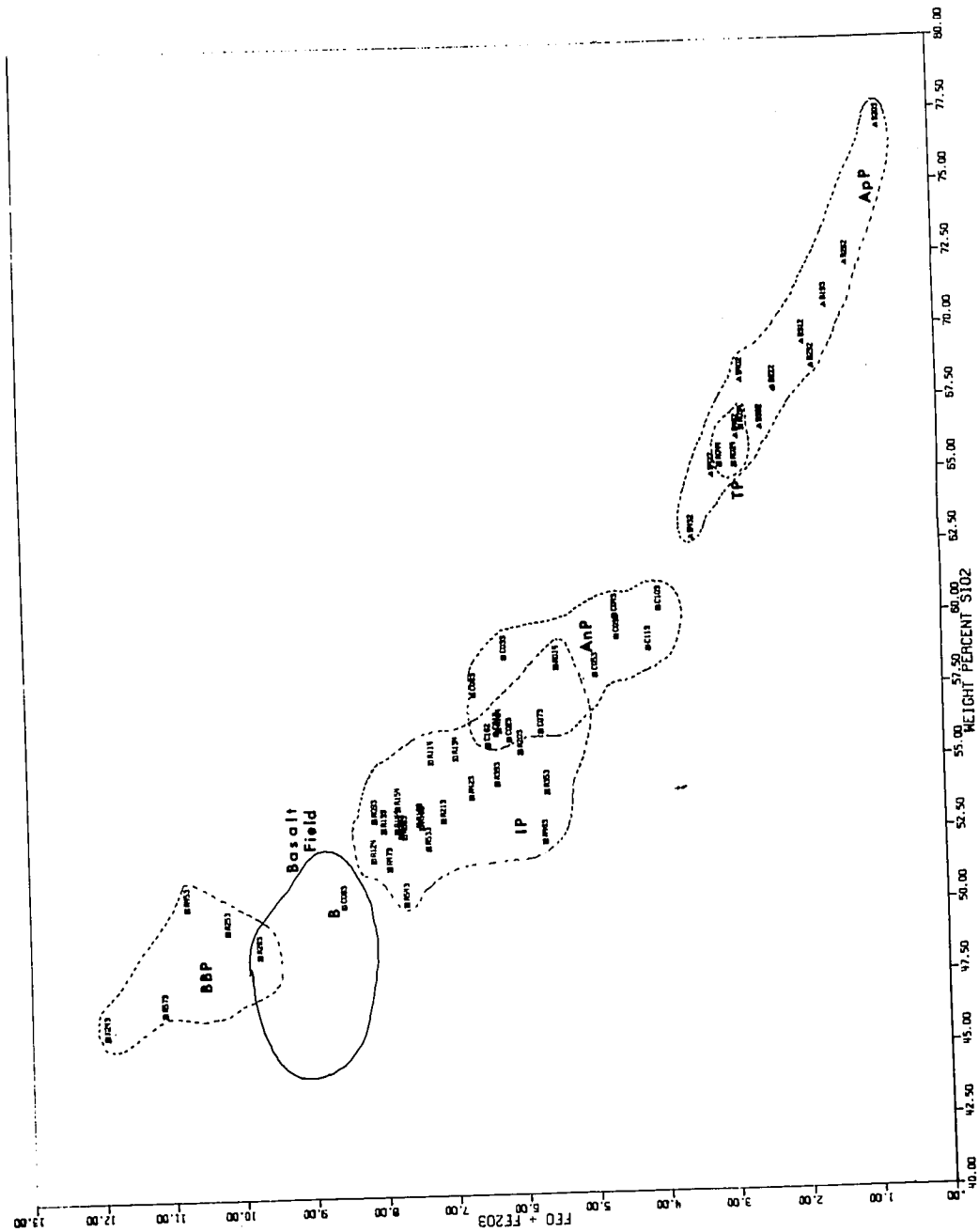

Figure 72. $FeO+Fe_2O_3-SiO_2$ Diagram.
Compare with Figure 73.
For explanation of symbols see Figure 61.

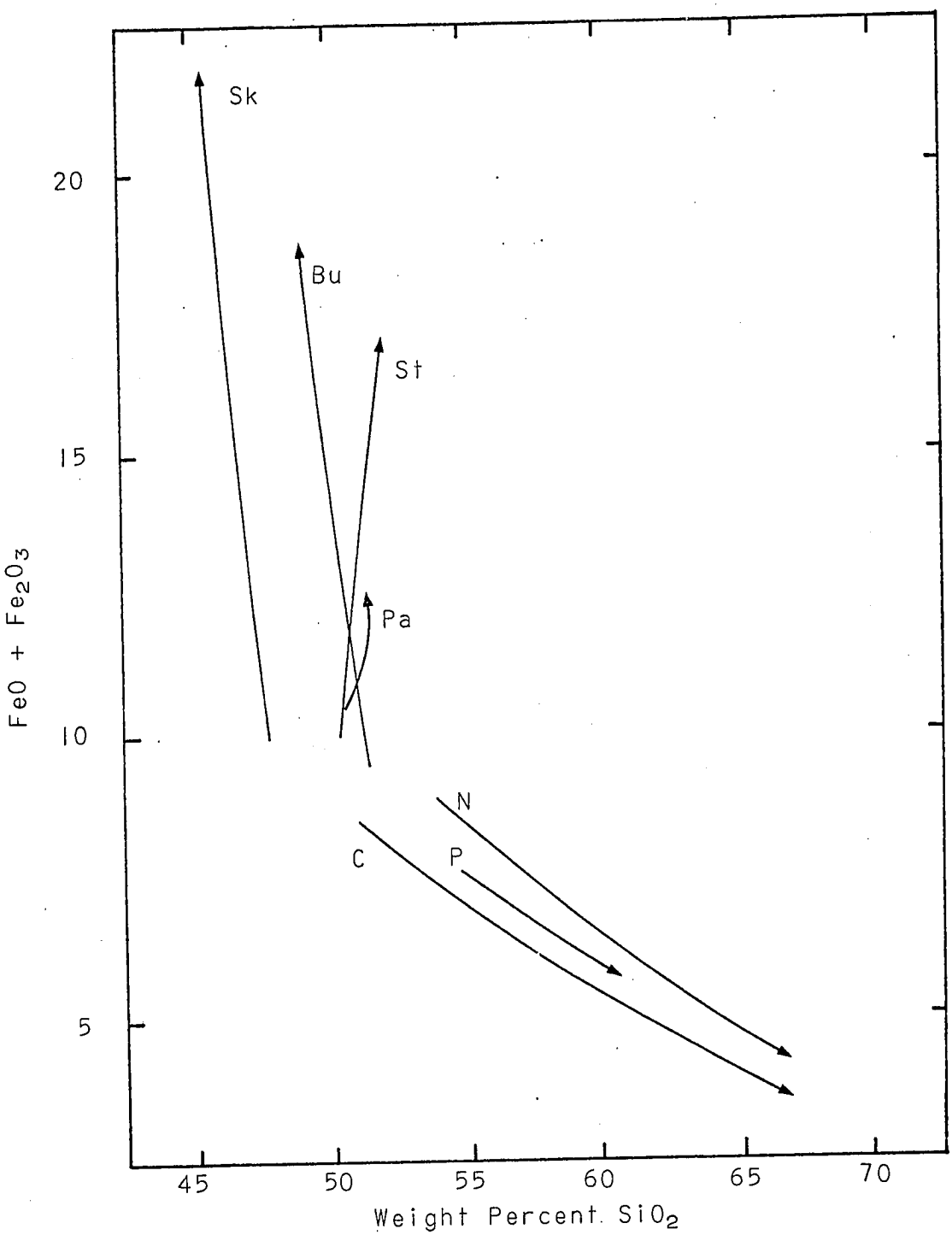

Figure 73. Two groups of rock series. Compare with Figure 72. Sk=Skaergaard liquids, Bu=Bushveld, St=Stillwater, Pa=Palisade diabase, N=Nockolds' averages, P=Paricutin lavas, C=Cascades series. (From Osborn, 1962)

it can readily be seen that two, and possibly three, phases of plutonic activity (in addition to the aplitic phase), plus two phases of post-plutonic dikes (basalt and andesite) are present for the Big Timber complex. If the same point of origin is used as in Osborn's figure (Figure 73), two distinct trends, both originating in the basalt field, become obvious. The five rocks comprising the basic border group have an iron-enrichment trend (fractionation-differentiation) which is moving toward the upper part of the diagram. The remainder of the series has a calc-alkaline (silica-enrichment trend). The iron enrichment trend corresponds closely to the trend of the Skaergaard, Bushveld (South Africa), Palisades Sill (New Jersey) and Stillwater (Montana), while the silica enrichment trend compares favorably with those of the Paricutin (Mexico), the Cascades series (Northwestern United States), and Nockolds' averages (1954).

Sugimura Diagram (Figure 74). Sugimura (1960) has recently shown that by plotting weight percent SiO_2 versus the cationic equivalent ratio $(Na_2O+K_2O)/Al_2O_3$, the latter being a general expression of the amount of normative alkali feldspar, several interesting relationships for the enrichment of alkalis in the crystallization sequence emerge. Sugimura plotted the chemical analyses for several volcanoes found in Japan on which sufficient analyses had

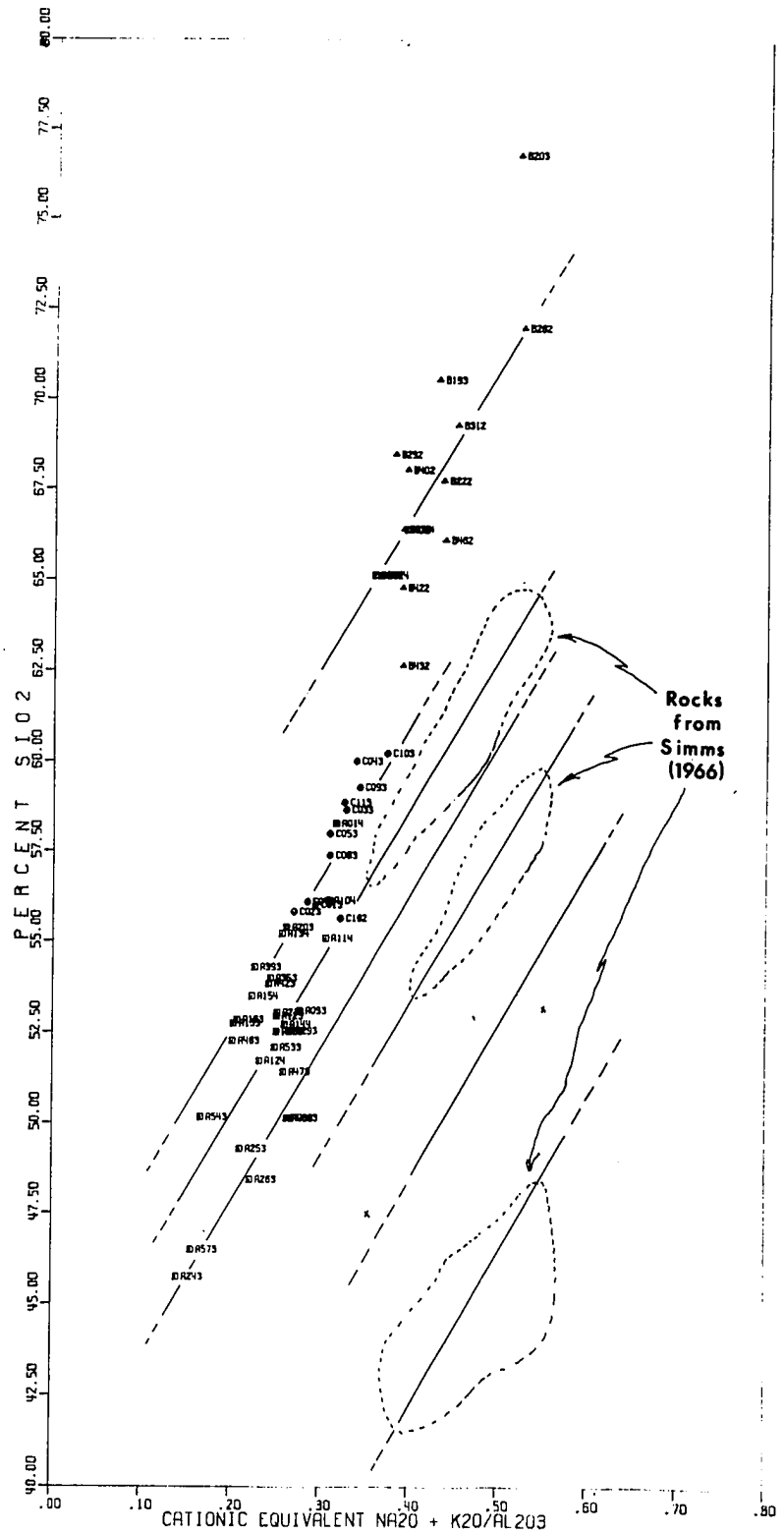

Figure 74. Sugimura Diagram
For explanation of symbols see Figure 61

already been performed. By applying the method of least squares to the data so plotted, a series of regression lines ($y = a+bx$) were fitted to the data for each of these volcanoes. In this calculation x = the molecular proportion of $(Na_2O+K_2O)/Al_2O_3$ and y = weight percent SiO_2. From this regression analysis Sugimura found that for each of the volcanoes with sufficient chemical data the value for b equalled 47. He then proceeded to evaluate the volcanoes in and around Japan, working on the basic assumption that all the lines of regression were parallel. For some volcanoes two or three parallel lines of regression were present with each subsequent line showing an increase in silica.

Data for both the Big Timber igneous complex and for the rocks within the northern part of the Crazy Mountain basin were plotted on similar diagrams. Using lines of regression with the same slope used by Sugimura, it has been found that there appears to be a genetic relationship between the rocks of these two areas. No genetic relationship could be found between the mildly alkaline rocks of the northern part of the basin and rocks within the Big Timber complex. Since it is the opinion of the writer that the plutonic igneous phases were intruded syntectonically, it is possible that since some of the rocks of the northern area follow the same lines of re-

gression as the rocks of the Big Timber complex, they may also be related directly in space and time. Lack of time has prevented the writer from exploring this possibility further.

Summary

In each of the diagrams except Figure 65 the various igneous phases of the complex have been outlined, and it can readily be seen that the general chemical trend of the igneous rocks of the Big Timber complex follows the average igneous rock trend. Since field relationships have established the sequence of intrusion to be: (1) early basic plutonic phase, (2) intermediate plutonic phase, (3) terminal plutonic phase, (4) basaltic dike phase, (5) aplitic dike phase, and (6) andesitic dike phase, any overlap or superposition present can be explained.

From the above discussion of the variation diagrams for the rocks of the Big Timber igneous complex several salient features have appeared. No continuous chemical series between the intermediate and terminal plutonic phases is present. Whether or not a genetic relationship exists between either the intermediate plutonic phase and the terminal plutonic phase or the terminal igneous phase and the aplitic dike phase is at the present time a moot question.

By studying the overall chemistry of the various rock phases with emphasis on aluminum, iron, magnesium, calcium, and sodium plus potassium, it can be seen that no abnormalities are present except for the general slight iron-rich characteristic. This iron enrichment can account for the clustering of the points in Figure 65.

Generally, all phases of the Big Timber igneous complex show iron enrichment. In those diagrams in which iron is a variable the trend line for the rocks of the complex is shifted slightly toward the Fe (total) corner.

In those diagrams in which magnesium is introduced as a variable there occurs both a greater degree of scattering and more irregular scattering than in diagrams where magnesium is not a variable. This fact can readily be illustrated by a comparison of Figures 71 and 72.

The ratio of sodium to potassium shows a slight variance, but the degree of variance appears to be insignificant. Neither aluminum nor calcium show deviation from the normal igneous rock trends.

PETROGENETIC ASPECTS

Field, petrographic, and chemical data support the probability that two different sets of physico-chemical conditions were imposed on the magma(s) which formed the rocks of the Big Timber complex. Figure 72 shows that the early basic phase has characteristics very similar to those of other rocks following the "tholeiitic" iron enrichment fractionation trend. The rocks comprising this phase of the Big Timber igneous complex show a mineralogy of olivine and pyroxenes in contrast with the magnetite and amphiboles of the remaining rocks of the complex.

Field investigations have shown the intermediate plutonic phase, terminal plutonic phase, basaltic dike phase, andesitic dike phase, and the aplitic dike phase to be separate and distinct phases of igneous intrusion. These phases essentially follow a continuous silica enrichment trend and apparently have crystallized under similar physico-chemical conditions.

During recent years there has been much written about chemical and mineralogical variations of basic and intermediate intrusions in consanguineous plutonic, hypabyssal and extrusive rock associations (Best, 1963; Kuno, 1960; and 1965; etc.). Strongly differentiated layered basic intrusions (See Figure 68), showing crystal cumulates (Wager and Deer, 1939) also show strong iron enrichment.

Only in the later stages, when 95 percent or more of the parental liquid has crystallized, as in the case of the Skaergaard (Wager, 1960), is there a significant increase in silica and alkalis. This fractionation-differentiation (crystal settling fractionation) is the constant bulk composition (≡tholeiitic trend) of Osborn (1959). In contrast to layered basic intrusions, the calc-alkaline (silica enrichment) suite of rocks, found peripheral to and within orogenic regions (Figure 68), shows a steady increase in alkalis and silica with varying degrees of iron depletion in the successive differentiates.

It was in the calc-alkaline suite that Bowen (1928) found supporting evidence for his proposed discontinuous reaction series involving olivine, pyroxene, amphibole, and then biotite. The validity of this reaction series has long been generally accepted, but it is also realized that differentiated basic intrusions of "tholeiitic"[1] affinities are typified by a mafic series free of hydrous minerals and involving essentially simultaneous crystallization of olivine and one or two pyroxenes (Boyd and Schairer, 1964).

During crystallization of a basaltic magma in an epizonal environment the trend of differentiation which will be followed appears to be dependent upon several factors:

---

[1] The reader is referred to a recent article by Chayes (1966) in which he presents a thorough discussion pertaining to the nomenclature used for basalts.

(1) Certain physical properties of the magmatic body and its envelope of country rocks, e.g. temperature, pressure, and size.

(2) The chemical composition of the initial magma. The published analyses of parental magmas, such as the Skaergaard (Wager, 1960), the Dillsburg sill (Hotz, 1953), the Red Hill dolerite (McDougall, 1962), and the extreme silica-alkali enrichment of the Katmai eruption (Fenner, 1926), show a common basaltic origin when plotted on a diagram similar to Figure 73. Of these, the Katmai eruption, as an example of a calc-alkaline suite, comes closest to the composite silica enrichment trend of the intermediate and terminal plutonic phases and of the dikes of the Big Timber complex.[2] Conversely, the rocks comprising the early basic plutonic phase have an iron enrichment trend similar to that of the Skaergaard layered basic igneous intrusion.

(3) The partition of major elements between solid and liquid phases and the types of solids forming from the liquid at any particular time during crystallization.

These three factors can operate either independently or interdependently.

Not considered among these factors is the assimilation of siliceous crustal material, the successive introduction

[2] It is interesting to note that when the rocks of the northern part of the Crazy Mountain basin are plotted on a similar diagram, a similar fractionation-differentiation trend results.

of magmas, and the weak to strong convection currents operative during the consolidation of the intermediate plutonic phase of the Big Timber complex. Viscosity, obviously low during the intermediate phase, as shown by layering and cut-and-fill structures, is governed by the composition of the magma. A high volatile content in the initial magma could affect the ultimate mineralogy and chemistry of a given crystallization process (Osborn, 1962).

Another important factor in the ultimate mineralogy of a cooling basaltic magma is the physico-chemical effect of the partial pressures of H_2O (P_{H_2O}) and O_2 (P_{O_2}). There is a growing body of opinion (Walker and Poldervaart, 1949; Kennedy, 1955; Kuno, 1960; and Fudali, 1965), based on experimental and field-related petrological studies, that the degree of iron enrichment in differentiated basic intrusions is governed to a great extent by the oxidation state of iron in the magma, which, in turn, is governed by the physico-chemical conditions which prevent or permit the oxidation or reduction of iron.

Cause of Iron Concentration Relative to Silica

Experimental investigations by Osborn (1959, 1962), Boyd and Schairer (1964), Buddington and Lindsley (1964), and Hamilton *et al.* (1964) on the crystallization of simple silicate systems having different P_{O_2} values have supple-

mented field-related petrological studies. Although such synthetic systems cannot duplicate precisely the behavior of much more complicated, natural basaltic magmas during crystallization, the experimental results are indicators of the general array of products forming from a magma under different environmental conditions.

The manner in which iron partitions itself under varying partial pressures of oxygen has been demonstrated by Osborn (1959, 1962) in the systems $CaSiO_3$-Mg_2SiO_4-SiO_2-FeO (low P_{O_2}) and $CaSiO_3$-Mg_2SiO_4-SiO_2-Fe_3O_4 (high P_{O_2}). These two quaternary systems are presented in Figures 75 and 76. The reader is referred to Osborn (1959) for a thorough discussion of the complex crystallization paths followed by synthetic basaltic liquid within the tetrahedra.

Figure 75 essentially represents the phases that can exist in equilibrium for these basaltic liquids crystallizing under low P_{O_2}. In this system magnetite does not occur as an early primary phase, because the low oxygen pressure will prevent the formation of ferric iron.

Conversely, in Figure 76 under high P_{O_2} conditions the liquidus volume of magnetite has become a large principal phase. In this system, under these conditions, liquids comparable in composition to natural basaltic magmas cannot move to the iron-rich, SiO_2-poor region of the system even by extreme fractionation. Hamilton et al. (1964) have also

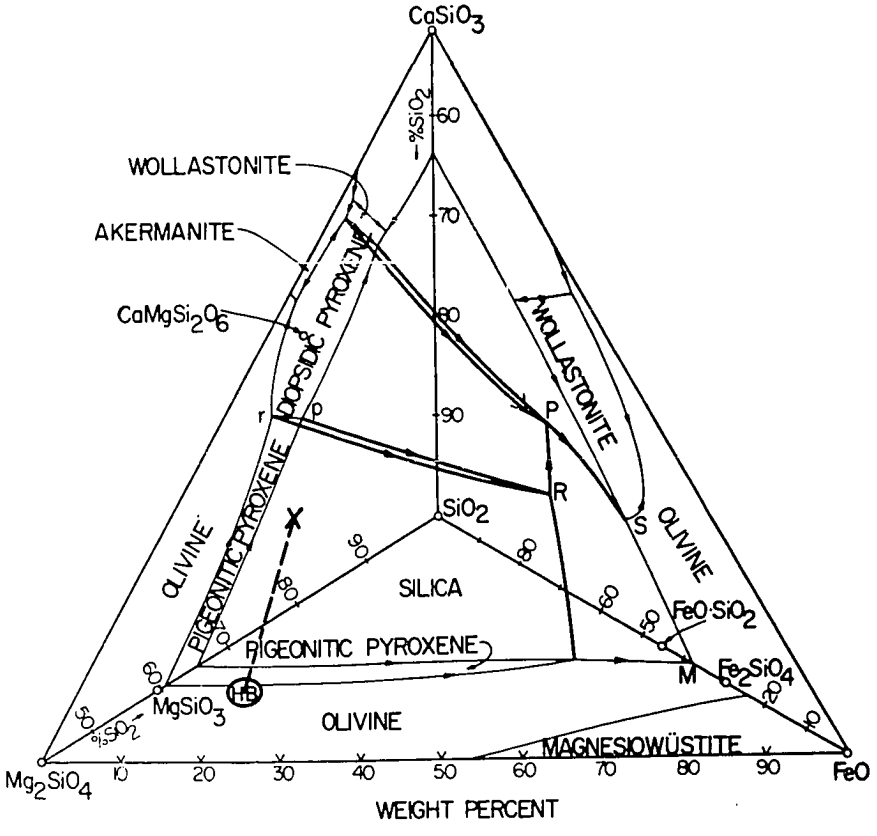

Figure 75. Tetrahedron illustrating the liquidus phase relations in the system Mg_2SiO_4-FeO-$CaSiO_3$-SiO_2 under very low partial pressure of oxygen. For a discussion of crystallization paths, see Osborn, 1962 (Taken from Osborn, 1962).

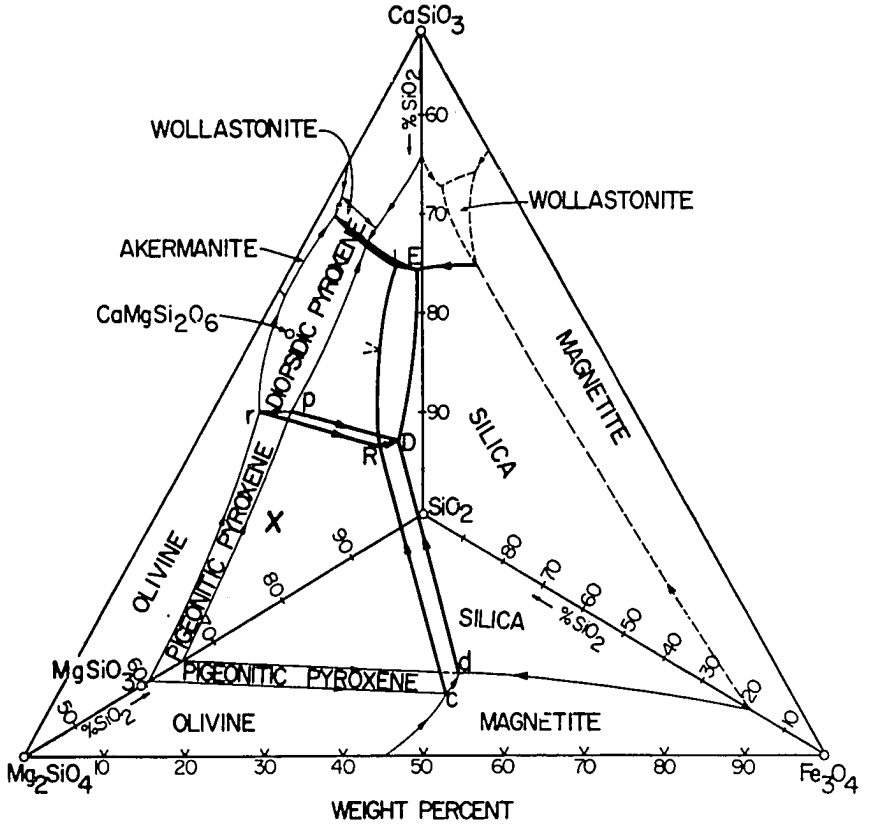

Figure 76. Tetrahedron illustrating the liquidus phase relations in the system Mg_2SiO_4-Fe_3O_4-$CaSiO_3$-SiO_2 at a constant oxygen pressure of 0.21 atm. For a discussion of the paths a liquid will follow during crystallization, see Osborn, 1962 (Taken from Osborn, 1962).

shown experimentally that high oxygen pressure (fugacity) causes early separation of magnetite in a basaltic melt under 1 kb water pressure. The fractionation trend in which iron decreases steadily while SiO_2 increases is generally believed to be characteristic of the calc-alkaline rock series.

Bowen (1928) regarded this as the normal trend for basaltic magmas. Osborn (1959) has stated that the maintenance of nearly constant oxygen pressure in magma, which he supposed to be essential for producing the calc-alkaline trend of fractionation, is made possible only by a sufficient supply of water to the crystallizing magma and by the ability of the hydrogen to escape from the system. In this instance, water plays the role of a buffer. He has suggested that water could be supplied to the melt from the wetter country rock surrounding the magma reservoir.

From the chemical data presented earlier, it can readily be seen (See Figures 71, 72, and 74) that within the Big Timber complex variable conditions were present during the crystallization of the different phases. The early basic phase shows mineralogical variations strongly suggesting crystallization under low P_{O_2} conditions (e.g. olivine and pyroxene with a paucity of primary magnetite).

However, the later intrusive phases, with the exception of the basalt, appear to have crystallized under essentially

high P_{O_2} conditions. The intermediate phase, as shown in Figure 72, originating within the diagram at essentially the same point as the early basic phase, shows a silica enrichment trend. Application of the data of Osborn (1959) to the intermediate phase, consisting of amphibole and abundant primary magnetite, has revealed that this phase could not have formed under low P_{H_2O} and P_{O_2} conditions.

The andesitic dike phase, slightly more rich in silica than the intermediate phase, appears to have crystallized under the same P_{O_2} conditions as the intermediate phase. The mineralogy (abundant hydrous mafic minerals and ubiquitous euhedral magnetite) also strongly suggests high P_{O_2} conditions.

The aplitic dike phase has affinities to late residual magmatic fluids and would normally crystallize under high P_{O_2} conditions, since it has been shown through experimental and field evidence that later magmatic liquids are saturated with H_2O (Tuttle and Bowen, 1958; Wager, 1960). Similar conditions appear to have existed during the crystallization of the terminal plutonic phase.

Reaction Series

The evaluation of the resulting ferro-magnesian fractions is shown in Figure 77. The fractional crystallization of a magma (basaltic) can produce an iron-rich residual liquid,

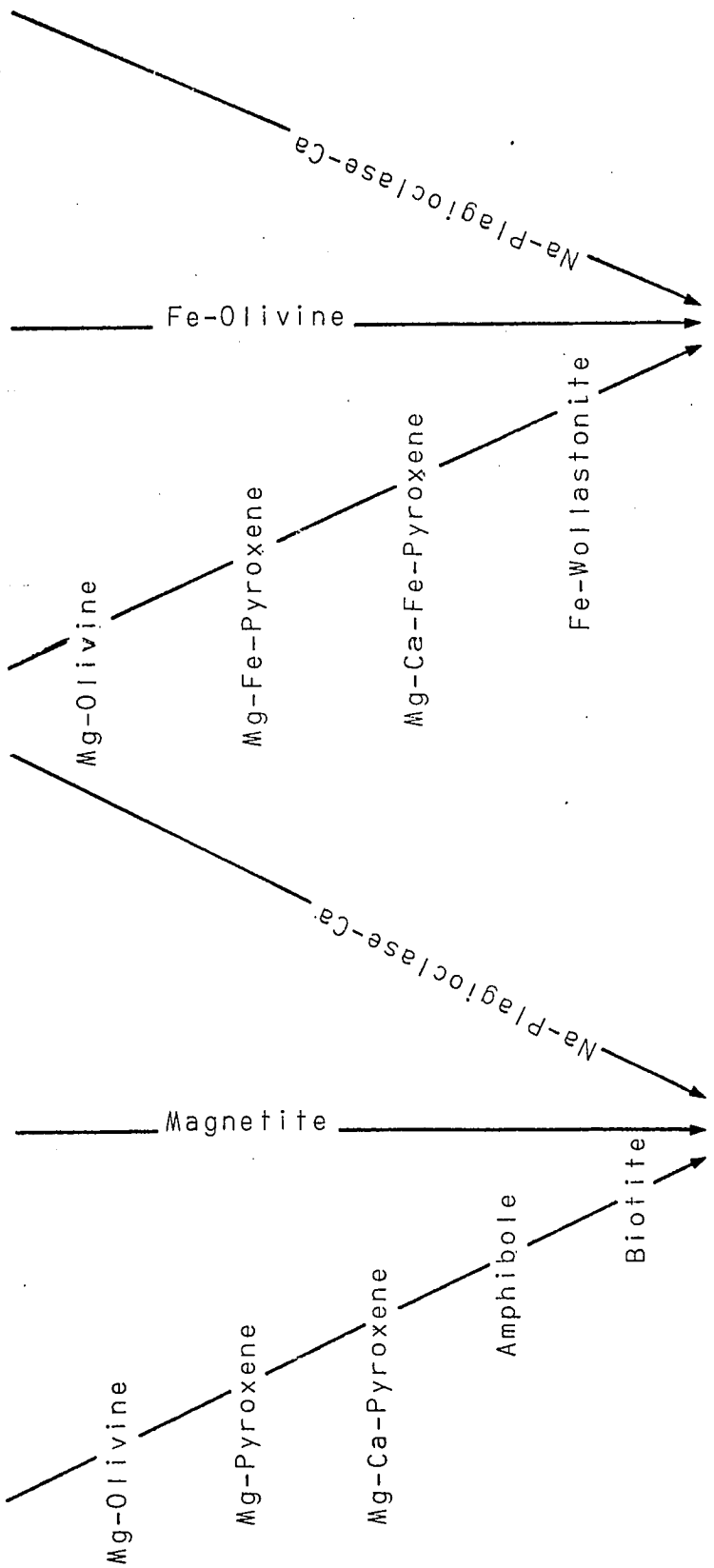

Figure 77. Two groups of reaction series for subalkaline igneous rocks. Group (a) is related to Figure 76 and to calc-alkaline rocks of orogenic regions. Group (b) is related to Figure 75 and to gabbroic layered intrusions. The vertical line for magnetite and that for Fe-olivine signify continued precipitation over the length of the line, just as does the line for plagioclase (From Osborn, 1962).

e.g. the Skaergaard complex and the early basic phase of the Big Timber complex, resulting in the observed mineral relations as shown in (b) of Figure 77. To produce the reaction series as shown in (a) of Figure 77 Osborn postulates that the maintenance of a fairly high oxygen pressure, ca. 10^{-7}, would be required.[3]

From this experimental data it has been shown that under high P_{O_2} the calc-alkaline suite of rocks can be produced from a basaltic magma solely by fractional crystallization. This type of genesis appears to be a possibility for all the rocks comprising the post-early basic phase of the Big Timber complex.

The question which arises at this point is whether or not fractionation during crystallization under high P_{O_2} conditions can alone give rise to the formation of all the rocks of the calc-alkaline suite. That this process may be a contributory factor has been suggested by Fudali (1965) but cannot alone account for the volumetric prominence of granite-granodiorite in orogenic belts. Currently a substantial body of evidence indicates that there are important roles played by processes such as rheomorphism of the sialic crust (Hess, 1960) and the contamination of basaltic magma by sialic crystalline material (Kuno, 1959; and Burnham,

[3] Fudali (1965) has shown that the partial pressure of oxygen (fugacity) required to produce rocks of the Mt. Hood area would vary from 10^{-9} for the most basic to $10^{-6.5}$ for the most acid.

personal communication). These processes could also have contributed to the development of the later phases of the Big Timber igneous complex.

Crystallization-differentiation need not be accepted as the only process operating during the formation of the Big Timber igneous complex. Small-scale chemical and mineralogical factors, such as reaction with the enclosing country rock, diffusion of ionic species, gaseous transfer of elements, late stage pneumatolytic effects and post-magmatic metasomatism may have contributed to the modification of and interference with magmatic consolidation. These various processes would tend to add heterogeneity into the chemical system, but in the Big Timber igneous complex the available chemical data seem to indicate that each separate igneous intrusion (except for the aplitic dikes) is regularly homogeneous.

Many authors feel that palingenesis of crustal materials was a principal factor in the formation of many igneous bodies similar in composition to the Big Timber igneous complex (Deer, 1935). The general paucity of crustal xenolithic material (except for scattered quartzose fragments) rules out the possibility of any wholesale assimilation process. The analysis of Caledonian granitic rocks by Mercy (1963) reveals that any process involving anatexis should show an anomalous proportion of Mg, Fe, Na, K, and Ca. Except for the variability of Mg the elements in the

rocks of the Big Timber complex show moderate regularity; the variation of Mg can possibility be accounted for by the resorption of forsteritic olivine within the mantle. The study of chemical analyses and mineralogical variations have convinced the writer that palingenesis was not of significant importance in the formation of this complex.

Evaluation of the chemical analyses of the rocks in the Big Timber complex leads to the conclusion that two differentiation trends are present. The early border group, whether having crystallized in situ or at depth, crystallized under low partial pressures of oxygen, while the intermediate and terminal phases crystallized under high P_{O_2} conditions. From these two trends there is evidence that at least two phases of magmatic intrusion could have occurred in the formation of the main body of the Big Timber complex.

The most facile explanation for this two-fold magmatic intrusion is that the initial magma, having low volatile content, was intruded under conditions of low partial pressure of oxygen. Water content may have originated in the crust due to major faulting extending through the crust to the upper mantle. The mechanism for this operative process can be explained by lateral movement along either the Nye-Bowler or the Lake Basin megashears, causing secondary faulting along the axis of the Crazy Mountain basin. Smith (1965) considers other igneous

bodies of the Transverse Igneous Belt of the Montana Platform to be related to these megashears which extend through the basement complex. This hypothesis is strongly favored by the writer.

SUMMARY AND CONCLUSION

The Big Timber igneous complex consists of an epizonal stock composed of three distinct phases of intrusion followed by three periods of dike intrusion. The basic border plutonic phase was probably intruded from depth as a crystal mush and was completely consolidated prior to the intrusion of the intermediate phase. This latter phase was essentially wholly liquid and possessed strong convection currents causing agmatite, lamination, and layering. The terminal plutonic phase, containing essential quartz, was intruded centrally into the pluton. The relationship between this phase and the earlier plutonic phases or the aplitic phase has not been established.

After the intrusion of this plutonic phase, basaltic dikes were injected; these dikes were followed by aplitic dikes, which net-veined both the pluton and the metamorphic aureole. Andesitic dike intrusion, the final period of igneous activity, cuts all the earlier phases, transects the metamorphic aureole, and terminates north and south of the pluton in unmetamorphosed sediments.

All the igneous events are proably related to secondary faulting associated with movement along either the Nye-Bowler or the Lake Basin megashears. Fracture patterns within the complex can be geometrically related to a secondary fault system probably extending through the basement complex into

the mantle.

Chemical and petrographic data strongly suggest two different oxidizing conditions present during the crystallization of the several phases of the complex. The early basic phase crystallized under a low partial pressure of water and oxygen as indicated by the presence of olivine and anhydrous ferromagnesian minerals. All post-early basic phase intrusions crystallized under high partial pressure of water and oxygen which is indicated by the absence of olivine and the presence of magnetite and hydrous ferromagnesian minerals. Whether or not a genetic relationship exists between the rocks comprising the Big Timber igneous complex and the sills, dikes, and laccoliths located west and north of the complex has not been established. Future mapping and analysis may reveal what relationship exists between the rocks in these two groups.

SELECTED BIBLIOGRAPHY

Ahrens, L.H., R.A. Edge, and R.R. Brooks, 1963. Investigations on the development of a scheme of silicate analysis based principally on spectrographic and ion exchange techniques: Anal. Chim. Acta, v.28, pp.551-573.

Anderson, E.M., 1951, The dynamics of faulting: Edinburgh, Oliver and Boyd, Ltd., 206pp.

Best, M.G., 1963, Petrology of the Guadalupe igneous complex, South-western Sierra Nevada foothills, California: Jour. Petrology, v.4, pp.223-259.

Bowen, N.L., 1928, The evolution of igneous rocks: Princeton, Princeton University Press, 332pp.

Boyd, F.R. and J.F. Schairer, 1964, The system $MgSiO_3$-$CaMgSi_2O_6$: Jour Petrology, v.5, pp.275-309.

Buddington, A.F., 1959, Granite emplacement with special reference to North America: Geol. Soc. America Bull., v.70, pp.671-747.

Buddington, A.F. and D.H. Lindsley, 1964, Iron titanium oxide minerals and synthetic equivalents: Jour. Petrology, v.5, pp.310-357.

Carmichael, I.S.E., 1964, The petrology of Thingmuli, a Tertiary volcano in Eastern Iceland: Jour. Petrology, v.5, pp.435-460.

Chamberlin, R.T., 1919, A peculiar belt of oblique faulting: Jour. Geology, v.27, pp.602-613.

Chapman, C.A., 1962, Diabase-granite composite dikes, with pillow-like structure, Mount Desert Island, Maine: Jour. Geology, v.70, pp.539-564.

Chayes, F., 1966, Alkaline and subalkaline basalts: American Jour. Science, v.264, pp.128-145.

Chinnery, M.A., 1966a, Secondary faulting, I. Theoretical aspects: Canadian Jour. Earth Sciences, v.3, pp.163-174.

_____, 1966b, Secondary faulting, II. Geological aspects: Canadian Jour. Earth Sciences, v.3, pp.175-190.

Crowell, J.C., 1962, Displacement along the San Andreas fault, California: Geol. Soc. America Spec. Paper 71.

Daly, R.A., 1933, Igneous rocks and the depths of the earth: New York, McGraw-Hill, 598pp.

Davis, E., 1965, Southern Crazy Mountain dike swarm: Unpublished bachelor's thesis, The University of Cincinnati.

Debras-Guedon, J. and I.A. Voinovitch, 1963, Analyse des silicates par spectrophotometrie de flamme en milieu "oxine": American Ceramic Soc. Jour., pp.29-36.

Deer, W.A., 1935, The Cairnsmore of Carsphairn igneous complex: Geol. Soc. London Quart. Jour., v.91, pp.47-76.

Eardley, A.S., 1962, Structural geology of North America: New York, Harper and Row, 743pp.

Elwell, R.W.D., R.R. Skelhorn and A.R. Drysdall, 1962, Net-veining in the diorite of N.E. Guernsey, Channel Islands: Jour. Geology, v.70, pp.215-226.

Fenner, C.N., 1926, The Katmai magmatic province: Jour. Geology, v.34, pp.675-772.

Fleischer, M. and R.E. Stevens, 1962, Summary of new data on rock samples G-1 and W-1: Geochim et Cosmochim. Acta, v.26, pp.525-543.

Fudali, R.F., 1965, Oxygen fugacities of basaltic and andesitic magmas: Geochim. et Cosmochim. Acta, v.29, pp.1063-1075.

Gilbert, G.K., 1877, Report on the geology of the Henry Mountains: U.S. Geog. and Geol. Survey, Rocky Mountain Region, 160pp.

Green, J. and A. Poldervaart, 1958, Petrochemical fields and trends: Geochim. et Cosmochim. Acta, v.13, pp.87-122.

Hamilton, D.L., C.W. Burnam, and E.F. Osborn, 1964, The solubility of water and effect of oxygen fugacity and water content on crystallization in mafic magmas: Jour. Petrology, v.5, pp.21-39.

Hatch, F.H., A.K. Wells, and M.K. Wells, 1961, Petrology of the igneous rocks: New York, Hafner, 515pp.

Hayden, F.V., 1872, Sixth annual report of the United States Geological and Geographical Survey of the territories, embracing portions of Montana, Idaho, Wyoming, and Utah, being a report of progress of the exploration for the year 1872.

Hess, H.H., 1960, Stillwater igneous complex, Montana: Geol. Soc. America Mem. 80, 230pp.

Hotz, P.E., 1953, Petrology of granophyre in diabase near Dillsburg, Pennsylvania: Geol. Soc. America Bull., v.64, pp.675-704.

Iddings, J.P. and W.H. Weed, 1894, Livingston, Montana: U.S. Geol. Survey Geol. Atlas, Folio no.1.

Ingamells, C.O. and N.H. Suhr, 1963, Chemical and spectrochemical analysis of standard silicate samples: Geochim. et Cosmochim. Acta, v.27, pp.897-910.

Johannsen, A., 1939, A descriptive petrography of the igneous rocks, I. Introduction, textures, classifications and glossary: Chicago, University of Chicago Press, 318pp.

_____, 1937, A descriptive petrography of the igneous rocks, III. The intermediate rocks: Chicago, University of Chicago Press, 360pp.

Kelley, W.N., Jr., 1966, Gravity study of the Crazy Mountains, Montana: Princeton University, Dept. of Geological Engineering, Rep. no. 66-2.

Kemp, J.F. and P. Billingsley, 1921, Sweet Grass Hills, Montana: Geol. Soc. America Bull., v.32, pp.437-478.

Kennedy, G.C., 1955, Some aspects of the role of water in rock melts, pp.489-504 in A. Poldervaart, ed., Crust of the earth -- a symposium: Geol. Soc. America Spec. Paper 62, 762pp.

Kuno, H., 1959, Origin of Cenozoic petrographic provinces of Japan and surrounding areas: Bull. Volcan., 2nd ser., v.20, pp.37-76.

_____, 1960, High-alumina basalt: Jour. Petrology, v.1, pp.121-145.

_____, 1965, Fractionation trends of basalt magmas in lava flows: Jour. Petrology, v.6, pp.302-321.

Langmyhr, J. and S. Sveen, 1965, Decomposability in hydrofluoric acid of the main and some minor and trace minerals of silicate rocks: Anal. Chim. Acta, v.32, pp.1-7.

Larsen, E.S., 1940, Petrographic Province of Central Montana: Geol. Soc. America Bull., v.51, pp.887-948.

Lensen, G.J., 1960, Principal horizontal stress directions as an aid to the study of crustal deformation, pp.389-403 in A symposium on earthquake mechanism: Publ. Dominion Obs. Ottawa, v.24.

McDougall, I., 1962, Differentiation of the Tasmanian dolerites: Red Hill dolerite-granophyre association: Geol. Soc. America Bull., v.73, pp.279-316.

McMannis, W.J., 1955, Geology of the Bridger Range, Montana: Geol. Soc. America Bull., v.66, pp.1385-1430.

_____, 1957, The Livingston formation: Billings Geol. Soc., 8th annual field conference, pp.80-84.

Mansfield, G.R., 1909, Glaciat . in the Crazy Mountains of Montana: Geol. Soc. America Bull., v.19, pp.558-567.

Mercy, E.L.P., 1963, The geochemistry of some Caledonian granitic and metasedimentary rocks, pp.189-216 in The British Caledonides, ed. Johnson and Stewart.

Moody, J.D. and M.J. Hill, 1956, Wrench-fault tectonics: Geol. Soc. America Bull., v.67, pp.1207-1248.

Murata, K.J., 1960, A new method of plotting chemical analyses of basaltic rocks: Amer. Jour. Science, 258A, pp.247-252.

Nockolds, S.R., 1954, Average chemical compositions of some igneous rocks: Geol. Soc. America Bull., v.65, pp.1007-1032.

Oki, Y., S. Oki, and H. Shibata, 1962, The systematic analysis of silicate rocks using ion exchange resin: Chem. Soc. Japan Bull., v.35, pp.273-275.

Osborn, E.F., 1959, Role of oxygen pressure in the crystallization and differentiation of basaltic magma: Amer. Jour. Science, v.257, pp.609-647.

_____, 1962, Reaction series for subalkaline igneous rocks based on different oxygen pressure conditions: Amer. Min., v.47, pp.211-226.

Reynolds, D.L., 1954, Fluidization as a geological process and its bearing on the problem of intrusive granites: Amer. Jour. Science, v.252, pp.577-613.

Riley, J.P., 1958, The rapid analysis of silicate rocks and minerals: Anal. Chim. Acta, v.19, pp.413-428.

Shapiro, L. and W.W. Brannock, 1952, Rapid analysis of silicate rocks: U.S. Geol. Survey Circ.165.

_____, 1956, Rapid analysis of silicate rocks: U.S. Geol. Survey Bull. 1036-C.

Simms, E., 1966,[title unknown]: Unpublished doctoral dissertation, The University of Cincinnati.

Smith, J.G., 1965, Fundamental transcurrent faulting in Northern Rocky Mountains: Amer. Assoc. Petroleum Geologists Bull., v.49, pp.1398-1409.

Stevens, R.E., et al., 1960, Second report on a cooperative investigation of the composition of two silicate rocks: U.S. Geol. Survey Bull. 1113, 126pp.

Sugimura, A., 1960, Zonal arrangements of some geographical and petrological features in Japan and its environs: Journal of the Faculty of Science, University of Tokyo, Sect. II, v.12, pp.133-153.

Turner, F.J. and J. Verhoogen, 1960, Igneous and metamorphic petrology: New York, McGraw-Hill, 694pp.

Tuttle, O.F. and N.L. Bowen, 1958, Origin of granite in the light of experimental studies in the system $NaAlSi_3O_8$-$KAlSi_3O_8$-SiO_2-H_2O: Geol. Soc. America Mem. 74, 153pp.

Vogt, J.H.L., 1921, The physical chemistry of the crystallization and magmatic differentiation of igneous rocks: Jour. Geology, v.29, pp.318-350.

Wager, L.R., 1960, The major element variation of the layered series of the Skaergaard intrusion and a re-estimation of the average composition of the hidden layered series and of the successive residual magmas: Jour. Petrology, v.1, pp.364-398.

Wager, L.R. and W.A. Deer, 1939, The petrology of the Skaergaard intrusion, Kangerdlugssuaq, East Greenland: Medd. om Grønland, v.105, no.4, 352pp.

Walker, F. and A. Poldervaart, 1949, Karroo dolerites of the Union of South Africa: Geol. Soc. America Bull., v.60, pp.591-706.

Webber, G.R., 1965, Second report of analytical data for CAAS syenite and sulphide standards: Geochim et Cosmochim. Acta, v.29, pp.229-248.

Weed, W.H., 1899, Geology of the Little Belt Mountains, Montana: U.S. Geol. Survey Ann. Rep. 20, pt.3, pp.257-581.

Wegman, C.E., 1938, Geological investigations in Southern Greenland, Part I: Medd. om Grønland, v.113, pp.1-149.

Wells, M.K., 1954, The structure and petrology of the hypersthene gabbro intrusion, Ardnamurchan, Argyllshire: Geol. Soc. London Quart. Jour., v.10, pp.367-397.

Wilson, C.W., 1936, Geology of Nye-Bowler lineament, Stillwater and Carbon Counties, Montana: Amer. Assoc. Petroleum Geologists Bull., v.20, pp.1161-1197.

Windley, B.F., 1965, The composite net-veined diorite intrusives of the Julianehåb district, South Greenland: Medd. om Grønland, v.172, pp.1-60.

Wolff, J.E., 1938, Igneous rocks of the Crazy Mountains, Montana: Geol. Soc. America Bull., v.49, pp.1569-1628.

Yoder, H.S., Jr. and C.E. Tilley, 1962, Origin of basalt magmas: an experimental study of natural and synthetic rock systems: Jour. Petrology, v.3, pp.342-532.

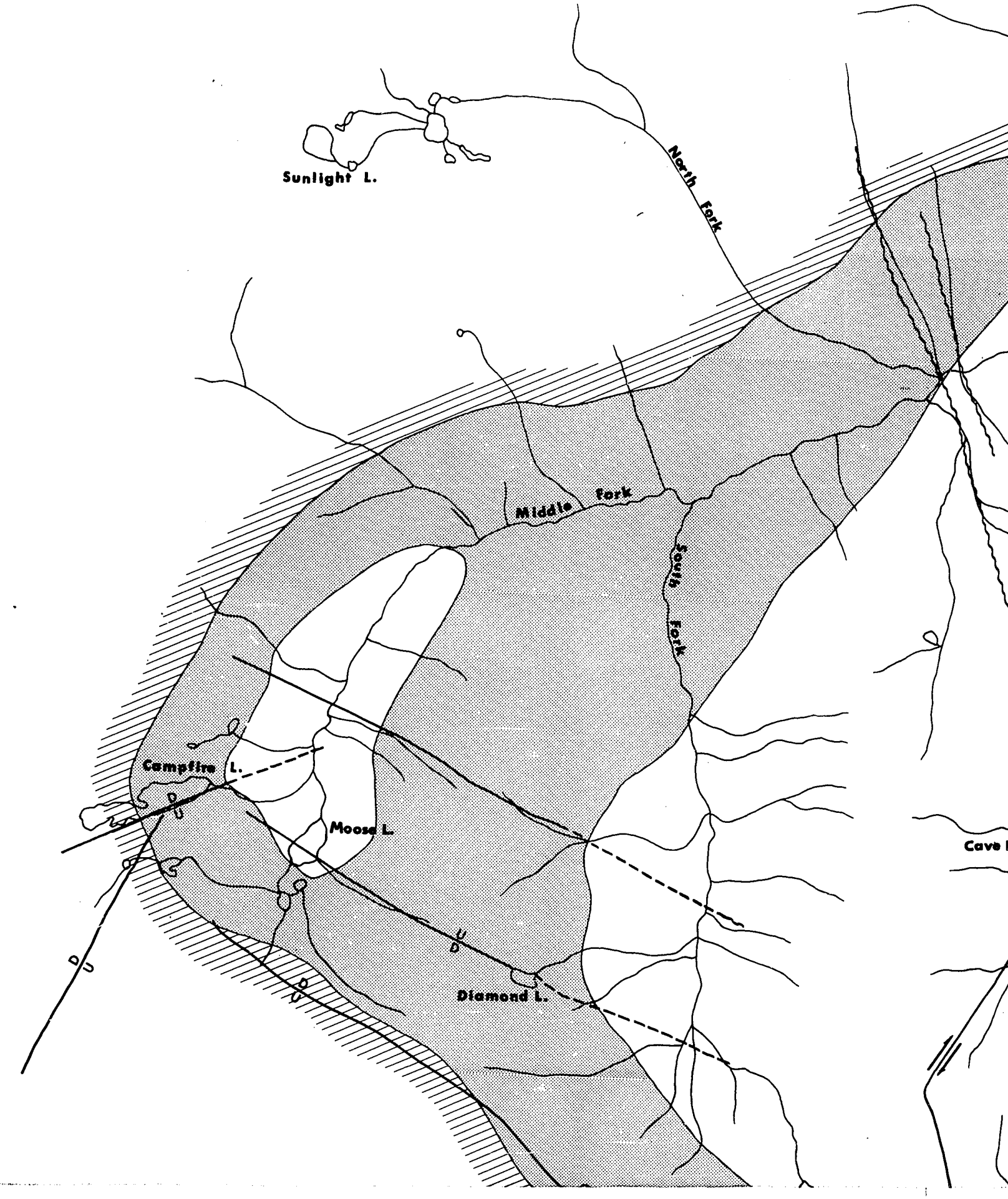

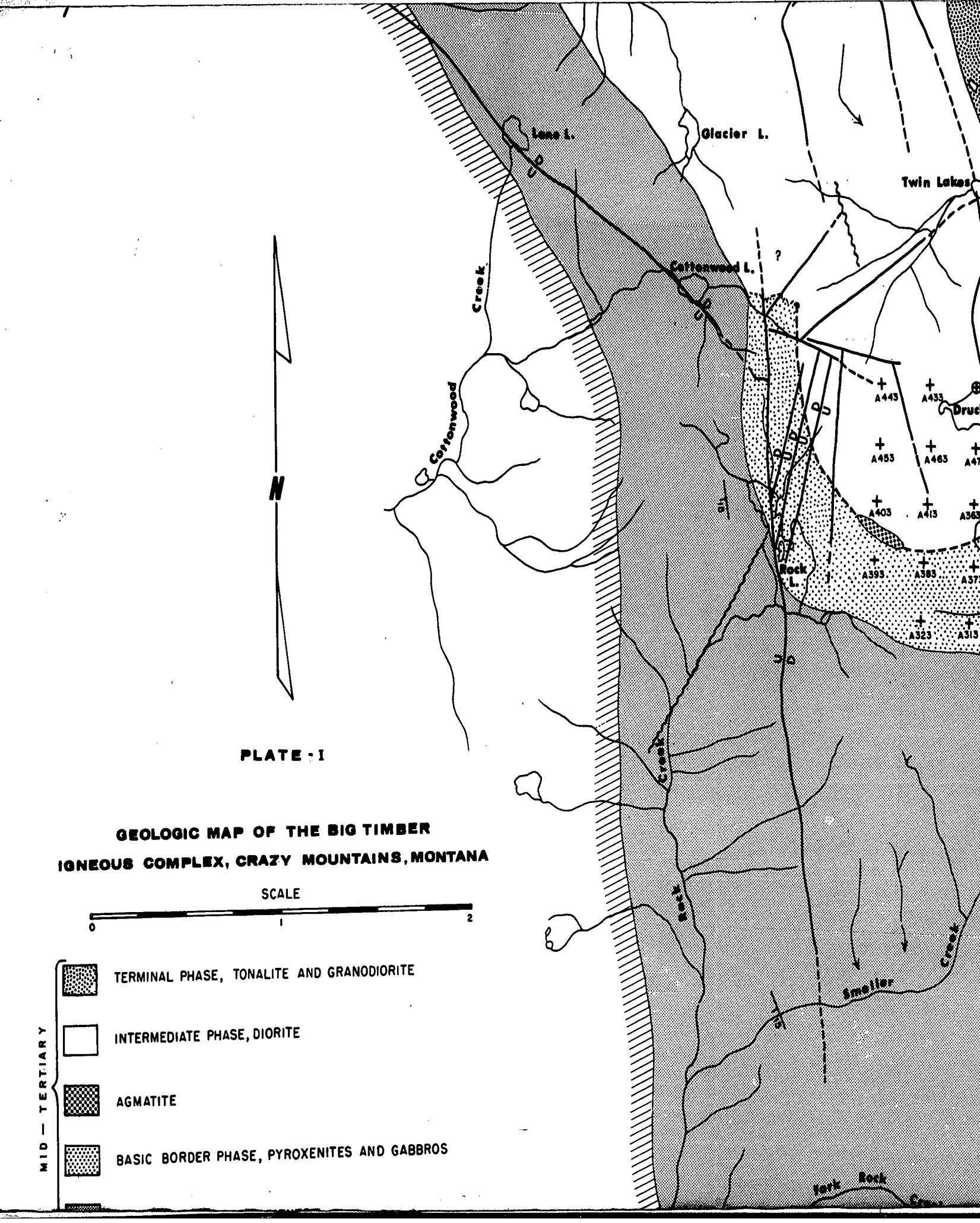

PLATE - I

GEOLOGIC MAP OF THE BIG TIMBER IGNEOUS COMPLEX, CRAZY MOUNTAINS, MONTANA

SCALE

0 1 2

MID — TERTIARY

- TERMINAL PHASE, TONALITE AND GRANODIORITE
- INTERMEDIATE PHASE, DIORITE
- AGMATITE
- BASIC BORDER PHASE, PYROXENITES AND GABBROS

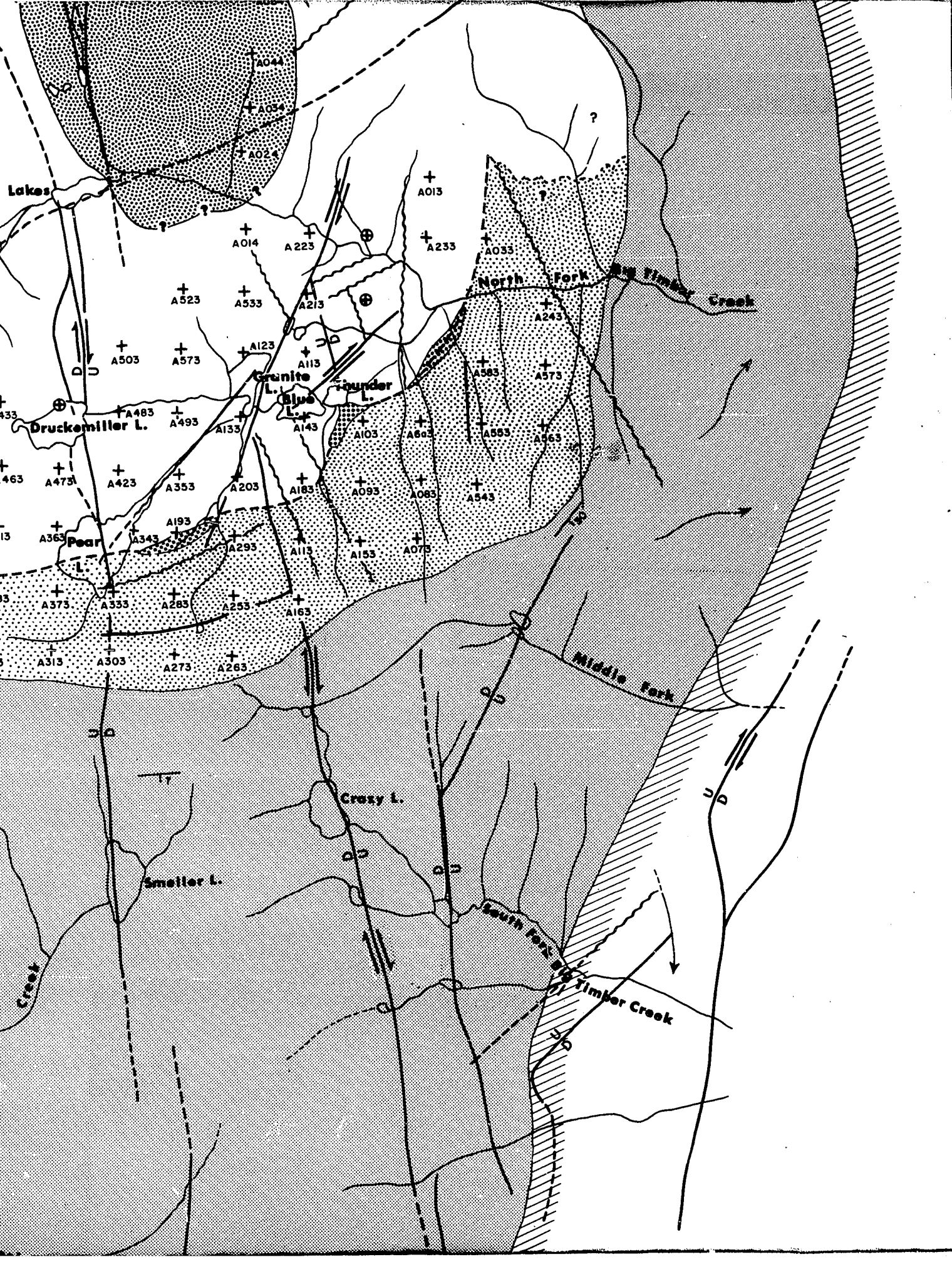

IGNEOUS COMPLEX, CRAZY MOUNTAINS, [illegible]

SCALE

0 1 2

MID — TERTIARY

TERMINAL PHASE, TONALITE AND GRANODIORITE

INTERMEDIATE PHASE, DIORITE

AGMATITE

BASIC BORDER PHASE, PYROXENITES AND GABBROS

METAMORPHOSED SEDIMENTS

CRETACEOUS PALEOCENE

LIVINGSTON GROUP & FORT UNION FORMATION, UNDIFFERENTIATED

110 STRIKE AND DIP OF SEDIMENTS

CONTACTS ARE GRADATIONAL

FAULTS, NORMAL & STRIKE-SLIP, ARROWS SHOW RELATIVE MOVEMENT

SHEARS

+ A 083 LOCATION OF SAMPLE ⊕ -SAMPLE UNOBTAINABLE

DUE TO SCALE, DIKES HAVE NOT BEEN SHOWN

MAP COMPILED FROM U.S. FOREST SERVICE, 2 INCH PLANIMETRIC MAPS AND U.S.G.S. 7½ MINUTE QUADRANGLES.

GEOLOGY BY JOHN TAPPE